NOTE TO USERS

This reproduction is the best copy available.

UMI

MULTI-PORPHYRIN ARRAYS:

SELF-ASSEMBLY, SOLUTION DYNAMICS AND DEPOSITION ON SURFACES

by

TATJANA MILIĆ

A dissertation submitted to the Graduate Faculty in Chemistry in partial fulfillment of the requirements for the degree of Doctor of Philosophy, The City University of New York

2003

This manuscript has been read and accepted for the Graduate Faculty in Chemistry in satisfaction of the dissertation requirements for the degree of Doctor of Philosophy.

1/27/03
Date

Prof. Charles Michael Drain
Chair of Examining Committee

1/28/2003
Date

Prof. Gerald Koeppl
Executive Officer

Prof. James D. Batteas

Prof. Max Diem

Prof. George W. Flynn

Supervisory Committee

THE CITY UNIVERSITY OF NEW YORK

Abstract

MULTI-PORPHYRIN ARRAYS:

SELF-ASSEMBLY, SOLUTION DYNAMICS AND DEPOSITION ON SURFACES

by

Tatjana Milić

Adviser: Professor Charles Michael Drain

Porphyrins and metalloporphyrins are versatile molecules that play an important role in nature; in photosynthesis and other oxido-reduction events. They are also excellent building blocks for the synthesis of large multiporphyrin systems, which may be used as biomimetic models or components of molecular electronics and novel materials.[1]

In nature, weak noncovalent interactions between molecules lead to the spontaneous formation of highly complex and functional molecular assemblies. Similarly, in modern material chemistry, introduction of specific noncovalent molecular interactions is seen as the most promising way toward the synthesis of functional nanoscale materials. Among many types of noncovalent interactions, metal-ion coordination has proved to be a successful approach for design of multi-porphyrin arrays because of its directionality, stability and tunability of the photophysical and electronic properties of the final assemblies.

[1] J. Wojaczynski, L. Latos-Grazynski, *Coord. Chem. Rev.***20 00**, *204*, 113-171 and references therein.

In this work we utilized external ligand-metal interactions to bring together various meso-(4-pyridyl)porphyrin derivatives using platinum(II) or palladium(II) dichloride complexes. By choosing the appropriate porphyrin substitution and metal ion binding geometry, various structures can be formed. In case of the formation of the most complex array made of nine porphyrin units: 4 "L" - shaped porphyrins serve as corners, 4 "T" - shaped porphyrin as sides, and 1 "+" - shaped porphyrin as the center. Self-assembly of these porphyrin units is accomplished by addition of 12 equivalents of a metal complex.

However, self-assembly and supramolecular reorganization proceeds through many stages, and the final products are columnar stacks that are ~ 6 nm in diameter and 0.4 nm to ~ 10 nm tall. If nine equivalents of a first-row transition metal, such as Co(II) or Zn(II), are added to the solution that forms the self-assembled multi-porphyrin array, each porphyrin in the array coordinates the added metal internally, so that the final result is the self-organization of 30 to ~ 300 entities, of five different chemical types.

The size of the aggregates is pre-determined by the choice of appended alkyl group, solvent, porphyrin metalation, and an understanding of the secondary organization kinetics. Moreover, these materials can be deposited onto a variety of surfaces with high structural fidelity, with the choice of surface chemistry affording an additional modality for size selection.

Acknowledgments

I would like to express my profound gratitude to my mentor Professor Charles Michael Drain for his kind help, guidance and support during my doctoral thesis studies. The experience I gained in the Prof. Drain's laboratory has been of great importance for me. I was involved in a very stimulating multi-disciplinary project, which broadened my knowledge of chemistry and helped me mature as a scientist.

I would also like to thank Prof. James Batteas from College of Staten Island for his co-mentorship and help. I am also grateful to Prof. George Flynn for his contribution in our microscopic studies and to Prof. Max Diem for his suggestion during my thesis work. Thanks to Prof. Klaus Grohmann for his help.

My dear co-workers, Dr. Ning Chi, Dr. Dalia Yablon, Dr. Fotis Nifiatis, Dr. Xinxu Shi, Dr. Xianchang Gong, Kaifun Cheng and Dr. Cliff Soll, helped me a lot during my research. My warmest thanks to Xin Chen, Isabelle Sylvain, Nadya Kobko, Artem Masunov and Gabriela Smeureanu whose friendship made my years at Hunter College particularly enjoyable.

My deepest gratitude to my father Nikola, my brother Miodrag and my husband Paolo for their scientific and intellectual help and more importantly for their love and continuous support during the years I spent in the doctoral program.

Posvećeno,

mami, tati i Mišku

Table of Contents

List of Tables

List of Figures

List of Schemes

Abbreviations

AFM	Atomic Force Microscopy
Bn	Benzonitrile
DLS	Dynamic Light Scattering
ESI-MS	Electrospray Mass Spectroscopy
IR	Infra-red
M	Metal
STM	Scanning Tunneling Microscopy
NMR	Nuclear Magnetic Resonance
TtBuPP	tetrakis-(4-*tert*-butylphenyl)porphyrin
TMePP	tetrakis-(4-methylphenyl)porphyrin
TDdcylPP	tetrakis-(4-dodecyloxyphenyl)porphyrin
TPyP	tetrakis-(4-pyridyl)porphyrin
5-PytBuPP	5-(4-pyridyl)-10,15,20-tris-(4-*tert*-butylphenyl)porphyrin
5-PyMePP	5-(4-pyridyl)-10,15,20-tris-(4-methylphenyl)porphyrin
5-PyDdcylPP	5-(4-pyridyl)-10,15,20-tris-(4-dodecyloxyphenyl)porphyrin
5,15-PytBuPP	5,15-bis-(4-pyridyl)-10,20-bis-(4-*tert*-butylphenyl)porphyrin
5,15-PyMePP	5,15-bis-(4-pyridyl)-10,20-bis-(4-methylphenyl)porphyrin
5,15-PyDdcylPP	5,15-bis-(4-pyridyl)-10,20-bis-(4-dodecyloxyphenyl)porphyrin
5,10-PytBuPP	5,10-bis-(4-pyridyl)-15,20-bis-(4-*tert*-butylphenyl)porphyrin
5,10-PyMePP	5,10-bis-(4-pyridyl)-15,20-bis-(4-methylphenyl)porphyrin
5,10-PyDdcylPP	5,10-bis-(4-pyridyl)-15,20-bis-(4-dodecyloxyphenyl)porphyrin
5,10,15-PytBuPP	5,10,15-tris-(4-pyridyl)-20-(4-*tert*-butylphenyl)porphyrin
5,10,15-PyMePP	5,10,15-tris-(4-pyridyl)-20-(4-methylphenyl)porphyrin
5,10,15-PyDdcylPP	5,10,15-tris-(4-pyridyl)-20-(4-dodecyloxyphenyl)porphyrin

1.

INTRODUCTION

1. 1. Supramolecular Chemistry

Supramolecular[1] chemistry is a modern multidisciplinary branch of chemical science that is progressing continuously since 1980's.[2] Nowadays it is a frontier of science that opens new perspectives toward design of the novel materials with unique properties and a wide range of applications.

There are two important factors that contributed to the rapid development of supramolecular chemistry. One of them is a long-term scientific need for strategic design of highly complex and functional molecular systems built from the simple molecules.[3] Another factor arises from the recent demands of the microelectronics industry and has influenced significantly the course of research in supramolecular chemistry. Advances in this industry currently use lithography methods that strive to decrease the size of existing silicon components. Because this miniaturization has limitations due to the difficulties in signal insulation and high speed signal processing, it is obvious that new ways for building electronic structures should be found.[3]

---

[1] *Supra* – prefix meaning "above" or "beyond limits" of molecule.
[2] J. M. Lehn, *Angew. Chem. Int. Ed.* **1990**, *29*, 1304-1319.
[3] D. Philp, J. F. Stoddart, *Angew. Chem. Int. Ed.* **1996**,*35* , 1154 –1196.

Supramolecular chemistry offers a new approach. It is focused on distinct molecules (no more than a few nanometers in size) that arrange themselves spontaneously into a complex and functional entities that are tens of nanometers to micrometers in size by means of intermolecular noncovalent interactions. These interactions between subunits or subassemblies are weak, but if many are combined together a very stable structure can be achieved.[3]

Molecular assemblies that occur in nature are wonderful examples of highly complex and functional systems. For example, specific amino acid sequences in proteins dictate the folding of the protein polymer into specific structures. Oftentimes these structures self-assemble (by themselves or with other proteins) into three-dimensional architectures that perform functions, such as catalysis and recognition. Similarly, the complex topology of RNA, thus its activity as a ribosome, arises from the information programmed into the molecule via its sequence. The liquid crystalline properties of membranes are also due to the intermolecular interactions of the lipids. Another example is the remarkable efficiency of photosynthesis that rests in the careful organization of pigment molecules with appropriate HOMO-LUMO energy gaps. The chlorophylls in the photosynthetic antennas complex, for example act in concert to harvest light with near 100 % quantum efficiency.

Much of the work contained herein acknowledges biological inspiration, but the overall goals are to discover new photonic materials rather then to mimic specific biological processes using porphyrins. The new materials might have surprising electronic, magnetic or photophysical properties, and a vast number of beautiful and

complex molecular assemblies has already been synthesized and reported in the literature.[4] However, the incorporation of designed functionality still presents a challenge.

1. 2. Self-Assembly

Self-assembly involves many noncovalent intermolecular interactions, that might be arranged in the following four categories:

- Coordination bonding (metal-ligand)
- Hydrogen bonding
- Electrostatic forces (π-π stacking, van der Waals and dipole-dipole interactions)
- Hydrophobic/hydrophilic interactions

There are a large number of synthetic advantages that self-assembly provides:[3]

- S*elf-assembly is highly efficient process*. A large, complex structure requires only a small number of different molecule types. If there are any defective or incorrectly attached subunits they will be eliminated from the growing structure, ensuring the correct assembly of the final thermodynamic product.
- *Noncovalent forces introduce flexibility into the system.* This property is commonly found in biological systems, where functionality is achieved through many reversible changes in conformation.
- *Self-assembly can utilize both covalent and noncovalent bonding.* Therefore, it is easy to form a hybrid material made of organic, inorganic and biological components with a combination of properties.

---

[4] L. F. Lindoy, I. M. Atkinson, *Self-assembly in supramolecular systems*, RSC, October **2000**.

- *Self-assembly is often a cooperative process.* Usually, it displays positive cooperativity, which means faster incorporation of subsequent units.
- S*elf-assembly often operates under equilibrium control.* A growing structure has time to reorganize itself in order to maximize complementary surface contacts, and the final structure usually represents the thermodynamic minimum.

However, self-assembly has some disadvantages that are a source of synthetic and characterization difficulties.

- *Noncovalent interactions are usually weak and reversible.* Labile systems that operate under equilibrium control may display multiple and complex reaction pathways. The final product may be trapped in one of the kinetic stages instead of the thermodynamic minimum.
- *Products may be concentration dependent* (discrete self-assembled species are more favored in a dilute solutions) *and thermally labile.*
- *Equilibria also pose problems in characterization* of self-assembled systems.

1. 3. Objectives of Our Research

As mentioned before, the essence of nanotechnology lies in the ability to design precise functional materials on the molecular level. With the remarkable progress in the self-assembly of molecular components into specific arrays and polymers, there are many other recent examples of supramolecular species that are proposed as components of nanoscaled devices.[2,5,6,7]

---

[5] J. S. Lindsey, *New. J. Chem.***19 91**, *15*, 153-180.
[6] P. J. Stang, B. Olenyak, *Acc. Chem. Res.* **1997**,*30* , 502-518.
[7] M. Fujita (Ed.), *Structure and Bonding* **2000**,*96* , 149-201.

But, there are several critical factors to be considered. Since the vast majority of molecular self-assembly processes are carried out in solution and utilize relatively weak intermolecular forces, can the desired products be reliably deposited onto surfaces and still retain their intended structure and function? Since the components of the self-assembled structures are organic or coordination compounds, how stable are they electrochemically, thermally, and to oxidation? If self-assembled entities are to be used in large-scale applications, an important, yet often unacknowledged requirement is that highly pure molecular components or building blocks must be readily synthesized on large scales in high yields

In this work we report the self-assembly of porphyrinic arrays and clusters that address these issues. More specifically, we have utilized the self-assembly of a multi-porphyrin arrays and tapes mediated by coordination of exocyclic pyridyl groups to *trans*-palladium(II) or *cis*-platinum(II) complexes. We monitored the actual process of self-assembly and determined the factors that influence the molecular self-organization and aggregation in solution. Moreover, we have deposited these materials onto a variety of surfaces to explore their stability, surface three-dimensional structures and possibilities for future molecular manipulation. Various spectroscopic techniques are combined for the characterization of self-assembled arrays in solution, and atomic force and scanning tunneling microscopy were used for imaging of final surface structures.

2.

PREPARATION AND CHARACTERIZATION OF PORPHYRIN BUILDING BLOCKS

2. 1. Introduction

Porphyrins and metalloporphyrins are versatile molecules that play an important role in nature; in photosynthetic processes and many other oxido-redox events. They are also excellent building blocks for the construction of large multicomponent architectures because of their facile synthesis, good stability and a variety of physico-chemical properties.[1] By simple modification of the peripheral substituents at the meso-positions on the porphyrin macrocycle, various supramolecular architecture can be formed. The main reason for this is that the peripheral functional groups at either the β-pyrrole or the meso position are held rigidly at pre-defined positions, which facilitates both design and reinforces structure.

The application of coordination chemistry in the formation of self-assembled systems has proved to be a very successful approach for design of multi-porphyrin arrays because of an easy templating effect of the binding metal center and coordination bond's strength

[1] J. Wojaczynski, L. Latos-Grazynski, *Coord. Chem. Rev.***20 00**, *204*, 113-171 and references therein.

(which can vary over ~ 1 order of magnitude from a couple of kcal/mol to tens of kcal/mol). Furthermore, the metals contained in the arrays may add some interesting electronic, optical or sensing properties.[2] A large variety of supramolecular assemblies are reported in the literature, where external metal ions bring together two or more porphyrin units, creating rings, squares, grids, ladders, capsules and different polymeric architectures. [3,4,5]

2. 1. 1. Choice of porphyrin building blocks

In order to form a coordination bond between a metal ion and the porphyrin building block it is necessary to choose the appropriate peripheral groups on the porphyrin macrocycle, usually at the meso position, suitable for the metal ion coordination. Usually, donor groups bearing nitrogen or oxygen atoms at the porphyrin periphery are good coordination sites for many transition metals. Due to the versatility of pyridyl ligands toward different metal ions, many discrete arrays as well as polymeric structures were formed by taking advantage of either axial metalloporphyrin-pyridyl or bridging metal-pyridylporphyrin interactions.[1] Other derivatives of pyridine, such as bipyridyl or terpyridyl ligands are also commonly used, and the main reason is that they all act as good sigma and π-donors as well as π-acceptors, so that the bound metal ion is coordinatively stabilized making the assembly thermodynamically stable.[2]

In this work we utilized external ligand-metal interactions, to bring together various meso-(4-pyridyl)porphyrin derivatives using platinum(II) or palladium(II) dichloride

---

[2] Z. Qin, H. Jenkins, S. Coles, K. Muir, R. Puddephatt, *Can. J. Chem.* **1999**,*77*, 155-157.
[3] L. Lindoy and I. Atkinson, *Self-assembly in Supramolecular Systems*, RSC, October **2000** and references therein.
[4] C. M. Drain, J.-M. Lehn, *J. Chem. Soc. Chem. Commun.* **1994**, 2313-2315.
[5] C. M. Drain, F. Nifiatis, A. Vasenko, J. D. Batteas, *Angew. Chem. Int. Ed.* **1998**,*37* (17), 2344-2347.

complexes. This strategy is a continuation of Lehn's and Drain's approach for the formation of various supramolecular arrays.[4,5]

The porphyrins used as building blocks in this work have either peripheral methylphenyl, *tert*-butylphenyl or dodecyloxyphenyl substituents at the remaining meso positions. Because of their different solubility in organic solvents, the final self-assembled porphyrin arrays have somewhat different aggregation properties in solution and absorption properties on surfaces. Nevertheless, this can be an important factor in the controlled formation of surface structures for various potential applications.

2. 1. 2. Choice of metal-binding complex

Precise geometrical structure of transition metal complexes can be used as a directional mode for binding organic ligands with a predetermined angle or shape. *Trans*-bis-(benzonitrile)palladium dichloride, $[(PhCN)_2PdCl_2]$, is one of the most widely used square planar palladium(II) complexes.[6] It was prepared for first time by *Kharasch et al* [7] in 1936 by heating palladium chloride with benzonitrile. This complex readily looses benzonitrile ligands upon coordination of stronger binding ligands and it is soluble in a wide variety of organic solvents (benzene, alcohol, chloroform, toluene, etc.). For all these reasons it is very suitable for use in the formation of self-assembled systems.

Because benzonitrile groups are weakly bound to the palladium, this complex decomposes in solution to give, after a while, palladium(II) dichloride.[8] A palladium(II) dichloride can form several stable polymorphs. The α-form consists of linear chains in which each palladium atom coordinates four chlorine atoms, while each chlorine atom

---

[6] Peter M. Maitlis, *The Organic Chemistry of Palladium*, Academic Press **1971**.
[7] M. S. Kharasch and T. A. Ashford, *J. Am. Chem. Soc.* **1936**,*58* , 1733.
[8] M. M. Olmstead, P. Wei, A. S. Ginwalla and A. L. Balch, *Inorg. Chem.* **2000**,*39* (20), 4555-4559.

bridges two-palladium atoms.[8] The β-form consists of discrete molecules of Pd_6Cl_{12} that are arranged in a octahedral array, in which every palladium atom is surrounded by four equivalent chlorine atoms.[8] Because of *bis*-(benzonitrile)palladium dichloride lability we can expect $PdCl_2$ and other chloro-bridged compounds, such as Pd_2Cl_6 and Pd_6Cl_{12} to be present in a solution. The presence of chloro-bridged ligand, Pd_2Cl_6, in toluene does not present an obstacle for the use in self-assembly reaction, as tested and described in experimental part 2. 3. 1.

Other metal salts commonly used in self-assembly reactions include related *cis*-bis-(benzonitrile)platinum(II) dichloride, palladium(II) and platinum(II) bisphosphane, palladium $(DMSO)_2Cl_2$ and other complexes.

2. 2. Results and discussion

2. 2. 1. Synthesis of porphyrin building blocks

All porphyrin monomers used for construction of supramolecular arrays are synthesized according to the Alder method.[9,10,11] This one-step reaction involves refluxing pyrrole with the appropriate benzaldehyde in propionic acid under oxidizing conditions. The mechanism of this reaction is thought to proceed through formation of carbonium ion after protonated aldehyde attacks the α-position on another pyrrole to give a meso-substituted dipyrrlymethane.[12] The reaction continues until tetrapyrrlycarbinols and black poly-pyrrolic by-products are formed. Ring closure follows until porphynogens are formed, which oxidize in air to porphyrins, and phlorins, which tautomerise to

[9] A. D. Adler, F. R. Longo, J. D. Finarelli, J. Goldmacher, J. Assour, L. Korsakoff, *J. Org. Chem.***19 67**, *32*, 476.
[10] A. D. Adler, F. R. Longo, W. Shergalis, *J. Am. Chem. Soc.***19 64**,*86* , 3145-3149.
[11] R. G. Little, J. A. Anton, P. A. Loach, J. A. Ibers, *J. Heterocycl.Chem.* **1975**, *12*, 343-349.
[12] Lionel R. Milgrom, *The colors of life*, Oxford University Press **1997**.

chlorins and oxidize slowly to porphyrins. The Adler method is used for several reasons. It is simple and suitable for large-scale porphyrin synthesis.[12] The porphyrins synthesized can be isolated and crystallized from the reaction mixture. Five out of six porphyrins resulting from a mixture of two aldehydes in this synthesis are useful building blocks in our studies.

The other frequently used approach, developed by Lindsey and coworkers[13,14,15,16] for synthesis of porphyrins involves anaerobic condensation of the pyrrole with the aldehydes at low temperature, until a maximum yield of porphyrinogen is obtained, and then the mixture is oxidized with an oxidation agent such as 2,3-dichloro-5,6-dicyanobenzoquinone (DDQ).[17] This approach was not used because the best reaction conditions vary from porphyrin to porphyrin, which makes difficult to simultaneously synthesize more then one porphyrin at the time. The low or erratic yields of pyridyl porphyrins are also common if this method is used.

2. 2. 2. Spectroscopic characterization of porphyrins building blocks

UV-Vis characterization

The absorption of light in the UV-Vis spectral region is the most important property of porphyrins and metalloporphyrins. The UV-Vis absorption spectra of porphyrins are related to their physicochemical properties and are very useful in terms of identification and quantification of a certain porphyrin fraction. The most typical and intense absorption band, common for all porphyrins, is located around 400 nm (Figure 2. 1.) and

---

[13] J. S. Lindsey, I. C. Schreiman, H. C. Hsu, P. C. Kearney, A. M. Marguerettaz, *J. Org. Chem.* **1987**,*52* , 827-836.
[14] J. S. Lindsey, K. A. MacCrum, J. S. Tyhonas, Y.-Y. Chuang, *J. Org. Chem.* **1994**,*59* , 579.
[15] D. Gryko, J. S. Lindsey, *J. Org. Chem.* **2000**,*65* (7), 2249-2252.
[16] P. D. Rao, B. J. Littler, G. R. Geier III, J. S. Lindsey, *J. Org. Chem.***20 00**,*65* , 1084-1092.
[17] R. A. W. Johnstone, M. L. P. G. Nunes, M. M. Pereira, A. M. d'A. Rocha Gonsalves, A. C. Serra, *Heterocycles* **1996**,*43* (7), 1423-1437.

was discovered by Soret in 1883. The molar extinction coefficient of the Soret band is in the range 2 - 5 × 10^5 [L/mol × cm] and it is 10-20 times more intense then the other visible bands.[18]

The visible spectra of porphyrins in neutral solvent have four characteristic bands, typically labeled I-IV. These bands are called Q-bands and their intensity ratio is different depending of the porphyrin type.

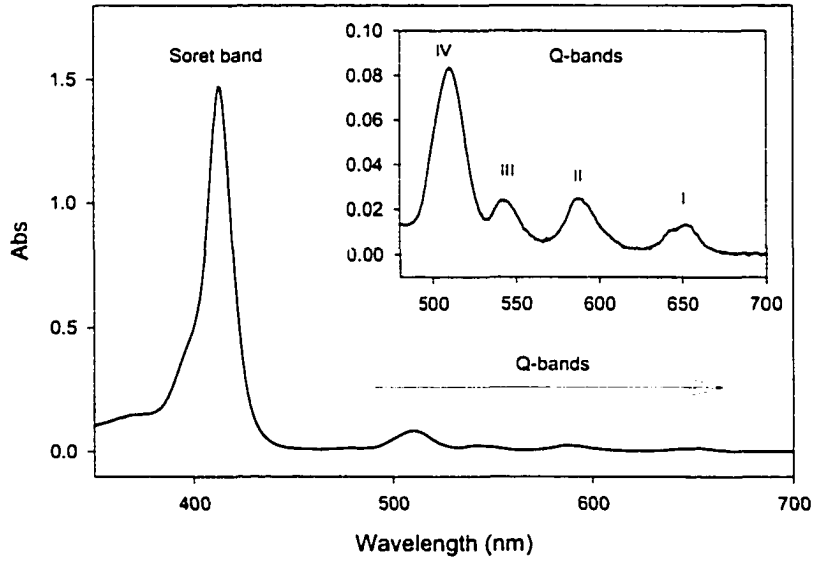

Figure 2. 1. UV-Vis spectrum of tetrakis-(4-pyridyl) porphyrin in ethanol

The number of bands in the UV-Vis spectral region is also an indication of protonation or metalation of macrocycle. If the porphyrin molecule is protonated or metalated, only two main visible bands, α and β, are found. The change in UV-Vis spectrum is due to the increased symmetry (usually D_{4h}) relative to the free-base porphyrin (usually D_{2h}).

[18] J. E. Falk, *Porphyrins and Metalloporphyrins*, Vol. 2, Elsevier New York, **1964**.

Fluorescence characterization

Fluorescence characterization is a very convenient method for porphyrin detection and determination. When porphyrins are irradiated with UV light they usually fluoresce and this property can be used in TLC chromatography, where spots containing only 5 nanograms of a porphyrin can be detected.[15] The intensity of fluorescence varies with pH and is greatly influenced by the presence of inorganic ions. If porphyrins have internal transition metal ion within its macrocycle, usually no fluorescence is found, and this will be discussed more in the following chapters. Fluorescence characterization provides several advantages compared to other spectrophotometric methods. It is 100-1000 times more sensitive and faster then the other spectrophotometric methods.[19]

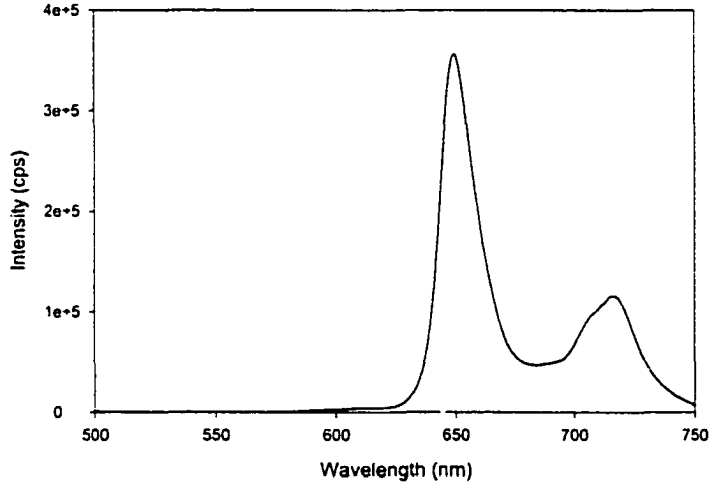

Figure 2. 2. Fluorescence emission spectrum of tetrakis-(phenyl)porphyrin

In general, the emission maxima (Figure 2. 2.) are close to the absorption maxima but at a longer wavelength than that of absorption band I, i.e. there is a small Stoke's shift.[18]

[19] E. Dufour, *American Laboratory*, May **2002**, *34* (10), 50-56.

NMR characterization

NMR spectroscopy is a powerful tool for all structural identification, and it can be successfully applied for identification of individual porphyrin molecules. From the NMR studies it is easy to observe aromatic nature of porphyrin macrocycle.[12] Diamagnetic ring current deshields both beta-pyrrole protons and meso-protons, and they can be found in the aromatic region of the spectra above 7 ppm. Meso-protons are attached to electron-deficient carbons and they are shifted more downfield then the beta-pyrrole protons. Since, ring current deshields protons from the external magnetic field outside the macrocycle, if there are protons inside the macrocycle, such as inner N-H protons, they will be shielded from the external magnetic field. Therefore, inner N-H protons are shifted upfield, beyond tetramethylsilane (0 ppm), and they are usually found between –2 and –3 ppm. NMR spectra of porphyrins used in our studies are given in Appendix, 2. 4.

Mass spectroscopy characterization

Electrospray ionization mass spectroscopy is commonly used method for characterization of free base porphyrin monomers. The porphyrin macrocycle is stable under mass spectroscopic conditions making the analysis facile and straightforward. ESI-MS spectra of porphyrins we used can be found in Appendix, 2. 4.

2. 3. Experimental

2. 3. 1. Preparation of bis-(4-pyridine)palladium(II) dichloride

As described before, even a fresh solution of bis(benzonitrile)palladium(II) dichloride shows the presence of free palladium(II) dichloride and chloro-bridged Pd_2Cl_6, due to the weakly bound benzonitrile ligands. The mass spectrum analysis of a freshly prepared and

diluted (12 μM) bis-(benzonitrile)palladium dichloro solution, confirm the presence of palladium chloro-bridged dimers. The results are given below.

ESI-MS: Calculated for $C_{14}H_{10}N_2PdCl_2$ *m/z* (theoretical intensities): 378 (2.1), 379 (0.2), 380 (24.6), 381 (50.3), 382 (79.7), 383 (42.2), 384 (100), 385 (20.3), 386 (67.9), 387 (10.6), 388 (22.3), 389 (3.5), 390 (2.7), 391 (0.4). *m/z* ($M + H^+$, rel. intensities) found: $PdCl_2$ 175 (25), 177 (18), 179 (10); $[Pd(PhCN)_2Cl_2]$ 381 (12), 384 (45), 386 (11), 391 (8); Pd_2Cl_6 422 (28), 424 (15), 426 (31), 427 (40), 429 (100), 430 (56), 431 (29), 432 (18), 433 (35).

The test reaction **1** was done to confirm the hypothesis that strongly binding pyridyl ligands have no difficulties in breaking the chloro-bridged Pd_2Cl_6 complex to access palladium(II).

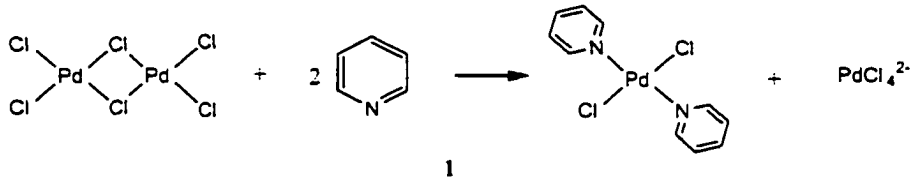

1

Scheme 2. 1. Formation of bis-(4-pyridine)palladium(II) dichloride complex

A 10 μM pyridine solution in toluene was prepared. This concentration is similar to the porphyrin concentration (9 μM) used in the typical self-assembly reaction. The pyridine solution was mixed with 5 μM solution of bis-(benzonitrile)palladium dichloride in toluene (2:1 ratio) and the product given for mass analysis. Results are given below.

ESI-MS: Calculated for $PdPy_2Cl_2$ *m/z* (theoretical intensities): 330 (2), 331 (0.2), 332 (25), 333 (50), 334 (79), 335 (40), 336 (100), 337 (16.3), 338 (68), 339 (8), 340 (22), 341

(3). *m/z* ($M + H^+$, rel. intensities) found: 179 (10) $PdCl_2$, 336 (18), 338 (100), 339 (25), 340 (8), 335 (5).

The results of reaction **1** confirm that ligands bearing nitrogen atoms, such as pyridyl ligands, can break apart chloro-bridged complexes, such as Pd_2Cl_6, and form a stable coordination bond with palladium(II).

Atomic force microscopy studies indicate that fresh and diluted 12 μM solutions of bis-(benzonitrile)palladium(II) dichloride when deposit on a glass plate, give rise to a small number of particles which can be easily removed by rinsing a plate with organic solvents. However, if solution of bis-(benzonitrile)palladium(II) dichloride is aged (more then 6 months) and concentrated (1.7 mM) it will show significant presence of small (3 - 4 nm) and well-distributed nanoparticles. In conclusions it is recommended that stock solution of bis-(benzonitrile)palladium(II) dichloride, used for self-assembly reaction, is prepared on a monthly basis using toluene or other non-chlorinated solvents.

2. 3. 2. Synthesis of porphyrins with *tert*-butylphenyl substituents

All compounds for the synthesis of porphyrins with *tert*-butylphenyl substituents (pyrrole, 4-*tert*-butylbenzaldehyde and 4-pyridinecarboxaldehyde) are commercially available and were purchased from Aldrich. Before the reaction, pyrrole and starting aldehydes were purified on small basic alumina columns. To a solution of 448 mL of propionic acid (preheated to 80°C), 4-*tert*-butylbenzaldehyde (1.87 mL, 11 mmol) and 4-pyridenecarboxaldehyde (1.34 mL, 14 mmol) were added and mixed, followed by addition of pyrrole (1.55 mL, 22.4 mmol). The reaction mixture was refluxed (boiling point of propionic acid is 140 °C) for 90 minutes in the dark. After the reaction, the reaction mixture was cooled and the propionic acid removed at reduced pressure. The

oily black-purple products were dissolved in 15 mL of toluene and allowed to crystallize in 400 mL of methanol overnight. Filtration and washing with methanol afforded 0.8 g (~17 % yield) of a purple crystalline product that contained the expected statistical mixture of six porphyrin compounds. The porphyrins were separated by flash silica gel column chromatography using a toluene/chloroform/ethyl acetate gradient, starting from 100% toluene and gradually ending with 100 % ethyl acetate.

2. 3. 3. Synthesis of porphyrins with methylphenyl substituents

Purified 4-pyridinecarboxaldehyde (6.8 mmol, 0.78 mL) and 4-methylbenzaldehyde (20.4 mmol, 1.89 mL) were added to a solution of 272 mL of preheated propionic acid. Pyrrole (27.2 mmol, 1.85 mL) was injected after 10 minutes into reaction mixture. The reaction was refluxed at 140 °C and stirred in the dark for 90 min. The product mixture was cooled and propionic acid removed. This crude product was dissolved in a mixture of 15 mL of chloroform and 10 mL of toluene, and then methanol was added to make 500 mL. The product was crystallized overnight in refrigerator. After crystallization and filtration 1.013 g of porphyrins remained (yield 21 %). The statistical mixture of porphyrins was analyzed on TLC with toluene/CH_2Cl_2/EtOAc/EtOH (1:3:3:1) eluent. Flash silica-gel column chromatography used to separate and purify the porphyrin fractions is described in 2. 3. 5.

2. 3. 4. Synthesis of porphyrins with dodecyloxyphenyl substituents

A statistical mixture of 4-pyridylcarboxaldehyde (0.33 mL, 3.4 mmol), 4-dodecyloxybenzaldehyde (1 g, 3.4 mmol) and pyrrole (0.48 mL, 6.9 mmol) was refluxed for 90 min in 138 mL of propionic acid (0.05 M) in the dark. A black-purple liquid remained after the propionic acid has been removed. Separation of the six statistical

products was achieved by flash silica-gel column chromatography with a toluene/ethylacetate gradient as eluent.

2. 3. 5. Purification of porphyrin building blocks

Table 2. 1. Summary of the solvents used for the purification of porphyrins by flash silica gel column chromatography

PORPHYRIN FRACTION	ELUENT USED
TtBuPP	hexane/toluene (1:1)
5-PytBuPP	toluene/2.5% ethylacetate
5,15-PytBuPP	toluene/5% ethylacetate
5,10-PytBuPP	toluene/10% ethylacetate
5,10,15-PytBuPP	toluene/ethylacetate (3:2).
TMePP	toluene 100 %
5-PyMePP	toluene/ethylacetate (1:1)
5,15-PyMePP	CH_2Cl_2/ethylacetate
5,10-PyMePP	ethylacetate 100 %
5,10,15-PyMePP	ethylacetate/ethanol
TDdcylPP	toluene 100 %
5-PyDdcylPP	toluene/acetonitrile (2:1)
5,15-PyDdcylPP	toluene/ethylacetate (5:1)
5,10-PyDdcylPP	toluene/ethylacetate (1:2)
5,10,15-PyDdcylPP	toluene/ethylacetate (1:5) or toluene/acetonitrile (1:1)

2. 3. 6. Characterization of porphyrin building blocks

NMR: All NMR measurements were done on a QE 300 MHz in $CDCl_3$. (^{1}H-NMR and ^{13}C spectra for the *tert*-butylphenyl and methylphenyl porphyrins are reported in the doctoral thesis " Supramolecular Architecture: Formation and Characterization of Multi-Porphyrin Arrays" by Fotis Nifiatis).

ESI-MS: An Agilent Technologies HP 1100 LC/MSD mass spectrometer was used. In our studies sample was usually dissolved in a mixture of toluene/acetonitrile 1:1 and 1% of trifluoroacetic acid. Five microliters of this mixture is injected. Typically solvent acetonitrile/water 1:1 + 0.1% HOAC is used, positive ion mode, and the fragmentor voltage of 100-350 mV.

UV-VIS: Varian Cary Bio-3 UV-visible spectrophotometer. Typically, we used a double beam method with a wavelength range of 350-700 nm with < 10 μM solutions in a 1 cm cuvettes.

Table 2. 2. Tetrakis-(4-*tert*-butylphenyl)porphyrin

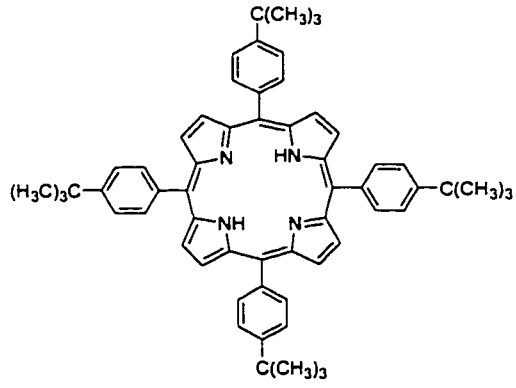

^{1}H-NMR: (300 MHz, $CDCl_3$) δ 8.88 (8H, s, β-pyrrole), 8.15 (8H, d, 3,5-phenyl, J = 8.1 Hz), 7.76 (8H, d, 2,6-phenyl, J = 8.1 Hz), 1.62 (36H, s, *tert*-butyl), -2.70 (2H, s, internal pyrrole).

ESI-MS: Calculated for $C_{60}H_{62}N_4$ *m/z* (theoretical intensities): 839 (100), 840 (67), 841 (22), 842 (5), 843 (0.8). *m/z* ($M+H^+$, relative intensities) found: 840 (100), 841 (63), 842 (23), 843 (8).

UV-Vis: λ, nm in toluene ($\varepsilon \times 10^4$ $cm^{-1}M^{-1}$) 420.5 (50), 515.5 (2.0), 550.5 (1.1), 592.5 (0.56), 649 (0.52).

Table 2. 3. 5-(4-pyridyl)-10,15,20-tris-(4-*tert*-butylphenyl)porphyrin

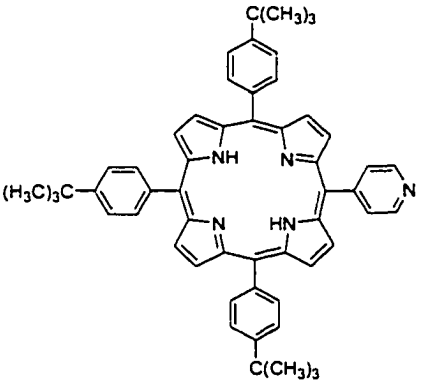

^{1}H-NMR: (300 MHz, $CDCl_3$) δ 9.04 (2H, d, 2,6-pyridyl, J = 5.5 Hz), 8.94 (2H, d, β-pyrrole, J = 4.8 Hz), 8.90 (4H, s, β-pyrrole), 8.78 (2H, d, β-pyrrole, J = 4.8 Hz), 8.20 (2H, d, 3,5-pyridyl, J = 5.5 Hz), 8.15 (6H, d, 3,5-phenyl, J = 8.1 Hz), 7.77 (6H, d, 2,6-phenyl, J = 8.1 Hz), 1.60 (27H, s, tert-butyl), -2.83 (2H, s, internal pyrrole).

ESI-MS: Calculated for $C_{55}H_{53}N_5$ *m/z* (theoretical intensities) 783 (100), 784 (62), 785 (19), 786 (4), 787 (0.5). *m/z* ($M+H^+$) (relative intensities) found: 784 (100), 785 (62), 786 (18), 787 (3).

UV-Vis: λ, nm in toluene (ε × 10^4 $cm^{-1}M^{-1}$) 420.5 (42), 515.5 (1.8), 550 (0.90), 591.5 (0.56), 649 (0.43).

Table 2. 4. 5,15-bis-(4-pyridyl)-10,20-bis-(4-*tert*-butylphenyl)porphyrin

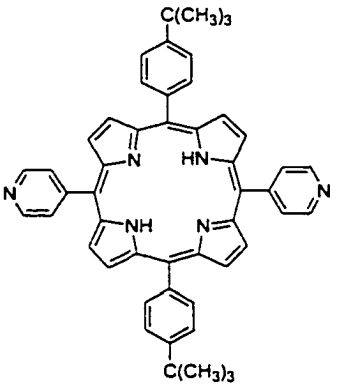

^{1}H-NMR: (300 MHz, $CDCl_3$) δ 9.04 (4H, d, 2,6-pyridyl, J = 5.9 Hz), 8.95 (4H, d, β-pyrrole, J = 4.4 Hz), 8.79 (4H, d, β-pyrrole, J = 4.8 Hz), 8.17 (4H, d, 3,5-pyridyl, J = 5.9 Hz), 8.13 (4H, d, 3,5-phenyl, J = 8.4 Hz), 7.78 (4H, d, 2,6-phenyl, J = 8.4 Hz), 1.70 (18H, s, tert-butyl), -2.86 (2H, s, internal pyrrole).

ESI-MS: Calculated for $C_{50}H_{44}N_6$ *m/z* (theoretical intensities) 728 (100), 729 (57), 730 (15), 731 (3), 732 (0.4). *m/z* ($M+H^+$, relative intensities) found: 729 (100), 730 (60), 731 (18).

UV-Vis: λ, nm in toluene ($\varepsilon \times 10^4$ $cm^{-1}M^{-1}$) 419.5 (26), 515 (1.2), 548 (0.5), 589 (0.36), 648 (0.23).

Table 2. 5. 5,10-bis-(4-pyridyl)-10,20-bis-(4-*tert*-butylphenyl)porphyrin

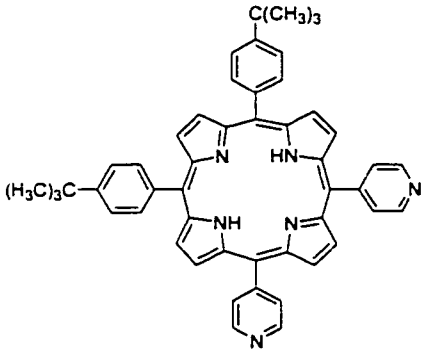

^{1}H-NMR: (300 MHz, $CDCl_3$) δ 9.05 (4H, d, 2,6-pyridyl, J = 5.9 Hz), 8.96 (2H, d, β-pyrrole, J = 4.8 Hz), 8.92 (2H, s, β-pyrrole), 8.84 (2H, s, β-pyrrole), 8.79 (2H, d, β-pyrrole, J = 5.5 Hz), 8.18 (4H, d, 3,5-pyridyl, J = 5.9 Hz), 8.15 (4H, d, 3,5-phenyl, J = 8.1 Hz), 7.79 (4H, d, 2,6-phenyl, J = 8.06 Hz), 1.63 (18H, s, *tert*-butyl), -2.83 (2H, s, internal pyrrole).

ESI-MS: Calculated for $C_{50}H_{44}N_6$ *m/z* (theoretical intensities) 728 (100), 729 (57), 730 (15), 731 (3), 732 (0.4). *m/z* ($M+H^+$, relative intensities) found: 729 (100), 730 (60), 731 (18).

UV-Vis: λ, nm in toluene (ε × 10^4 $cm^{-1}M^{-1}$) 419.5 (37), 514.5 (1.7), 548 (0.72), 592 (0.51), 645.5 (0.31).

Table 2. 6. 5,10,15-tris-(4-pyridyl)-20-(4-*tert*-butylphenyl)porphyrin

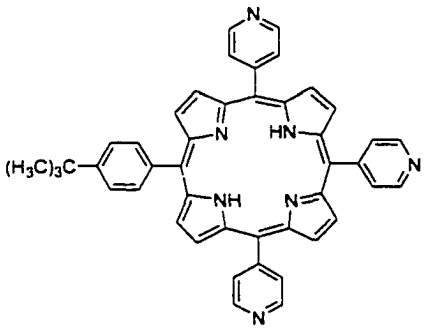

^{1}H-NMR: (300 MHz, $CDCl_3$) δ 9.07 (6H, d, 2,6-pyridyl, J = 5.9 Hz), 8.95 (2H, d, β-pyrrole, J = 4.8 Hz), 8.86 (4H, s, β-pyrrole), 8.81 (2H, d, β-pyrrole, J = 5.1 Hz), 8.18 (6H, d, 3,5-pyridyl, J = 5.5 Hz), 8.14 (2H, d, 3,5-phenyl, J = 8.1 Hz), 7.80 (2H, d, 2,6-phenyl, J = 8.1 Hz), 1.75 (9H, s, *tert*-butyl), -2.83 (2H, s, internal pyrrole).

ESI-MS: Calculated for $C_{45}H_{35}N_7$ *m/z* (theoretical intensities) 673 (100), 674 (52), 675 (13), 676 (2), 677 (0.2). *m/z* ($M+H^+$, relative intensities) found: 674 (100), 675 (53), 676 (10).

UV-Vis: λ, nm in toluene ($\varepsilon \times 10^4$ $cm^{-1}M^{-1}$) 419 (31), 513 (1.6), 547 (0.6), 590 (0.46), 645.5 (0.24).

Table 2. 7. Tetrakis-(4-methylphenyl)porphyrin

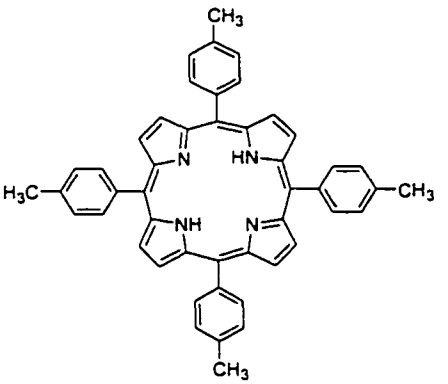

^{1}H-NMR: (300 MHz, $CDCl_3$) δ 8.85 (8H, s, β-pyrrole), 8.09 (8H, d, 3,5- phenyl, J = 8.06 Hz), 7.55 (8H, d, 2,6-phenyl, J = 7.8 Hz), 2.71 (12H, s, methyl), -2.75 (2H, s, internal pyrrole).

ESI-MS: Calculated for $C_{48}H_{38}N_4$ *m/z* (theoretical intensities) 670 (100), 671 (54), 672 (14), 673 (2.5), 674 (0.2) *m/z* ($M+H^+$) (relative intensities) found: 671 (100), 672 (58), 673 (10).

UV-Vis: λ, nm in $CHCl_3$ ($\varepsilon \times 10^4$ $cm^{-1}M^{-1}$) 420 (39), 513 (1.7), 549.5 (0.9), 595 (0.5), 650.5 (0.4).

Table 2. 8. 5,10-bis-(4-pyridyl)-15,20-bis-(4-methylphenyl)porphyrin

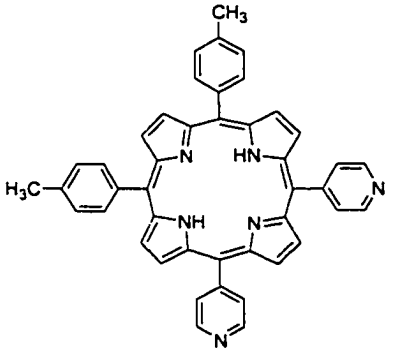

^{1}H-NMR: (300 MHz, $CDCl_3$) δ 9.03 (4H, d, 2,6-pyridyl, J = 5.5 Hz), 8.93 (2H, d, β-pyrrole, J = 4.76 Hz), 8.89 (2H, s, β-pyrrole), 8.83 (2H, s, β-pyrrole), 8.79 (2H, d, β-pyrrole, J = 4.76 Hz), 8.16 (4H, d, 3,5-pyridyl, J = 5.86 Hz), 8.09 (4H, d, 3,5-phenyl, J = 7.7Hz), 7.57 (4H, d, 2,6-phenyl, J = 7.7 Hz), 2.77 (6H, s, methyl), -2.83 (2H, s, internal pyrrole).

ESI-MS: Calculated for $C_{44}H_{32}N_6$ *m/z* (theoretical intensities) 644 (100), 645 (50), 646 (12), 647 (2), 648 (0.2). *m/z* ($M+H^+$, relative intensities) found: 645 (100), 646 (51), 647 (14).

UV-Vis: λ, nm in toluene (ε × 10^4 $cm^{-1}M^{-1}$) 419.5 (34), 513.5 (1.6), 549 (0.64), 591.5 (0.46), 646.5 (0.28).

Table 2. 9. 5,10,15-tris-(4-pyridyl)-20-(4-methylphenyl)porphyrin

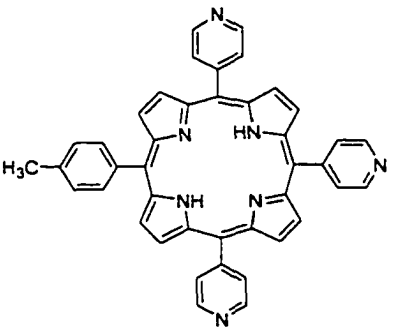

^{1}H-NMR: (300 MHz, $CDCl_3$) δ 9.06 (6H, d, 2,6-pyridyl, J = 5.9 Hz), 8.96 (2H, d, β-pyrrole, J = 4.8 Hz), 8.86 (4H, s, β-pyrrole), 8.82 (2H, d, β-pyrrole, J = 4.8 Hz), 8.18 (6H, d, 3,5-pyridyl, J = 5.9 Hz), 8.10 (2H, d, 3,5-phenyl, J = 7.7 Hz), 7.60 (2H, d, 2,6-phenyl, J = 7.7 Hz), 2.73 (3H, s, methyl), -2.87 (2H, s, internal pyrrole).

ESI-MS: Calculated for $C_{42}H_{29}N_7$ *m/z* (theoretical intensities) 631 (100), 632 (48), 633 (11), 634 (2), 635 (0.2). *m/z* ($M+H^+$, relative intensities) found: 632 (100), 633 (46), 634 (11).

UV-Vis: λ, nm in toluene (ε × 10^4 $cm^{-1}M^{-1}$) 419 (36), 513.5 (1.8), 547.5 (0.62), 590 (0.52), 645 (0.26).

Table 2. 10. Tetrakis-(4-dodecyloxyphenyl)porphyrin

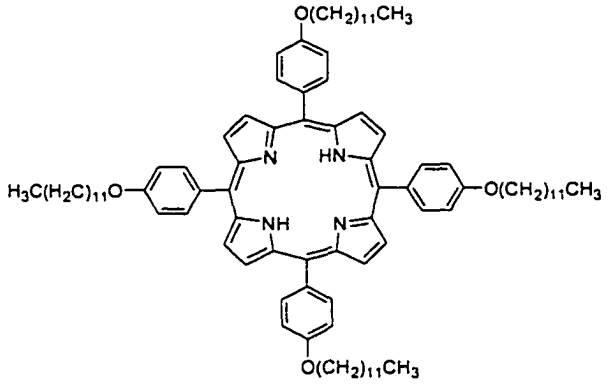

^{1}H-NMR: (300 MHz, $CDCl_3$) δ 8.86 (8H, s, β-pyrrole), 8.10 (8H, d, 3,5-phenyl, J = 8.4 Hz), 7.27 (8H, d, 2,6-phenyl, J = 8.4 Hz), 4.25 (8H, t, OCH_2, J = 6.5 Hz), 2.02 - 1.96 (80H, b, CH_2) 1.66 - 1.24 and 0.93 - 0.85 (12H, m, CH_3), -2.8 (2H, s, internal pyrrole).

ESI-MS: Calculated for $C_{92}H_{126}N_4O_4$ *m/z* (theoretical intensities): 1351 (97), 1352 (100), 1353 (52), 1354 (18), 1355 (5), 1356 (1). *m/z* ($M+H^+$) (relative intensities) found: 1352 (97), 1353 (100), 1354 (57), 1355 (16), 1356 (4).

UV-Vis: λ, nm in toluene (ε × 10^4 $cm^{-1}M^{-1}$) 423 (22), 518.5 (0.8), 554.5 (0.6), 594.5 (0.24), 653 (0.26).

Table 2. 11. 5-(4-pyridyl)-10,15,20-tris-(4-dodecyloxyphenyl)porphyrin

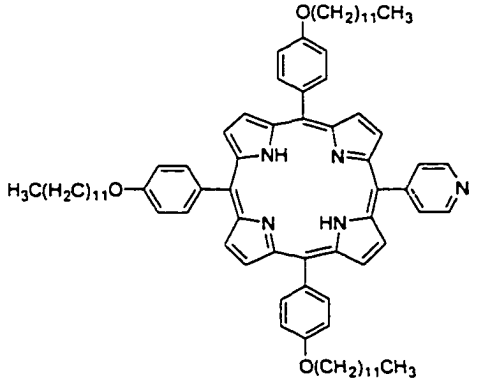

^{1}H-NMR: (300 MHz, $CDCl_3$) δ 9.03 (2H, d, 2,6-pyridyl, J = 6.2 Hz), 8.92 (2H, d, β-pyrrole, J = 5.1 Hz), 8.88 (4H, s, β-pyrrole), 8.76 (2H, d, β-pyrrole, J = 4.8 Hz), 8.18 (2H, d, 3,5-pyridyl, J = 5.9 Hz), 8.10 (2H, d, 3,5-phenyl, J = 8.8 Hz), 8.04 (4H, d, 3,5-phenyl, J = 8.8 Hz), 7.28 (2H, d, J = 8.8Hz, 2,6-phenyl), 6.93 (4H, d, J = 8.8 Hz, 2,6-phenyl), 4.26 (4H, t, OCH_2, J = 6.5 Hz), 4.02 (2H, t, OCH_2, J = 6.6 Hz), 2.07 - 1.41 (60H, b, CH_2), 1.40 - 1.02 and 1.00 - 0.78 (9H, m, CH_3), -2.78 (2H, s, internal pyrrole).

ESI-MS: Calculated for $C_{79}H_{101}N_5O_3$ *m/z* (theoretical intensities) 1168 (100), 1169 (89), 1170 (40), 1171 (12), 1172 (3) *m/z* ($M+H^+$, relative intensities) found: 1169 (100), 1170 (84), 1173 (3).

UV-Vis: λ, nm in toluene ($\varepsilon \times 10^4$ $cm^{-1}M^{-1}$) 423 (50), 518 (2.0), 554 (1.2), 594 (0.6), 650 (0.56).

Table 2. 12. 5,15-bis-(4-pyridyl)-10,20-bis-(4-dodecyloxyphenyl)porphyrin

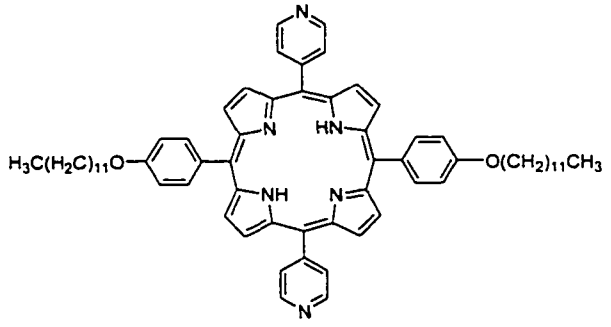

^{1}H-NMR: (300 MHz, $CDCl_3$) δ 9.04 (4H, d, 2,6-pyridyl, J = 5.5 Hz), 8.94 (4H, d, β-pyrrole, J = 4.8 Hz), 8.79 (4H, d, β-pyrrole, J = 4.8 Hz), 8.17 (4H, d, 3,5-pyridyl, J = 5.5 Hz), 8.10 (4H, d, 3,5-pyridyl, J = 8.4 Hz), 7.30 (4H, d, 2,6-pyridyl, J = 8.4 Hz), 4.26 (4H, t, OCH_2, J = 6.4 Hz), 2.07 - 1.97 (40H, b, CH_2), 1.69 - 1.27 and 0.92 - 0.88 (6H, m, CH_3), - 2.82 (2H, s, internal pyrrole).

ESI-MS: Calculated for $C_{66}H_{76}N_6O_2$ *m/z* (theoretical intensities) 985 (100), 986 (28), 988 (7), 989 (1). *m/z* ($M+H^+$, relative intensities) found: 986 (100), 987 (80), 988 (18), 989 (7).

UV-Vis: λ, nm in toluene (ε × 10^4 $cm^{-1}M^{-1}$) 421.5 (41), 516 (1.8), 551.5 (0.91), 593 (0.54), 649 (0.40).

Table 2. 13. 5,10-bis-(4-pyridyl)-15,20-bis-(4-dodecyloxyphenyl)porphyrin

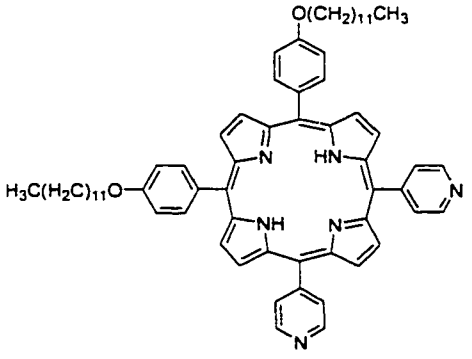

^{1}H-NMR: (300 MHz, $CDCl_3$) δ 9.04 (4H, d, 2,6-pyridyl, J = 5.9 Hz), 8.94 (2H, d, β-pyrrole, J = 4.8 Hz), 8.91 (2H, s, β-pyrrole), 8.82 (2H, s, β-pyrrole), 8.78 (2H, d, β-pyrrole , J = 4.8 Hz), 8.16 (4H, d, 3,5-pyridyl, J = 5.9 Hz), 8.10 (4H, d, 3,5-phenyl, J = 8.42 Hz), 7.29 (4H, d, 2,6-phenyl, J = 8.42 Hz), 4.27 (4H, t, OCH_2, J = 6.6 Hz), 2.02 - 1.96 (40H, b, CH_2), 1.66 - 1.31, 0.93 - 0.87 (6H, m, CH_3), -2.81 (2H, s, internal pyrrole).

ESI-MS: Calculated for $C_{66}H_{76}N_6O_2$ *m/z* (theoretical intensities) 985 (100), 986 (28), 988 (7), 989 (1). *m/z* ($M+H^+$, relative intensities) found: 986 (100), 987 (80), 988 (18), 989 (7).

UV-Vis: λ, nm in toluene (ε × 10^4 $cm^{-1}M^{-1}$) 421.5 (45), 516.5 (2.0), 551.5 (1.0), 593 (0.62), 649.5 (0.43).

Table 2. 14. 5,10,15-tris-(4-pyridyl)-20-(4-dodecyloxyphenyl)porphyrin

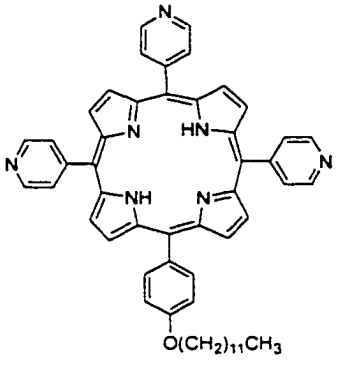

^{1}H-NMR: (300 MHz, $CDCl_3$) δ 9.05 (6H, d, 2,6-pyridyl, J = 6.3 Hz), 8.97 (2H, d, J = β-pyrrole, J= 4.8 Hz), 8.85 (4H, s, β-pyrrole), 8.81 (2H, d, β-pyrrole, J = 4.8 Hz), 8.16 (6H, d, 3,5-pyridyl, J = 5.9 Hz), 8.10 (2H, d, 3,5-phenyl, J = 8.4 Hz), 7.30 (2H, d, 2,6-phenyl, J = 8.4 Hz), 4.26 (2H, t, OCH_2, J = 6.4 Hz), 2.1 – 1.9, 1.8 – 1.2 (20H, m, CH_2) 1.0 – 0.8 (3H, m, CH_3), -2.86 (2H, internal pyrrole).

ESI-MS: Calculated for $C_{53}H_{51}N_7O$ *m/z* (theoretical intensities) 801 (100), 802 (61), 803 (18), 804 (4), 805 (0.5) *m/z* ($M+H^+$, relative intensities) found: 802 (100), 803 (78), 804 (22), 805 (6).

UV-Vis: λ, nm in toluene (ε × 10^4 $cm^{-1}M^{-1}$) 420 (33), 514 (1.7), 549 (0.7), 592 (0.5), 646 (0.3).

Table 2. 15. Tetrakis-(4-pyridyl)porphyrin

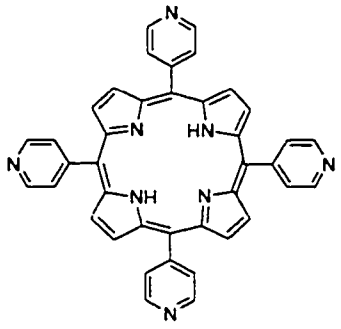

^{1}H-NMR: (300 MHZ, $CDCl_3$) δ 9.07 (8H, d, 2,6-pyridyl, J = 5.9 Hz), 8.87 (8H, s, β-pyrrole), 8.16 (8H, d, 3,5-pyridyl, J = 5.9 Hz), -2.95 (2H, s, internal pyrrole).

ESI-MS: Calculated for $C_{40}H_{26}N_8$ *m/z* (theoretical intensities) 618 (100), 619 (47), 620 (10), 621(2), 622 (0.2). *m/z* ($M+H^+$, relative intensities) found: 619 (100), 620 (46), 621 (12).

UV-Vis: λ, nm in $CHCl_3$ ($\varepsilon \times 10^4$ $cm^{-1}M^{-1}$) 418 (25), 516 (1.8), 550 (0.77), 590 (0.54), 646 (0.46).

2. 4. Appendix

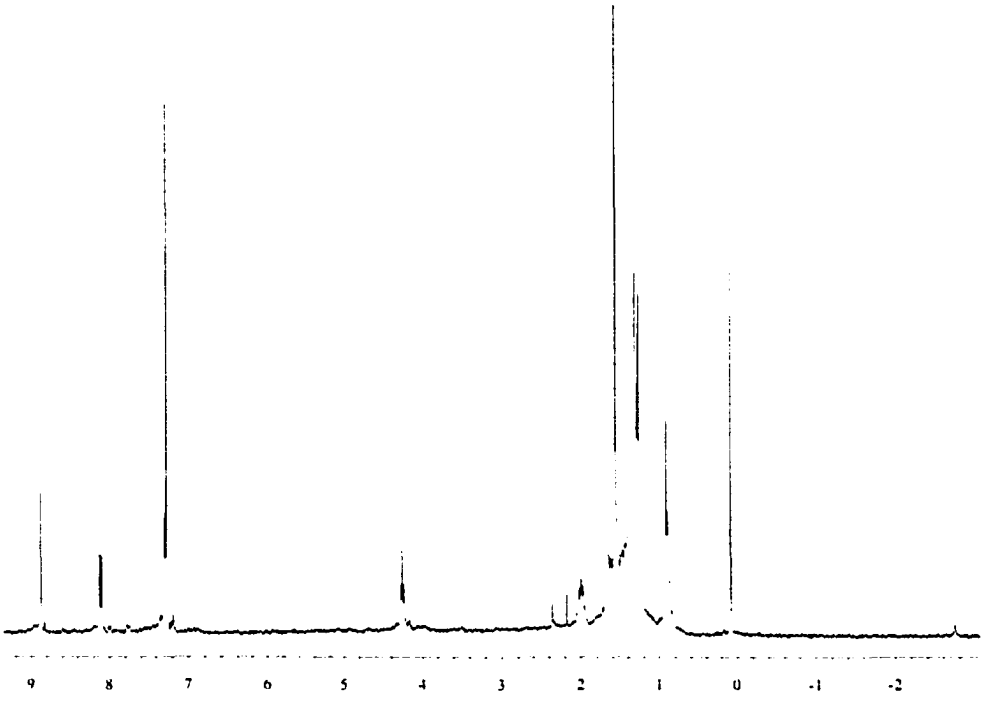

Figure 2. 3. ^{1}H-NMR spectrum of tetrakis-(4-dodecyloxyphenyl)porphyrin

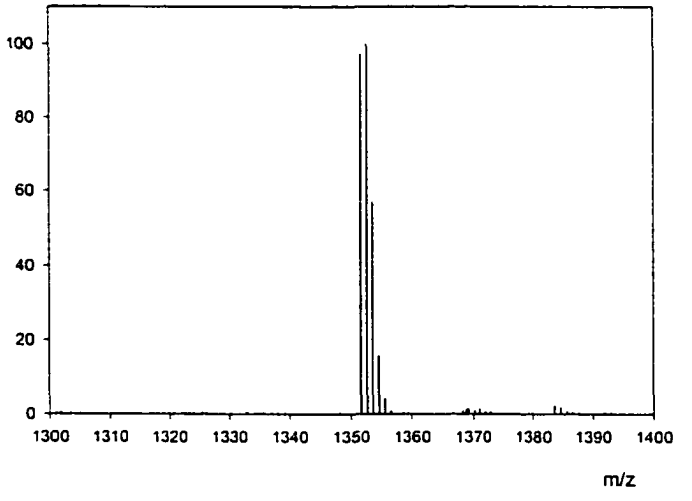

Figure 2. 4. ESI-MS spectrum of tetrakis-(4-dodecyloxyphenyl)porphyrin

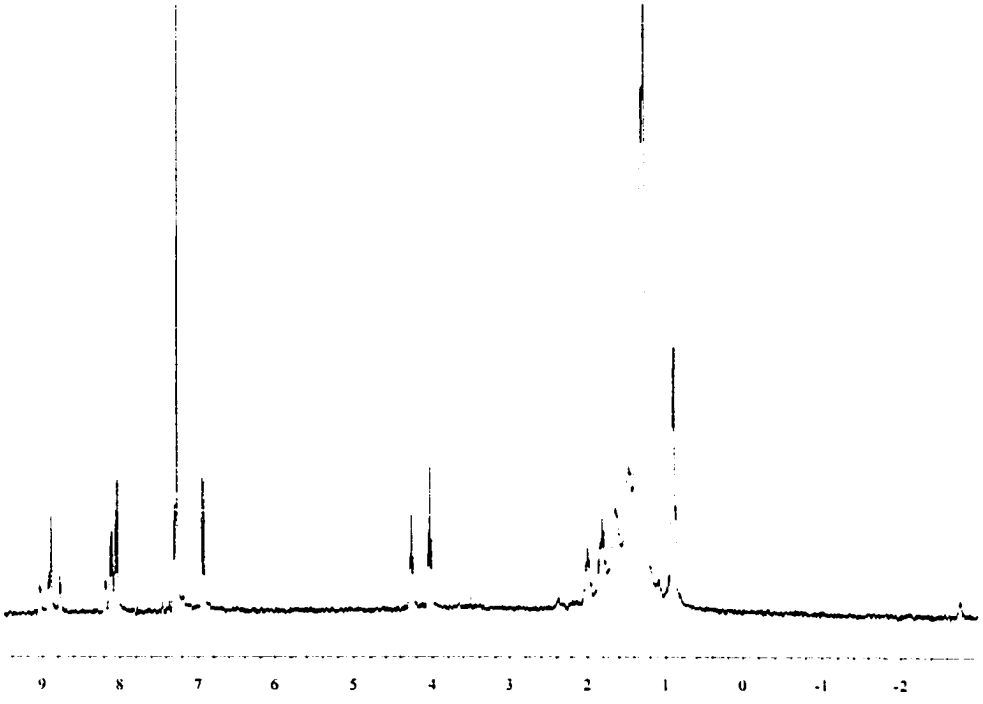

Figure 2. 5. ^{1}H-NMR spectrum of 5-(4-pyridyl)-10,15,20-tris-(4-dodecyloxyphenyl) porphyrin

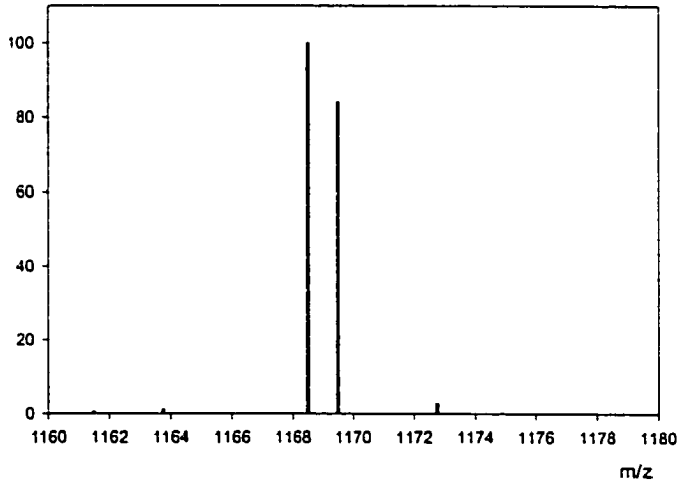

Figure 2. 6. ESI-MS spectrum of 5-(4-pyridyl)-10,15,20-tris-(4-dodecyloxyphenyl) porphyrin

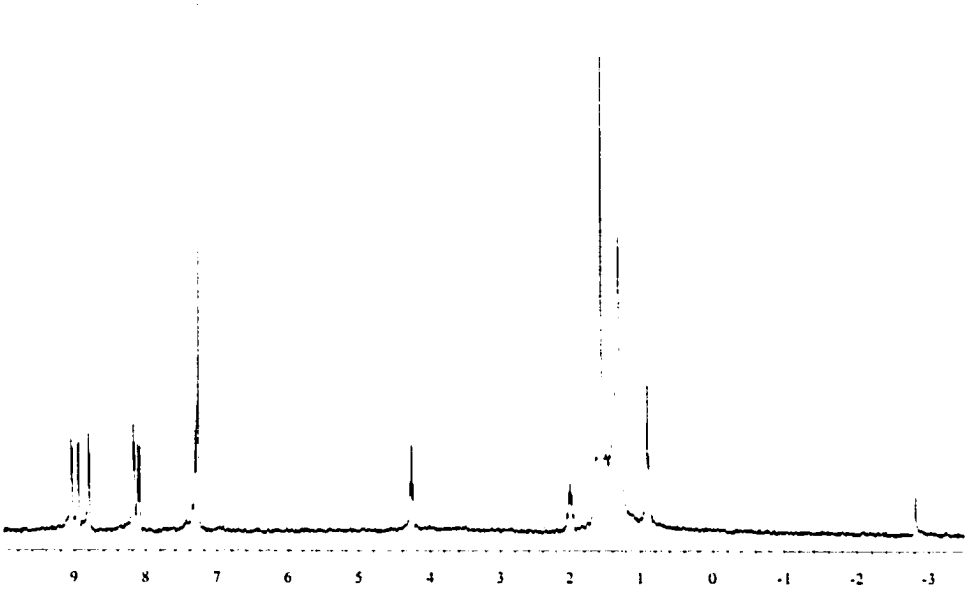

Figure 2. 7. ^{1}H-NMR spectrum of 5,15-bis-(4-pyridyl)-15,20-bis-(4-dodecyloxyphenyl) porphyrin

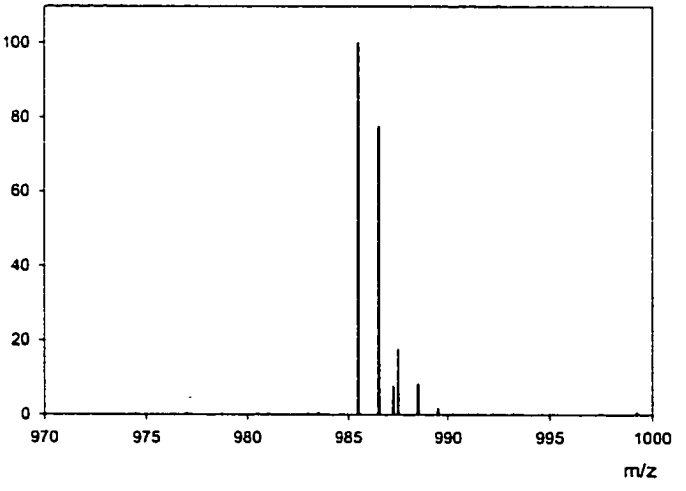

Figure 2. 8. ESI-MS spectrum of 5,15-bis-(4-pyridyl)-15,20-bis-(4-dodecyloxyphenyl) porphyrin

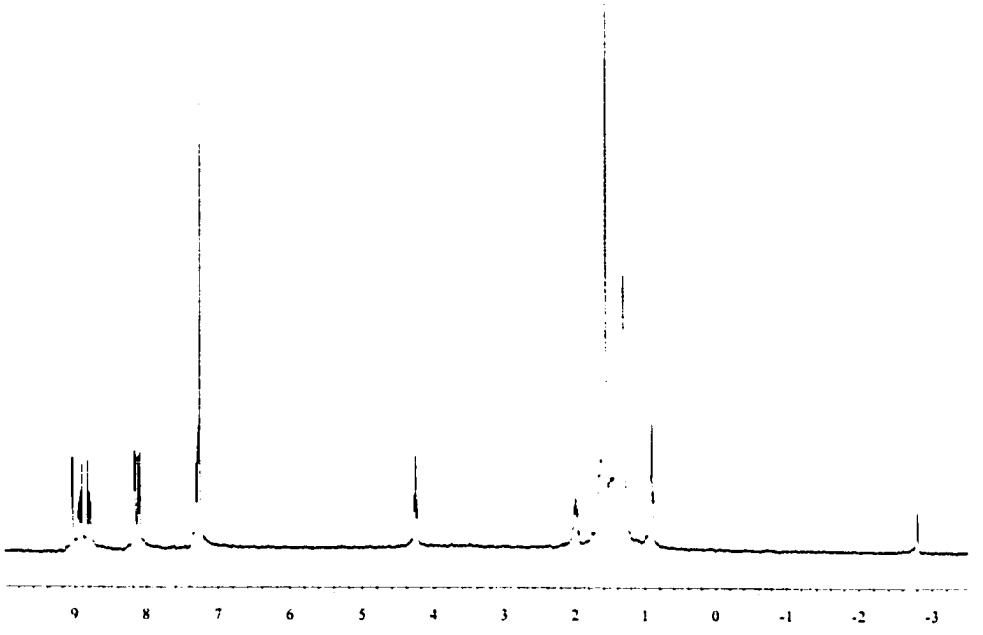

Figure 2. 9. ^{1}H-NMR spectrum of 5,10-bis-(4-pyridyl)-15,20-bis-(4-dodecyloxyphenyl) porphyrin

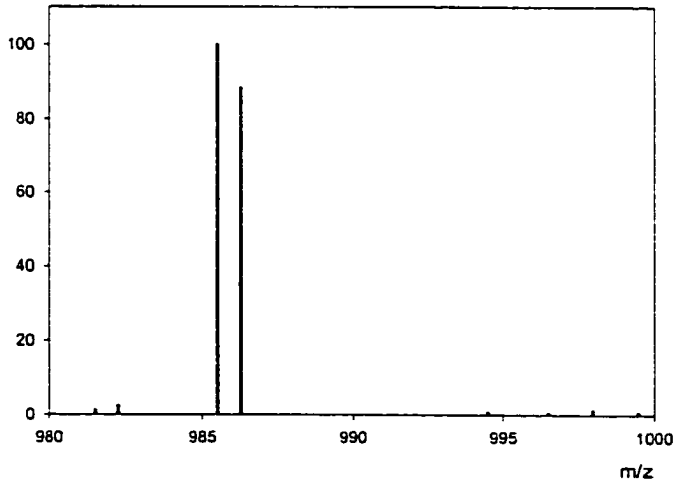

Figure 2. 10. ESI-MS spectrum of 5,10-bis-(4-pyridyl)-15,20-bis-(4-dodecyloxyphenyl) porphyrin

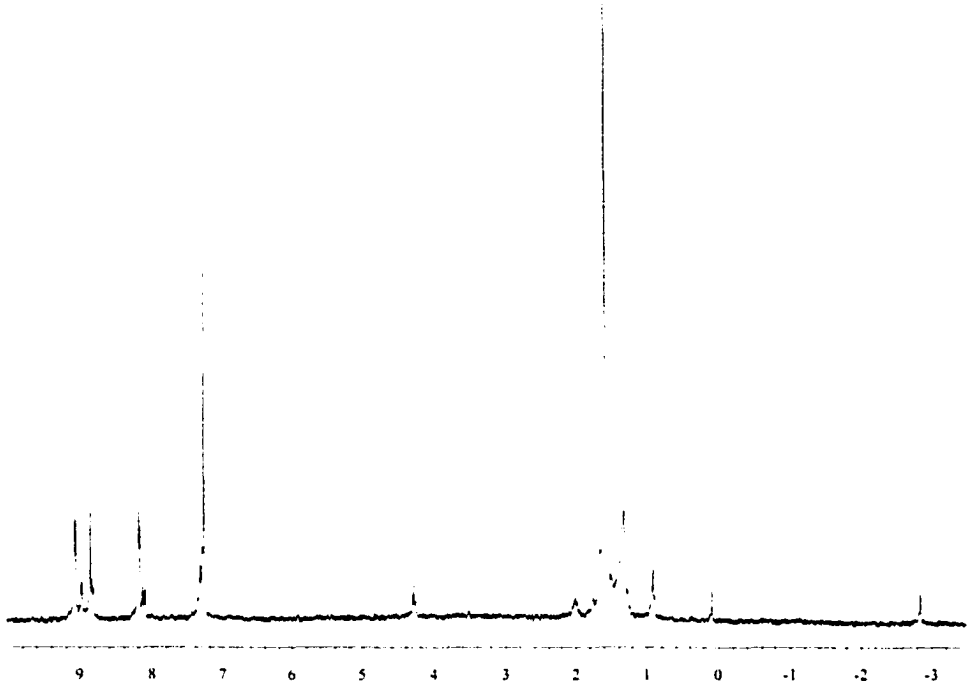

Figure 2. 11. ^{1}H-NMR spectrum of 5,10,15-tris-(4-pyridyl)-20-(4-dodecyloxyphenyl) porphyrin

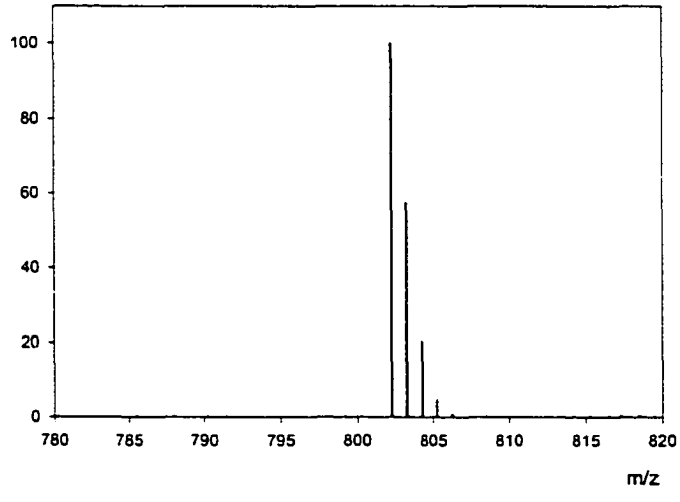

Figure 2. 12. ESI-MS spectrum of 5,10,15-tris-(4-pyridyl)-20-(4-dodecyloxyphenyl) porphyrin

3.

MULTI-PORPHYRIN ARRAYS: SELF-ASSEMBLY AND CHARACTERIZATION

3. 1. Introduction

Self-assembled multi-porphyrin structures have found an important place in all aspects of materials chemistry. A study of self-assembled multi-porphyrin arrays and tapes is an important part of microelectronics, due to the potential application as molecular wires,[1,2] molecular switches,[3] and components for information storage.[4] Construction of synthetic light-harvesting antennas is another important prospect for the utilization of self-assembled multi-porphyrin systems. They also could be promising components of new magnetic and conductive polymeric materials and of sensor systems.[5,6,7,8,9,10]

---

[1] J. Seth, V. Palaniappan, R. W. Wagner, T. E. Johnson, J. S. Lindsey, D. F. Bocian, *J. Am. Chem. Soc.* **1994**, *116*, 10578.
[2] R. W. Wagner, J. S. Lindsey, *J. Am. Chem. Soc.* **1994**,*11 6*, 9759.
[3] V. Marvaud, J. P. Launay, *Inorg. Chem.* **1993**,*32* , 1376.
[4] J. J. Hopfield, J. N. Onuchic, D. N. Beratan, *J. Phys. Chem.* **1989**, *93*, 6350.
[5] E. J. Brandon, R. D. Rogers, B. M. Burkhart, J. S. Miller, *Chem. Eur. J.***19 98**,*4* , 1938.
[6] D. Gust, T. A. Moore, *Top. Curr. Chem.* **1991**,*15 9*, 103.
[7] S. Prathapan, T. E. Johnson, J. S. Lindsey, *J. Am. Chem. Soc.***19 93**, *115*, 7519.
[8] H. J. Anderson, S. J. Martin, D. D. C. Bradley, *Angew. Chem. Int. Ed.* **1994**,*33* , 655.
[9] J. Sojaczynski, L. Latos-Grazynski, *Coor. Chem. Rev.* **2000**,*20 4*, 113-171.
[10] Lionel R. Milgrom, *Colours of Life*, Oxford University Press **1997**.

3. 1. 1. Self-assembly of porphyrins: Strategies

Intermolecular noncovalent interactions are common binding modes for all supramolecular architectures. These interactions can be specific and directional, such as hydrogen bonding or metal-ion coordination, or non-specific such as van der Waals and π-π aromatic interactions. Because the nature of noncovalent interactions is not fully understood, particularly in the case of non-specific interactions, hydrogen bonding and metal-ion coordination are frequently chosen as building modes in order to obtain more control over supramolecular structure.

Hydrogen-bond interactions have been explored extensively and utilized for linking porphyrins into a large, symmetrical supramolecular structure.[11] They are selective and stronger then the van der Waals interactions, but there is only a limited range of non-competing solvents that can be used in order to keep assembled structures stable in most cases.

In this regard, metal-ion coordination has synthetic advantages in terms of stability and directionality. Multi-porphyrin structures formed by coordination to metal ions are usually rigid and do not allow for flexible changes in the conformation, which make them suitable for construction of stable supramolecular architectures on surfaces. Furthermore, desired functionality in terms of various photophysical and electronic properties can be tuned by the choice of metal ion linker or metalloporphyrin.

---

[11] a) C. M. Drain, X. Shi, T. Milic, F. Nifiatis, *Chem. Commun.* **2001**, 287-288.
b) X. Shi, K. M. Barkigia, J. Fajer, C. M. Drain, *J. Org. Chem.* **2001**,*66* (20), 6513-6522.

3. 1. 2. Self-assembled multi-porphyrin systems: Characterization

New materials based on the self-assembly of molecular components have brought a number of challenges in terms of their structural and physical characterization.[12] The structural identification of supramolecular structures is often difficult because of their large size and noncovalent binding mode. Large molecules are often poorly soluble while labile noncovalent bonds cannot withstand certain characterization conditions such as in the ionization processes in mass spectroscopy. A detailed understanding of the structure is difficult to accomplish with a single technique, such as X-ray diffraction, due to difficulties in obtaining high quality crystals. For these reasons, a number of spectroscopic and microscopic techniques must be combined for complete characterization of these materials. Among the different solution techniques, the most commonly used are: UV-Visible spectroscopy, fluorescence spectroscopy, light scattering, nuclear magnetic resonance and mass spectroscopy. However a more precise structural characterization of supramolecules is needed, especially in order to understand how the structure modulates electronic and optical properties of a molecule.[12] Further development of analytical methods for characterization of self-assembled species will continue and there are the advances in Fourier transform IR and solid state NMR.[12]

Solution phase methods

UV-Visible spectroscopy is an especially valuable tool for the characterization of supramolecules that contain chromophoric groups. Multi-porphyrin assemblies are just one example where UV-Vis characterization plays an important role in monitoring the

[12] A. P. Alivisatos, P. F. Barbara, A. W. Castleman, J. Chang, D. A. Dixon, M. L. Klein, G. L. McLendon, J. S. Miller, M. A. Ratner, P. J. Rossky, S. I. Stupp, M. E. Thompson, *Adv. Mater.* **1998**,*10* (16), 1297-1336.

self-assembly process. Because of the linear relationship between absorbance and concentration, most of the time, reaction progress may be easily followed by UV-Vis spectroscopy. If the concentration of a ligand such as a metal-ion complex is changed stepwise while the concentration of porphyrin is held constant, it is common to observe an isosbestic point (the point where ε for both the free and complexed species are the same).[13] Typically, the presence of isosbestic points is an indication of only two reacting species in equilibrium under given conditions. In rare cases it also might be possible that more then two species are having same ε, and that more then one equilibrium is present. Sometimes, deviations from the Lambert-Beer's law are observed, that result from secondary aggregation processes of self-assembled supramolecules.

Fluorescence emission and excitation studies of self-assembled porphyrin arrays are commonly used for both solution studies of porphyrin self-assembly and energy transfer reactions.[10] In the case of metal-ion coordination a significant decrease (quenching) of fluorescence is observed and serves as an indication of metal-porphyrin association. This is due to the "heavy atom effect", which may be defined as an enhancement of the rate of a spin-forbidden process due to the presence of an atom of high atomic number. Fluorescence properties of porphyrin assemblies on solid surfaces may also be measured by front-face illumination.

Dynamic light scattering (DLS) is a conventional method for measurements of the sizes of organic polymers. More recently this technique has also been applied for nanoparticle characterization and in protein studies. This method is based on the measurement of the frequency spectrum of the scattered light by suspended particles.

---

[13] H-J. Schneider, A. Yatsimirsky, *Principles and methods in supramolecular chemistry*, Wiley **2000.**

Light scattered from a moving particle exhibits frequency fluctuation (due to the Doppler frequency shift), and the relaxation time for these fluctuations is measured and depends only on the diffusion behavior of the particles.[14] By using the Stokes-Einstein equation,

$$D = (kT)/(6\pi\eta r)$$

one can obtain a hydrodynamic radius r, if the solvent viscosity η and temperature T are known. k is the Boltzmann constant.

The main difficulty in DLS characterization is the background signal arising from the medium (for very diluted samples) and the limited size range of measured nanoparticles (detection limit for most instrument is a hydrodynamic radius of 1.5 nm). Otherwise it is a helpful technique for the measurement of self-assembled nanoparticles and their dynamic behavior, such as aggregation.

Mass characterization of noncovalent molecular assemblies still remains a challenge, but there is a growing trend of application of mass spectrometry for the study of supramolecular reactions. Here, the use of soft, non-destructive ionization techniques are most important, since they can produce large molecular ions held together even with weak noncovalent interactions. The main problem in mass spectrometry characterization is how to ionize molecules without destroying the intermolecular bonds that hold the supramolecule together.[3] Field desorption and fast atom bombardment are promising techniques, however electron spray ionization methods (ESI) also have shown success in studies of host-guest complexations.[15] Besides problems with characterization of insufficiently stable complexes, there is also a problem with non-specific interactions,

---

[14] R. F. Pasternack, P. J. Collings, *Science* **1995**,*26 9*, 935-939.
[15] M. Przybylski, M. O. Glocker, *Angew. Chem. Int. Ed.* **1996**,*35* , 806-826.

which may occur in the gas phase and become detectable by MS, yielding incorrect products.[3]

NMR methods for the structural characterization of self-assembled systems also have a few limitations. Since self-assembly is concentration dependent and discrete species are favored in a dilute solution (usually ~ 10^{-6} M), obtaining good NMR spectra at low concentrations is somewhat more difficult. Though NMR is widely used for the determination of association constants and equilibrium studies,[10] the precise structural characterization of complex self-assembled molecules still remains a challenge.

Solid phase methods

Because of the limitations of solution phase characterization methods, in many cases the complexity of the self-assembled structure requires direct imaging techniques. The development of scanning tunneling microscopy (STM), atomic force microscopy (AFM) and most recently near-field scanning optical microscopy (NSOM) have contributed crucially to progress in supramolecular chemistry.

Atomic force microscopy is a high resolution imaging technique used for the investigation of sample surface structure. The AFM probe is a sharp tip (typically 10-100 nm radius of curvature) at the end of a cantilever, which is attached to a piezoelectric scanner. As the probe is brought within close proximity of the sample, interatomic forces between the sample and tip cause the deflection of the cantilever. A laser beam reflecting off the cantilever into a detector generates a feedback signal and this information processed by computer to generate a 3D surface image.[16] By controlling the tip-sample distance, images may be collected in repulsive force (contact AFM mode) or long-range

[16] A. Ikai, *Surface Science Reports* **1996**, *26*, 261-332.

attractive force (non-contact AFM mode). The main advantage of AFM is that practically any surface may be scanned. However, the limitation of AFM lies in the rather large size of the conventional AFM tips (more then 10 nm radius of curvature) limiting the resolution of the instrument.[16]

In scanning tunneling microscopy a metallic tip senses the local electronic density of states in terms of the intensity of the tunneling current when a certain bias voltage is applied between the tip and sample. The space between the tip and the sample could be vacuum, gas, or liquid. In its application to the study of metal or semiconductor surfaces, STM is most commonly operated in an ultra-high vacuum of 10^{-8} Pa or in liquids to avoid surface contamination, but many STM studies are carried in air and at ambient conditions.[16]

Near-field optical scanning microscopy is an optical technique integrated with scanning probe microscope instrumentation. The sample is excited with light passing through a sub-micron aperture at the end of an optical fiber. The probe is held at the certain distance from the sample, which is regulated with piezo technology just like in AFM. The data are collected simultaneously but independently and contain both optical and topographical information about the sample. The most common imaging mode is fluorescence, but it might be also UV-Vis, IR or Raman.[12]

Advances in scanning probe microscopies have significantly aided in the actual fabrication and testing of nanodevices.

3. 2. Results and discussion

The focus of our research is the formation of the multi-porphyrin arrays via metal ion coordination. The following multi-porphyrin structures have been synthesized (Scheme 3. 1. **1-8**). For each self-assembled structure, UV-Vis spectral changes have been monitored to ensure the correct self-assembly. The arrays **1-8** were characterized by combination of solution spectroscopic methods and scanned probe microscopies.

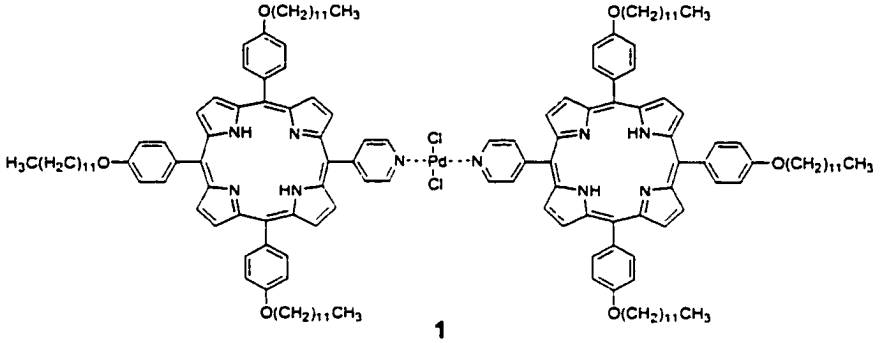

1

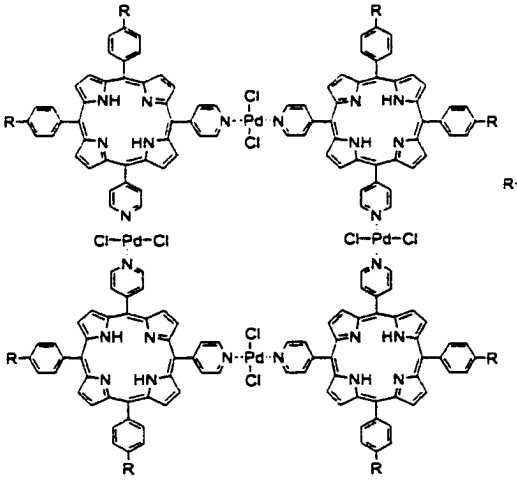

2 - R = *tert*-Bu
3 - R = $O(CH_2)_{11}CH_3$

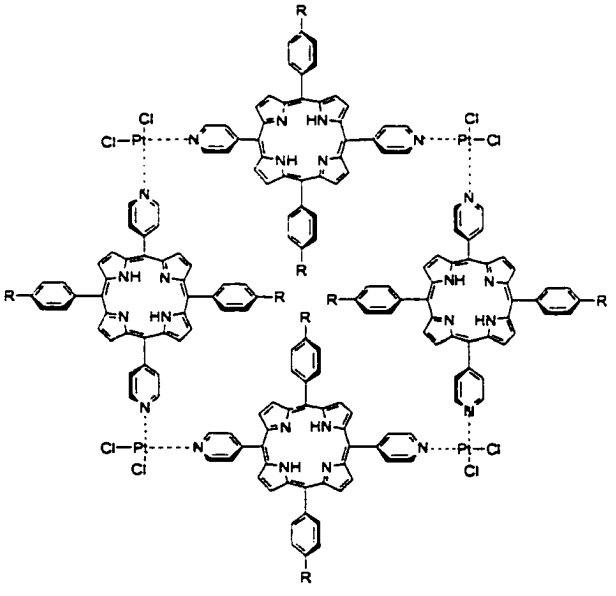

4 - R = *tert*-Bu
5 - R = $O(CH_2)_{11}CH_3$

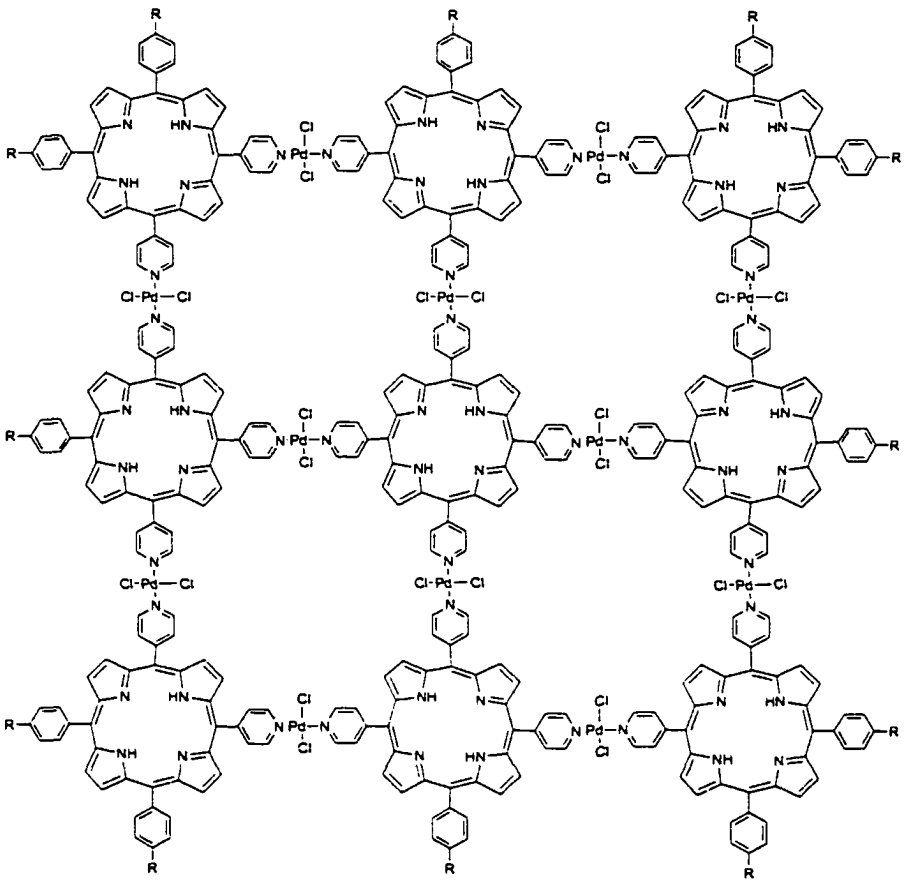

6 - R = CH_3
7 - R = $C(CH_3)_3$

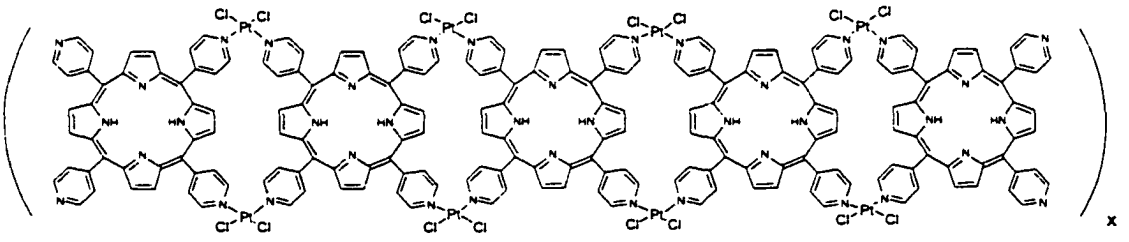

8

Scheme 3. 1. Various multi-porphyrin arrays (**1-8**) that have been synthesized using Pd or Pt-pyridyl interactions

In all of the self-assembly reactions we used dichloro Pt- or Pd- square planar complexes because of their well-defined ligand binding angles, selectivity and high

reaction yields. However, when these complexes bind to the porphyrins, the product is usually partially soluble in organic solvents. Because of this limited solubility, the growth of the X-ray crystals was difficult since the self-assembled species tend to precipitate at high concentrations as powders or microcrystals.

3. 2. 1. UV-Vis characterization

We have followed the changes in the UV-Vis spectra for all of the self-assembled reactions done in our laboratory. The total porphyrin concentration was less the 10 μM with absorbances less then 3 o.d. allowing facile UV-Vis monitoring. To ensure the correct self-assembly, it is necessary to use precise stoichiometric amounts of the reactant porphyrins and metal-binding complex in order to obtain the desired product.

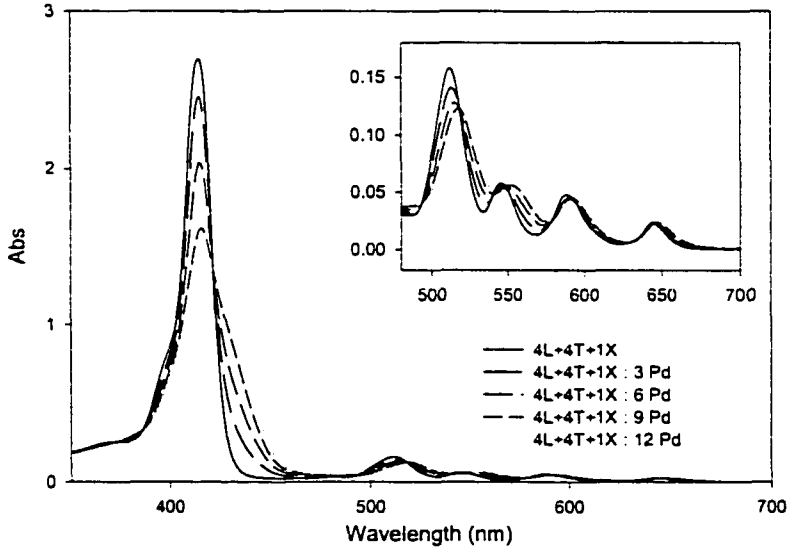

Figure 3. 1. UV-Vis titration reaction for the self-assembly of a multi-porphyrin array **6** in ethanol. Clear isosbestic points indicate that there are only two principle species in solution and that the sum of the porphyrin and nonamer concentration is held constant.

When bis-(benzonitrile)palladium(II) dichloride coordinates the pyridyl substituents on the meso-porphyrin positions, there is a perturbation of metal and ligand electronic levels, which produces a large spectral change in the most intense Soret band.[17] A strong exciton coupling causes a shift and broadening of the Soret band (Figure 3. 1.). This is a clear indication of the self-assembly reaction.

If the UV-Vis spectra of porphyrins used for the self-assembly are recorded as a function of palladium complex concentration, the stoichiometry of this reaction can be easily followed. The absorbance is measured at the Soret band maximum as a function of palladium concentration (Figure 3. 2). In our studies for the formation of array **6** made of nine porphyrin units, we combined nine equivalent of porphyrins (4T, 4L and 1X, see Chapter 4, Figure 4. 1.) with 12 equivalents of palladium(II) complex.

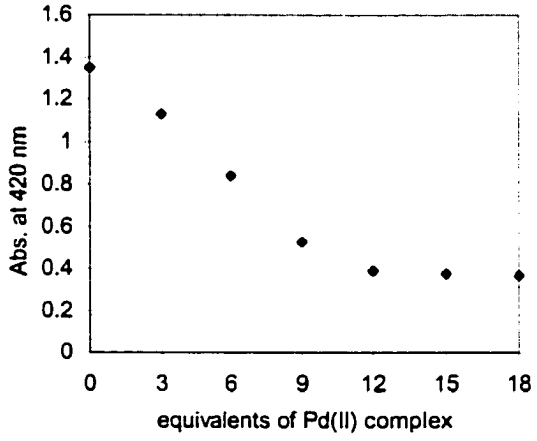

Figure 3. 2. The change of absorbance at 420 nm with stepwise addition of palladium(II) complex

[17] R. Margalit, N. Shaklai, S. Cohen, *Biochem. J.* **1983**, *209*, 547.

We can see (Figure 3. 2.) that the absorbance at the Soret band maximum decreases linearly until the right ratio Porph:Pd (9:12) is obtained. Further addition of palladium does not cause a significant change in absorbance although small deviations in the absorbance from the constant value are due to an additional secondary π-π stacking of formed self-assembled arrays.

The kinetics of the self-assembly reaction can be easily followed if palladium(II) complex is used. Because Pd(II) binds to the pyridyl groups of the porphyrins at room temperature quickly, the monitoring of the kinetics of the self-assembly reaction is facile, and equilibrium was achieved usually within 90 minutes. The comparison of UV-Vis kinetics curves for self-assembly of dimer, tetramer and nonamer via palladium (II) is given in Figure 3. 3.[18]

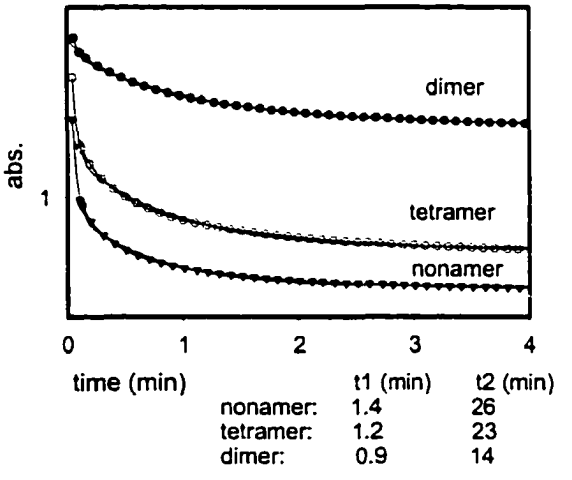

Figure 3. 3. The UV-Visible kinetic data for the self-assembly of the dimer, tetramer and nonamers (R = Me) in toluene.

[18] T. N. Milic, N. Chi, D. G. Yablon, G. W. Flynn, J. D. Batteas, C. M. Drain, *Angew. Chem. Int. Ed.***20 02**, *41* (12), 2117-2119.

The reaction in Figure 3. 3. was done at room temperature from a 5 μM solution of the porphyrin monomers. Changes in absorbance were monitored at the Soret band at 420 nm. These UV-visible studies on a series of porphyrin arrays and tapes self-assembled by the same $[Pd(PhCN)_2Cl_2]$ species[19] reveal a remarkable similarity in the formation kinetics under the same conditions of concentration, solvent and temperature. The rate of formation of the much more complex 21-particle nonameric array is only slightly slower than the formation of the simple 3-particle dimer or 8-particle tetramer- all occurring in less than 90 seconds (Table 3. 1.). This is an exquisite demonstration of the cooperative formation of thermodynamic products. The UV-visible spectral evolution for the arrays continues, revealing a second time constant on the order of ~ 25 minutes for the nonamer.

Table 3. 1. Formation kinetics of porphyrin arrays

Pd linked Assembly (# particles)	t1 (min)	t2 (min)
dimer (3)	0.9 ± 0.1	14 ± 5
square tetramer (8)	1.2 ± 0.1	23 ± 3
nonamer (21)	1.4 ± 0.2	26 ± 4

For the binding of platinum(II) complex higher reaction temperatures and longer times are needed in order to ensure the complete binding to the pyridyl groups of porphyrin. It is also interesting to notice that when platinum is binding to pyridyl groups on the porphyrin macrocycle, there is a small red-shift in the UV-Vis (~ 2 nm), due to the

[19] C. M. Drain, F. Nifiatis, A. Vasenko, J. D. Batteas, *Angew. Chem. Int. Ed.***19 98,** *37* (17), 2344-2347.

less extensive perturbations caused by platinum(II) to the electronic properties of the porphyrin.[20] The resulting complexes however are much more stable.

Changes in the porphyrin UV-Vis spectrum may also used to study aggregation processes.[21,22,23] If porphyrins are aggregated as J-type aggregates (head-to-tail), usually a red-shift of the Soret band is observed, while if they are aggregated face-to-face a blue shift results.[24] The Q-bands usually do not change much upon aggregation. Splitting of the Soret band can be an indication of edge-to-edge aggregation or partial protonation of the porphyrin macrocycle.

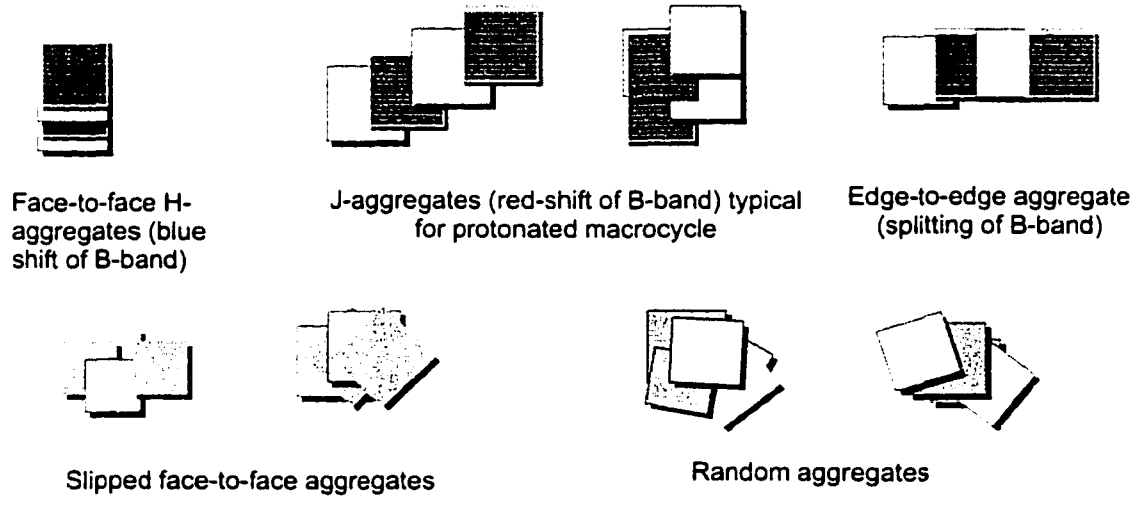

Scheme 3. 2. Possible modes of porphyrin π-π stacks aggregation

Because of the extensive π-nature of the porphyrin macrocycle, it is common to encounter aggregation of neutral porphyrins even in organic solvents. In our experiments we have used porphyrins with non-planar terminal groups, such as phenyl or *tert-*

[20] H. Yan, L. Thomas, L. K. Woo, *Inorg. Chem.* **1996**,*35* , 2808-2817.
[21] D. L. Akins, H.-R. Zhu, C. Guo, *J. Phys. Chem.***19 96**,*10 0*, 5420-5425.
[22] A. P. H. J. Schenning, D. Hubert, M. Feiters, R. J. M. Nolte, *Langmuir* **1996**,*12* , 1572-1577.
[23] K. Kano, H. Minamizono, T. Kitae, S. Negi, *J. Phys. Chem. A* **1997**, *101*, 6118-6124.
[24] R. F. Khairutdinov, N. Serpone, *J. Phys. Chem. B* **1999**, *103*, 761-769.

butylphenyl, so it is hard to envision exclusively pure H aggregation. More likely, the porphyrin aggregates stack one upon the other neither in a deck-of-cards arrangement (J-type) not in a face-to-face arrangement (H-type), but are off-set as in the non-chiral random aggregates (Scheme 3. 2.), particularly in case of nonameric arrays **6** and **7** (see Chapter 4 for more detailed discussion).

3. 2. 2. Other solution phase characterization methods

Fluorescence emission and excitation studies of our self-assembled systems confirm the metals binding to the exocyclic pyridyl groups. Substantial quenching of fluorescence intensity is observed upon Pd(II) and Pt(II) addition due to the heavy atom effect, and the formation of columnar π-stacks of aggregated porphyrin arrays.

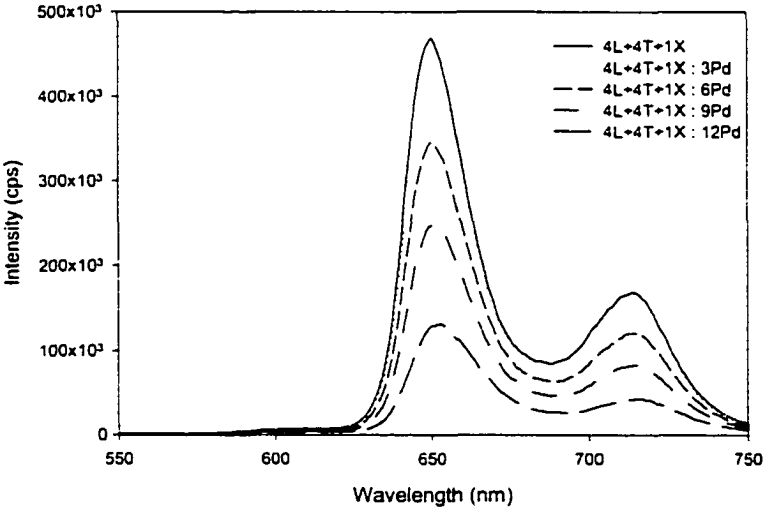

Figure 3. 4. Fluorescence emission spectra for self-assembly reaction of **6**. Titration of "4T+4L+1X" with bis-(benzonitrile)palladium(II) dichloride leads to the intense quenching of fluorescence.

^{1}H-NMR characterization studies of our self-assembled molecules resemble the ones already reported in the literature for the similar supramolecular species.[19,25,26] When pyridyl groups bind the metal ion, there is a characteristic downfield shift for the 2' and 6'-pyridyl protons. Upon self-assembly both the pyridyl protons and the protons on the β-pyrrole ring tend to have more complex resonances due to symmetry loss or multimer formation. For this reason, exact peak assignment and integration is often difficult. For further solution phase characterization dynamic light scattering studies were used for larger self-assembled arrays **6**, **7** and **8**, due to the detection limitation of an instrument (minimum radius of 1.5 nm). DLS results for array **8** are given in Figure 3. 20. and for arrays **6** and **7** in Chapter 4, Figure 4. 4.

Mass spectroscopic measurements were useful for the characterization of smaller species, such as array **1** and **3** (Figure 3. 9. and Figure 3. 13.). The main problem we encounter was the instability of the self-assembled structures during the mass spectroscopic measurement conditions, frequently yielding the decomposition products of the desired compound.

3. 2. 3. Surface phase characterization methods

Atomic force microscopy was used to investigate the deposition patterns of our synthesized assemblies. The arrays **4, 5** and **8** have been characterized on glass, while assemblies **6** and **7** were imaged on glass, gold and mica.

It is interesting to note that though array **3** is well characterized in solution it was difficult to prove the formation of self-assembled structure on surfaces, such as Au(111)

---

[25] C. M. Drain, J. –M. Lehn, *Chem. Commun.***19 94**, 2313.
[26] P. J. Stang, J. Fan, B. Olenyuk, *Chem. Commun.* **1997**, 1453.

since most of the particles found looked the same as individual porphyrin building units. One reason is that this structure is not stable under deposition conditions and during the absorption dissembles into constituent parts. Assemblies **6**,**7** and **8** are quite stable on the surface, allowing a contact mode AFM to be used to image the deposited nanostructures. We used contact mode AFM because of high scan speeds and higher resolution compared to non-contact AFM.

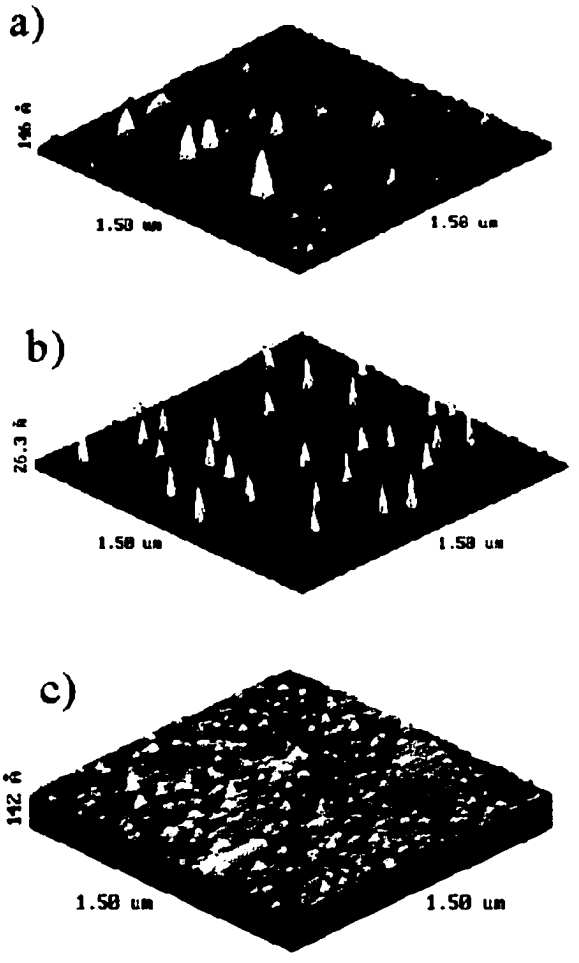

Figure 3. 5. Columnar stacks of free-base porphyrin nonamers **7** a) on glass, b) on mica and c) on Au(111). The size of the stacks is determined by the nature of a substrate.

In general for arrays **4**, **6** and **7** with terminal methylphenyl or *tert*-butylphenyl substituents we have observed randomly dispersed columnar nano-aggregates. The size of these aggregate depends on the surface used. Examples of aggregates of the nonameric array **7** on glass, mica and gold(111), are shown in Figure 3. 5. On graphite these arrays tend to conglomerate due to the weak interaction with hydrophobic surface. If the porphyrinic array has a terminal long alkyl chains at the periphery, such as array **5**, it will yield a more consistent monolayer film on glass or graphite as observed by AFM and this will be discussed in detail in Chapter 6. Detailed AFM studies of assemblies **6-7** are given in the Chapter 4.

Studies of the electronic properties of porphyrin arrays were carried out by STM. Because the nonameric array **7** on Au(111) forms single molecules deposit it was particularly amenable to utilize STM for higher resolution imaging (Figure 3. 6.).

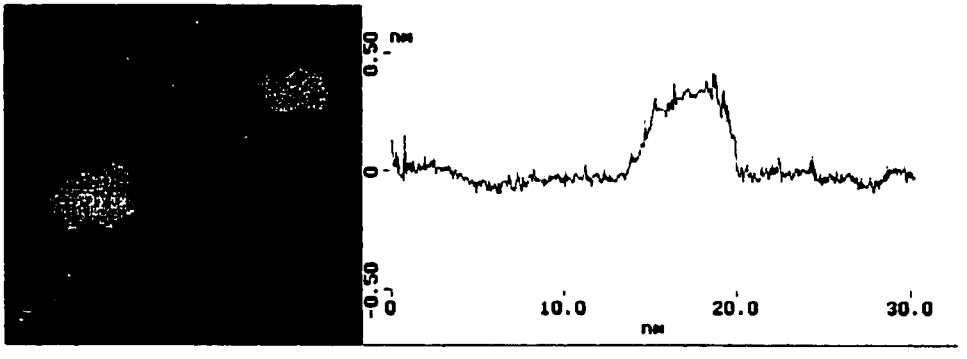

Figure 3. 6. STM constant current image (29nm x 29nm) of nonameric particles on Au(111) (I=250pA, V=1.2V). The nonameric particle is ~ 6 nm wide and ~0.4 nm high.

Free-base and zinc-based porphyrin nonamers were imaged on gold and their dimensions obtained are in a close agreement with the theoretical predictions. However, the internal structure of these nonamers could not be elucidated, possibly due to their

extended π-conjugated system and scanning conditions whereby multiple tunneling pathways may impact the image.

The multi-porphyrin tapes **8** yielded very peculiar surface organization as observed by the AFM. The polymeric tape is made when tetrakis-(4-pyridyl)porphyrin and *cis*-platinum(II) dichloride are mixed in 1:1.7 ratio and heated overnight at ~ 80 °C. This ratio stoichiometrically should produce tapes with about five connected porphyrins. However, because the tapes represent a linear (open) system, more likely a distribution of tape length is expected and observed.

The self-assembly of **8** was monitored by UV-Vis spectroscopy. The product shows a red-shift of ~ 2 nm compared to the starting monomeric porphyrin, which indicates electronic coupling between platinum and porphyrin units. Based on the dynamic light scattering results, the majority of the tapes are in polydispersed aggregates in solution at the concentration of ~ 10^{-5} M. Only ~ 10 % of particles have hydrodynamic radius around 7 nm, due to non-aggregated tapes.

The ^{1}H-NMR spectrum shows the presence of two broad signals, one centered at 9.34 ppm and one with lower intensity at 9.56 ppm, which can be assigned to the pyridyl groups. The broadening and the shifting of these signals to lower field are due to the coordination of the pyridyl groups to platinum. The ^{1}H-NMR spectrum shows also two doublets corresponding to the pyrrole rings. The first doublet resonates at 8.65 ppm, and it is coupled to a doublet at 7.98 ppm with a coupling constant J = 8.0 Hz. Other signals corresponding to the tape system are localized in the multiplets at 9.12-9.05, 8.97-8.81 and 8.24-8.10, and overlap with the resonances of the starting material. Despite many attempts it was not possible to separate the tape product from the porphyrin starting

material and from other impurities deriving from the bis-(benzonitrile)platinum(II) dichloride. Therefore an unambiguous assignment of the ^{1}H-NMR signals and the determination of the relative intensity of the peaks was not possible.

The tapes were deposited on glass by evaporation of porphyrin solution at room temperature. When the reaction product was deposited on a glass substrate, a ring structures were produced on the surface (Figure 3. 7.).

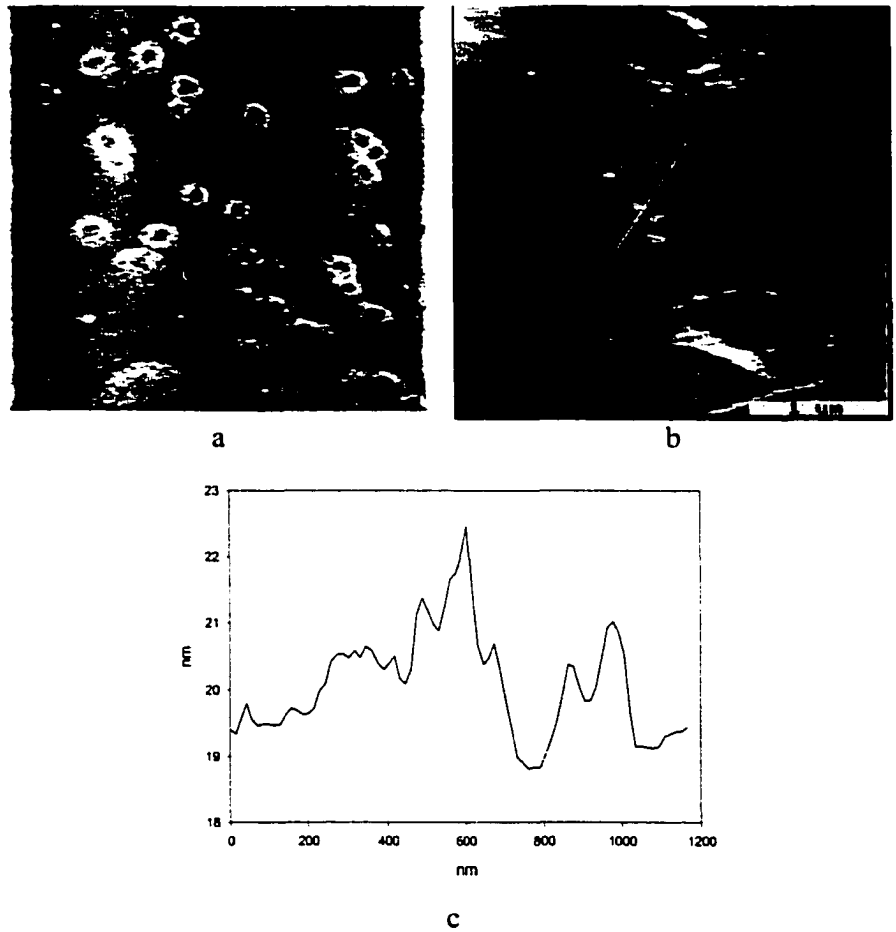

Figure 3. 7. a) 18 x 18 μm topographical AFM image (z = 3.6 nm), **b)** 3 x 3 μm topographical image AFM image (z = 5 nm) and line scan **c)** of the polymeric porphyrin tapes **8** on glass.

We observed a ring structures in repetitive experiments when deposition was done from ~ 10^{-6} M ethanol or THF solutions. Unlike any of the other porphyrin supramolecules formed, these tapes form aggregated ring structures. The rings range from ~ 1.1 – 1.7 μm in diameter and ~ 2 – 4 nm high. This thickness corresponds to ~ 4 – 10 π-stacked tapes of material.

The porphyrin tapes that constitute the rings can be in one of two arrangements (Scheme 3. 3.). The thickness of the ring walls, about 100-200 nm, reflects hundreds to over a thousand tapes, depending on their orientation. The proclivity for porphyrin assemblies to sit parallel to the glass surface, is in this case competing with the *cis*-chloride groups on the Pt(II). As such it is difficult to say at present, which orientation the porphyrins in the rings have. Based on the ring heights we can envision 4-10 porphyrin tapes stacked over each other.

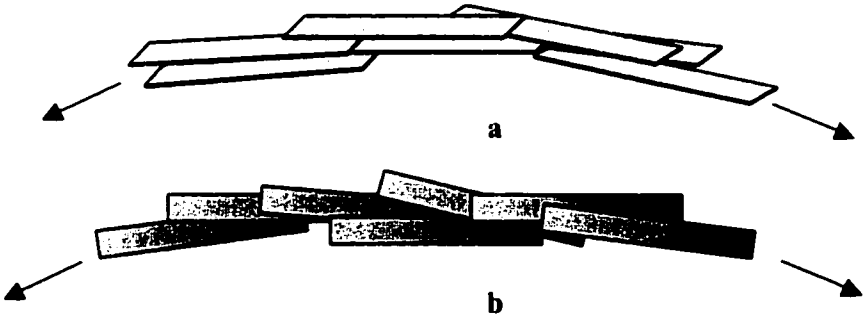

Scheme 3. 3. Simplified models of porphyrin stacks that form a ring structures; **a)** either the π-stacked porphyrin tapes lay parallel to the surface or **b)** lay edge-on to the surface. In each case they would overlap end-to-end.

Ring structures from deposited porphyrin assemblies have been observed before in the case of porphyrin dimers assembled with Pd(II) or Pt(II) dichloride in chloroform or 1,2,4-trichlorobenzene.[27,28,29,30] In these systems ring structures are formed within the concentration range 10^{-4}–10^{-6} M and they have diameter of 1-5 micrometers and average width and height of 10-100 nm. The ring formation was solvent dependent, and no rings were formed when toluene or THF was used. Nolte *et. al.* proposed two mechanisms for the formation of these structures. One mechanism is highly dependent on the aggregation mode of the porphyrins in solution and involves two-dimensional phase separation between porphyrin - rich and porphyrin - poor solution. This process occurs at nucleation sites where solid domains of porphyrins are formed, such as for two-dimensional assemblies of lipids or block copolymers.[31,32] The second mechanism is that presence of gas bubbles in the solution causes the formation of rings, as a result of complex hydrodynamic and surface effects.

Another way to explain the formation of rings made of nanocrystals is by Benard-Marangoni instabilities in the liquid films.[33] This effect is due to the temperature gradient between the substrate and a film during the process of solvent evaporation and it is solvent dependent. A change in the nanocrystal organization, from rings to random aggregates, is observed if hexane (b.p. 69 °C) is replaced by decane (b.p. 174 °C) or

---

[27] A. P. H. J. Schenning, F. B. G. Benneker, H. P. M. Geurts, X. Y. Liu, R. J. M. Nolte, *J. Am. Chem. Soc.* **1996**,*11 8*, 8549-8552.
[28] J. Hofkens, L. Latterini, P. Vanoppen, H. Faes, K. Jeuris, S. De Feyter, J. Kerimo, P. F. Barbara, F. C. De Schryver, *J. Phys. Chem. B.* **1997**,*10 1*, 10588-10598.
[29] H. A. M. Biemans, A. E. Rowan, A. Verhoeven, P. Vanoppen, L. Latterini, J. Foekema, A. P. H. J. Schenning, E. W. Meijer, F. C. De Schryver, R. J. M. Nolte, *J. Am. Chem. Soc.* **1998**, *120*, 11054-11060.
[30] L. Latterini, R. Blossey, J. Hofkens, P. Vanoppen, F. C. De Schryver, A. E. Rowan, R. J. M. Nolte, *Langmuir* **1999**,*15* , 3582-3588.
[31] R. M. Weis, H. M. McConnell, *J. Phys. Chem.* **1985**, *89*, 4453.
[32] J. H. Wang, C. Bohm, T. S. Ramalingam, E. Betzig, M. Edidin, *Science* **1995**,*27 0*, 610.
[33] M. Maillard, L. Motte, A. T. Ngo, M. P. Pileni, *J. Phys. Chem B.***20 00**,*10 4*, 11871-11877.

water (b.p. 100 °C), due to the different evaporation rates. The slower the evaporation rate causes less expressed temperature gradient and no rings are formed.

In our studies we observed rings when ethanol (b.p. 78 °C) and tetrahydrofuran (b.p. 67 °C) were used and they have a comparable boiling points to hexane (b.p. 69 °C). But solvent evaporation rate cannot be the only factor contributing to the ring formation. When square-shaped nonameric array **7** was prepared in ethanol no rings are observed. So, certainly aggregation of nanoparticles in solution and even a shape of molecule may play certain role in the final surface organization. The linear shape of the polymeric porphyrin assemblies seems important for particular aggregation tendencies and together with interplay between surface absorption and solvent evaporation contribute to the formation of circular structures.

3. 3. Experimental

3. 3. 1. Self-assembly of porphyrin dimer via *trans*-palladium(II) coordination

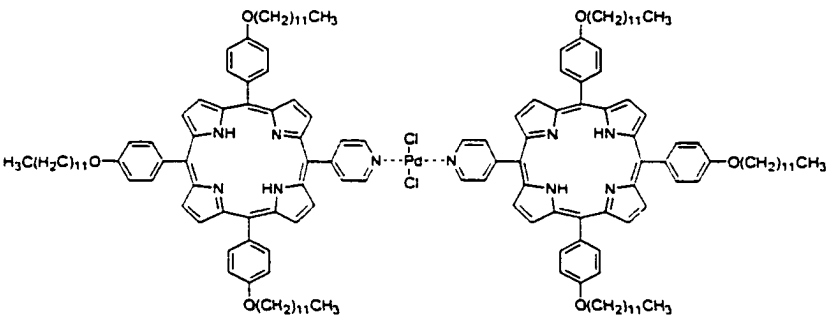

1

Synthesis (1): To a solution of 5-(4-pyridyl)-10,15,20-tris-(4-dodecyloxybenzyl) porphyrin (2.01 μM) *trans*-bis-(benzonitrile)palladium(II) dichloride was added in four aliquots at intervals of at least five minutes to reach a concentration of 1.00 μM (porphyrin:palladium ratio 2:1). The reaction was done in 3 mL cuvette in toluene at room temperature and stirring continuously. Due to the good solubility of product in toluene or dichloromethane, the reaction can be also done at higher concentrations. In this case *trans*-bis-(benzonitrile)palladium(II) dichloride (4.3 mg, 11 μmol) was added to the solution of 5-(4-pyridyl)-dodecyloxyphenyl porphyrin (23.7 mg, 20 μmol) in 10 mL of freshly distilled dichloromethane. The reaction was done at room temperature for 2 hours. The product was purified by preparative thin layer chromatography using the chloroform:hexane (8.5:1.5) as an eluent. The fraction with $R_f = 0.386$ was identified as dimer compound, **1** (12.9 mg, yield 44.3%).

UV-VIS - λ, nm in toluene ($\varepsilon \times 10^4$ $cm^{-1}M^{-1}$) 424 (89), 518 (4.1), 555 (2.8), 595 (1.3), 652 (1.3).

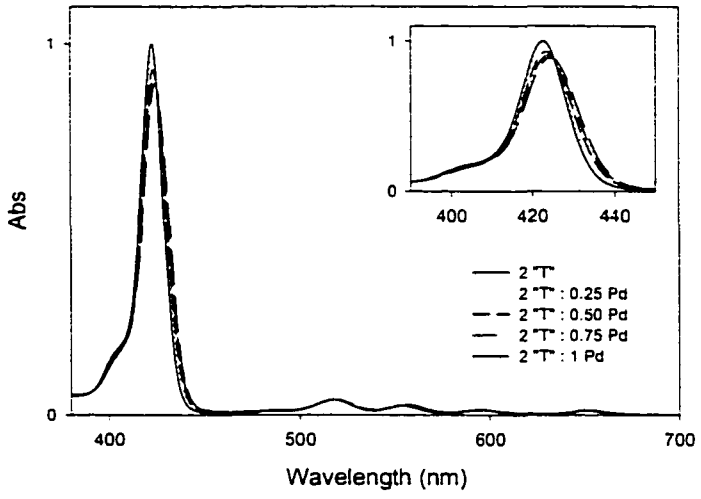

Figure 3. 8. UV-Vis titration for the formation of the dimer compound **1**

ESI-MS: *m/z* (theoretical intensities) calculated for $C_{158}H_{202}N_{10}O_6Cl_2Pd$: 2510 (8.8), 2511 (29.1), 2512 (45), 2513 (62), 2514 (90), 2515 (100), 2516 (93), 2517 (72), 2518 (48), 2519 (28), 2520 (17), 2521 (6), 2522 (2). *m/z* ($M+3H^+$, relative intensities) found: 839.3 (100), 840.2 (70), 841.3 (25), 842.3 (5).

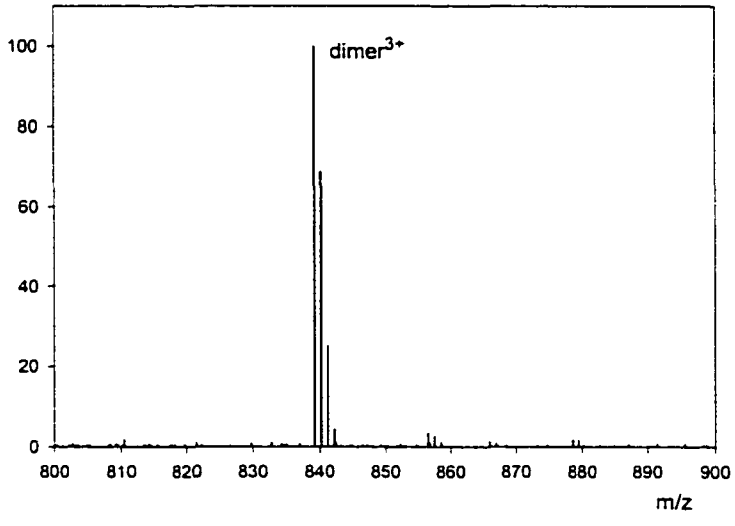

Figure 3. 9. ESI-MS spectrum of dimer **1**

^{1}H-NMR (300 MHz, $CDCl_3$): δ 9.39 (b, 2,6-pyridyl), 8.99 (d, J = 4.8 Hz, β-pyrrole), 8.96 (d, J = 5.1 Hz, β-pyrrole), 8.93-8.86 (m, β-pyrrole), 8.82 (d, J = 4.8 Hz, β-pyrrole), 8.77 (d, J = 5.1 Hz, β-pyrrole), 8.29 (d, J = 5.5 Hz, 3,5-pyridyl), 8.25 (d, J = 5.5 Hz, 3,5-pyridyl), 8.12 (d, J = 8.43, 3,5-phenyl), 8.07 (d, J = 8.43, 3,5-phenyl), 7.32-7.13 (m, 2,6-phenyl), 4.26 (b, OCH_2), 4.13-3.9 (b, OCH_2), 3.64 (d, OCH_2), 2.6-0.8 (m, CH_2), -2.74 (s, internal pyrrole).

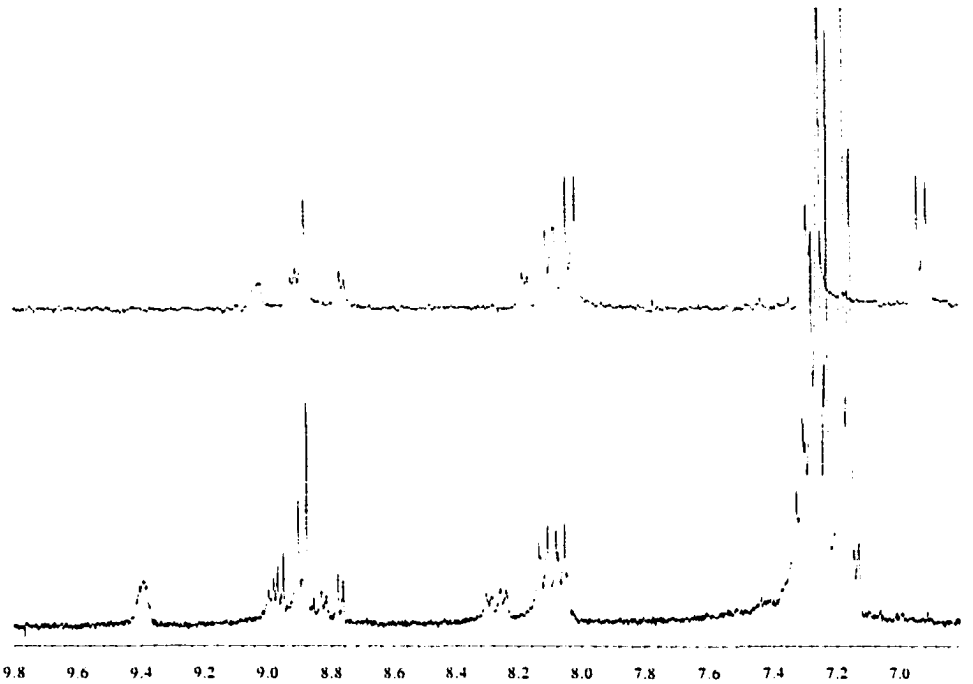

Figure 3. 10. ^{1}H-NMR spectra of the porphyrin building block (above) and resulting dimer **1** (below).

3. 3. 2. Self-assembly of tetrameric porphyrin array via *trans*-palladium(II) coordination

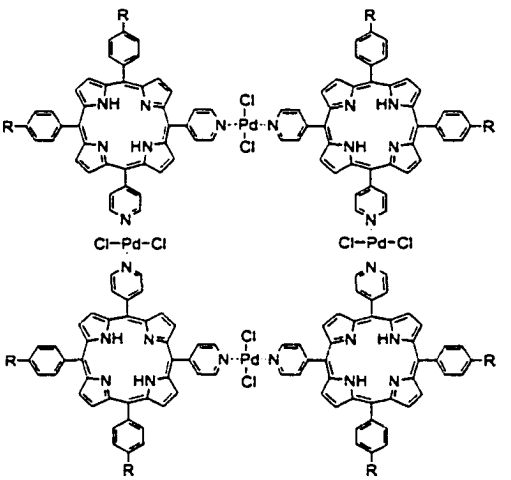

2 - R = *tert*-Bu
3 - R = $O(CH_2)_{11}CH_3$

Synthesis (2): To the 3 mL solution of mineral oil or toluene *trans*-bis-(benzonitrile)palladium(II) chloride solution (1.2×10^{-8} mol, 4.0 μM) is added in four aliquots to the solution of 5,10-PytBuPP (1.2×10^{-8} mol, 4.0 μM) until 1:1 stoichiometric ratio is reached. The reaction was stirred at room temperature. **UV-VIS**: - λ, nm in mineral oil ($\varepsilon \times 10^4$ $cm^{-1}M^{-1}$) 422 (75), 520 (9.3), 555 (6.8), 594 (5.8), 649 (5.0) (Figure 3. 11.)

Synthesis (3): *Trans*-bis-(benzonitrile)palladium(II) dichloride (1.2 mg, 3.25 μmol) was added to the stirring solution of 5,10-bis-(4-pyridyl)-15,20-(4-dodecyloxyphenyl) porphyrin (3.2 mg, 3.25 μmol) in 10 mL of dichloromethane. The reaction was left overnight at room temperature. The product was purified by Sephadex size exclusion

chromatography. **UV-VIS**: - λ, nm in toluene (ε × 10^4 $cm^{-1}M^{-1}$) 424 (128), 519 (7.6), 556 (4.5), 594 (2.7), 650 (1.9) (Figure 3.12.)

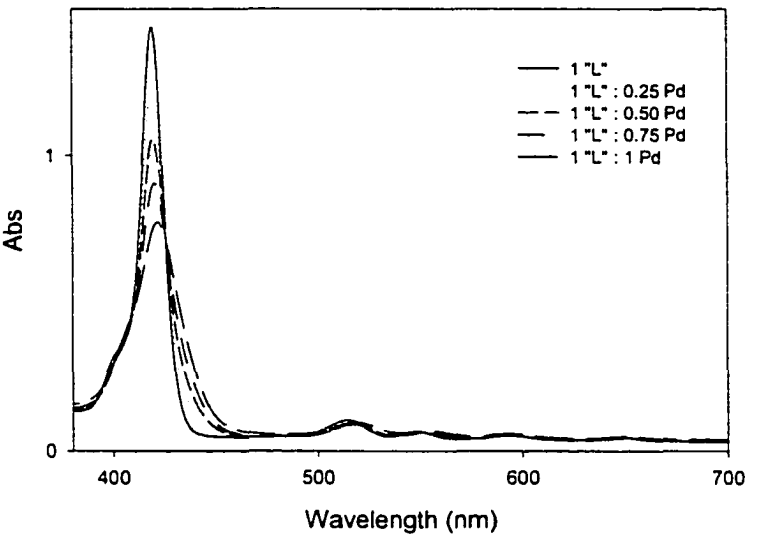

Figure 3. 11. UV-Vis titration spectrum for the formation of tetrameric array **2**

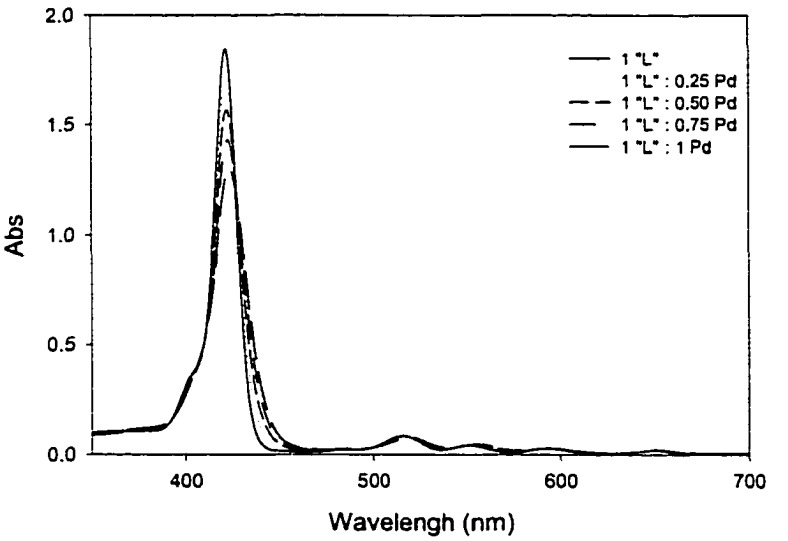

Figure 3. 12. UV-Vis titration spectrum for the formation of tetrameric array **3**

ESI-MS: *m/z* (theoretical intensities) calculated for $C_{264}H_{304}N_{24}O_8Cl_8Pd_4$ 4640 (8), 4641 (9), 4642 (15), 4643 (24), 4644 (34), 4645 (48), 4646 (62), 4647 (77), 4648 (88), 4649 (95), 4650 (100), 4651 (98), 4652 (95), 4653 (88), 4654 (77), 4655 (67), 4656 (54), 4657 (43), 4658 (35), 4659 (24), 4660 (16), 4661 (11), 4662 (8). *m/z* found: 1586.0 $(tetramer)^{2+}$-2Cl, 1168.5 $(tetramer)^{4+}$, 1025.5 $(tetramer)^{4+}$ - 4Cl, 985.5 (monomer), 824.5 $(tetramer)^{5+}$ - 3Cl, 780.5 $(tetramer)^{6+}$, 667.2 $(tetramer)^{6+}$ - 3Cl.

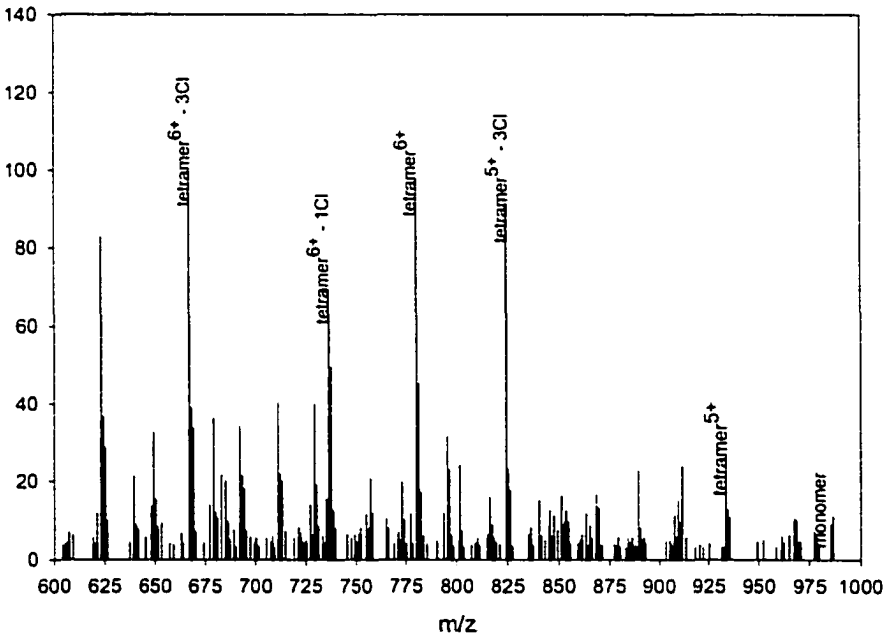

Figure 3. 13. ESI-MS spectrum of tetrameric array **3**

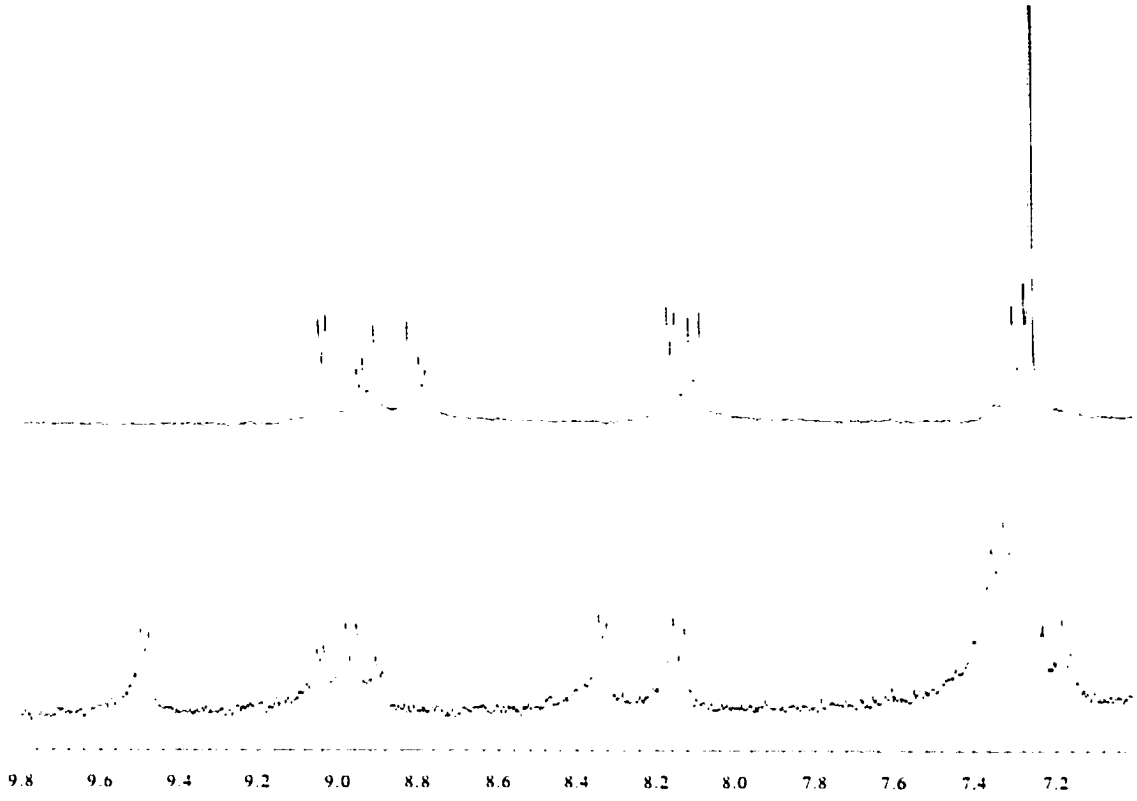

Figure 3. 14. ^{1}H-NMR spectrum of the monomer 5,10-PyDdcylPP (above) and corresponding tetrameric array **3** (below).

3. 3. 3. Self-assembly of tetrameric porphyrin array via *cis*-platinum(II) coordination

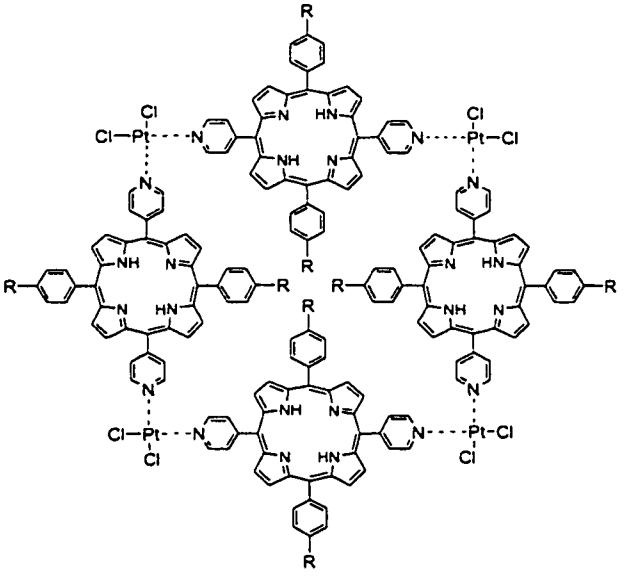

4 - R = *tert*-Bu
5 - R = $O(CH_2)_{11}CH_3$

Synthesis (4): 5,15-bis-(4-pyridyl)-15,20-bis-(4-*tert*-butylphenyl)porphyrin (4.06 mM) was mixed in 1:1 ratio with *cis*-bis-(benzonitrile)platinum(II) dichloride (4.06 mM) in 3 mL of toluene, and heated overnight at temperature ~ 90 °C. **UV-Vis**: λ, nm in toluene 421, 515, 550, 590, 648. (Figure 3. 15.)

Synthesis (5): *Cis*-bis-(benzonitrile)platinum(II) dichloride (2.4 μmol, 1.13 mg) was added with stirring to the solution of 5,15-bis-(4-pyridyl)-10,20-bis-(4-dodecyloxyphenyl)porphyrin (2.4 μmol, 2.36 mg) in 6 mL of toluene. The solution was refluxed overnight for 17 hours. Purification of the product was done by column chromatography on flash silica gel using toluene/ethyl acetate 15% as eluent. **UV-Vis**: λ, nm in toluene 423, 516, 553, 593, 650. (Figure 3. 16.)

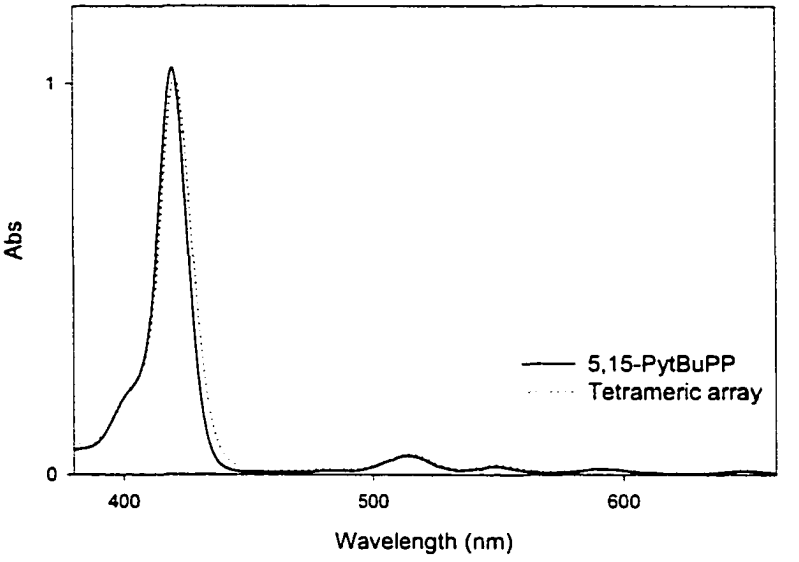

Figure 3. 15. UV-Vis spectal changes for the formation of tetrameric array **4**

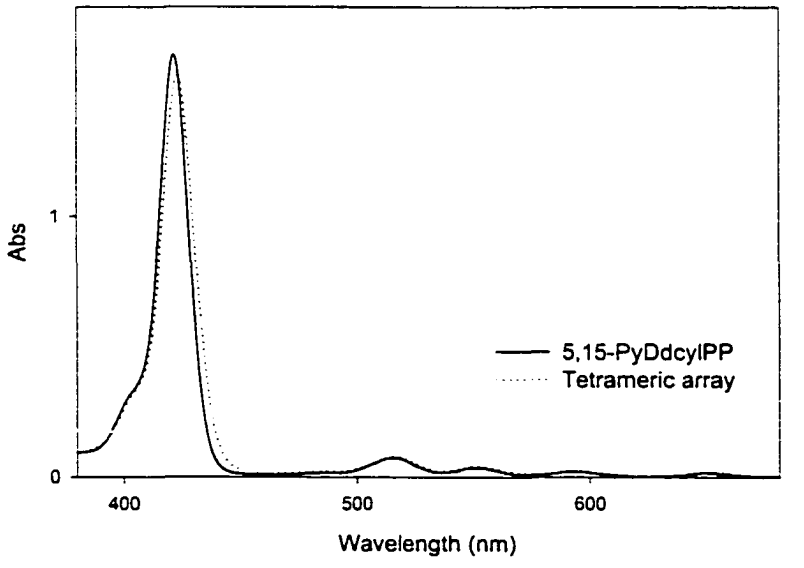

Figure 3. 16. UV-Vis spectal changes for the formation of tetrameric array **5**

ESI-MS: *m/z* (theoretical intensities) calculated for $C_{264}H_{304}N_{24}O_8Cl_8Pt_4$: 4996 (4), 4997 (8), 4998.5 (15), 5000 (28), 5001 (45), 5002 (64), 5003 (82), 5004 (95), 5005 (100), 5006 (84), 5007 (56), 5008 (40), 5009 (28), 5011 (17), 5012 (12), 5013 (6). *m/z* found: 2231.3 $dimer^{4+}$, 2114.0 ($dimer^{+}$–1Cl), 2077.7 ($dimer^{+}$ – 2Cl), 1409.5 ($monomer^{+}$ + 2Pt + 1Cl), 1375.0 ($monomer^{+}$ + 2Pt), 494.2 $monomer^{2+}$, 401 $(PtPhCN)_2$.

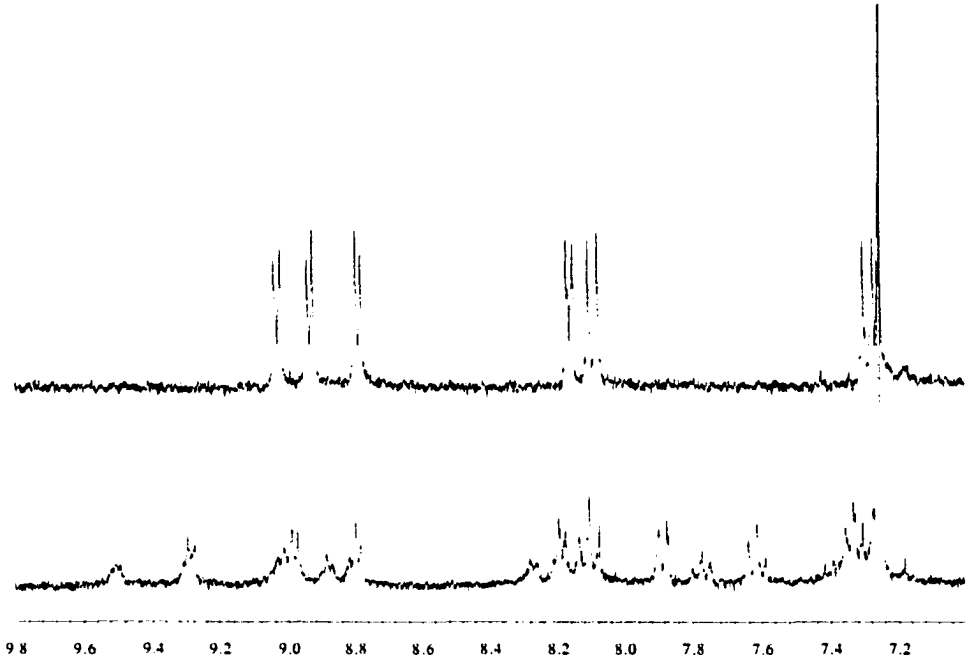

Figure 3. 17. ^{1}H-NMR spectra for the 5,15-PyDdcylPP (above) and corresponding tetrameric array **5** (below)

3. 3. 4. Self-assembly of tetrapyridylporphyrin-*cis*-platinum(II) tapes

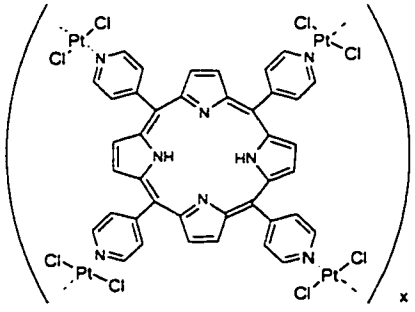

8

Synthesis (8): Tetrakis-(4-pyridyl)porphyrin (5.9 mg, 9.5 μmol) was dissolved in 23 mL of methanol/chloroform (1:1.5) at 45 °C, until completely dissolved. *Cis*-bis (benzonitrile)platinum(II) dichloride (7.8 mg, 16.5 μmol) was added (platinum:porphyrin 1.7:1 ratio) to the stirring solution. The reaction was done at 50 °C overnight for 18 hours. The product was a red-purple colloidal solution. The TLC analysis of the reaction mixture showed presence of three spots on silica-gel plate (eluent 100 % THF), one of them indicate presence of small amount of unreacted starting material. Because of the limited solubility of the product the chromatographical purification was not possible. Instead, the reaction mixture was evaporated, and product washed with hexane (Optima grade) using a Büchner vacuum filtration system. Then it was washed with chloroform to remove traces of unreacted porphyrin starting material. Most of the product remained on the filter in a form of purple crystalline powder (3.9 mg).

UV-VIS: Tetrakis-(4-pyridyl)porphyrin (6×10^{-9} mol, 2.0 μM) and bis-(benzonitrile)platinum(II) dichloride (1×10^{-8} mol, 3.3 μM) were added to a 3 mL solution of ethanol. The solution was stirred at 50 °C for 17 hours. The reaction done in

THF yields the similar results. **UV-Vis:** λ, nm in ethanol: 414.5, 511.0, 544.5, 587.5, 647.0. (Figure 3. 18.)

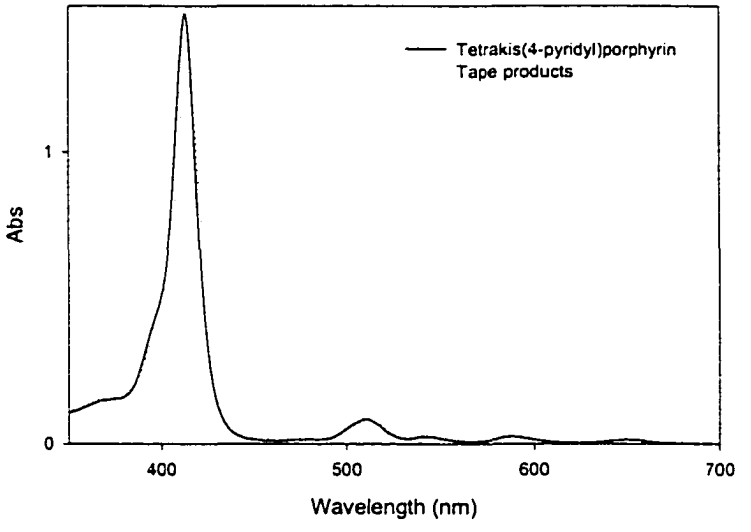

Figure 3. 18. UV-Vis spectra for the formation of **8** in ethanol

ESI-MS: *m/z* (theoretical intensities) calculated for $C_{200}H_{130}N_{40}Pt_8Cl_{16}$, if five porphyrins constitute a tape: 5209 (1.8), 5210 (3.6), 5211 (6.7), 5212 (11.5), 5213 (18.1), 5214 (27.1), 5215 (38.2), 5216 (50.8), 5217 (64.0), 5218 (76.7), 5219 (87.5), 5220 (95.5), 5221 (99.7). *m/z* found: 2911 (trimer$^+$), 1761 (dimer$^+$), 1468 (trimer^{2+} or dimer$^+$-1Cl), 1267 (trimer^{2+} -1Pt), 852 (monomer$^+$ + Pt + Cl), 619.0 (monomer$^+$).

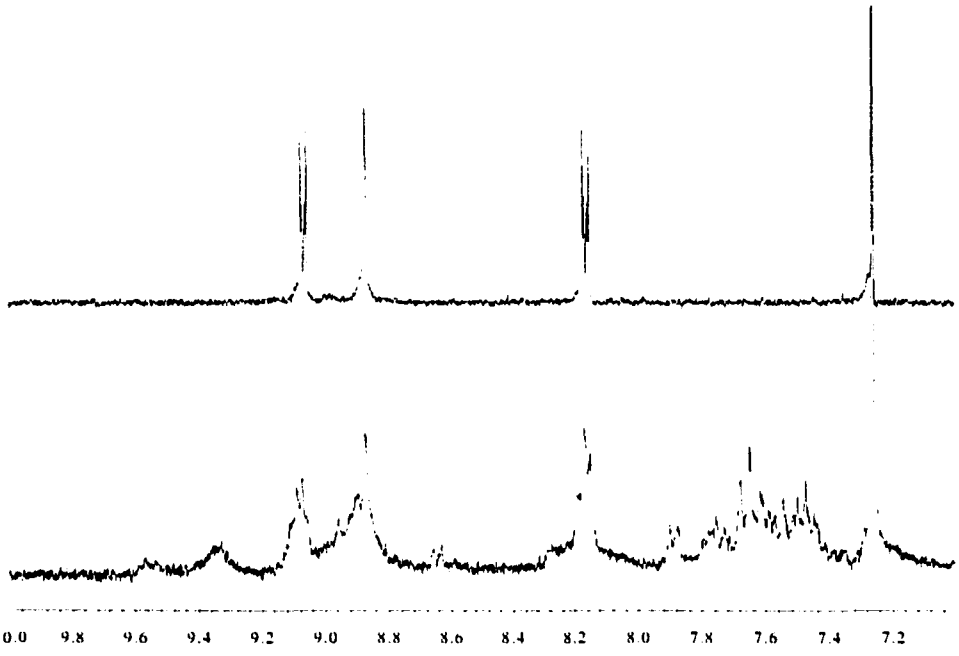

Figure 3. 19. ^{1}H-NMR spectra of the tape compound **8** (below) and TPyP (above)

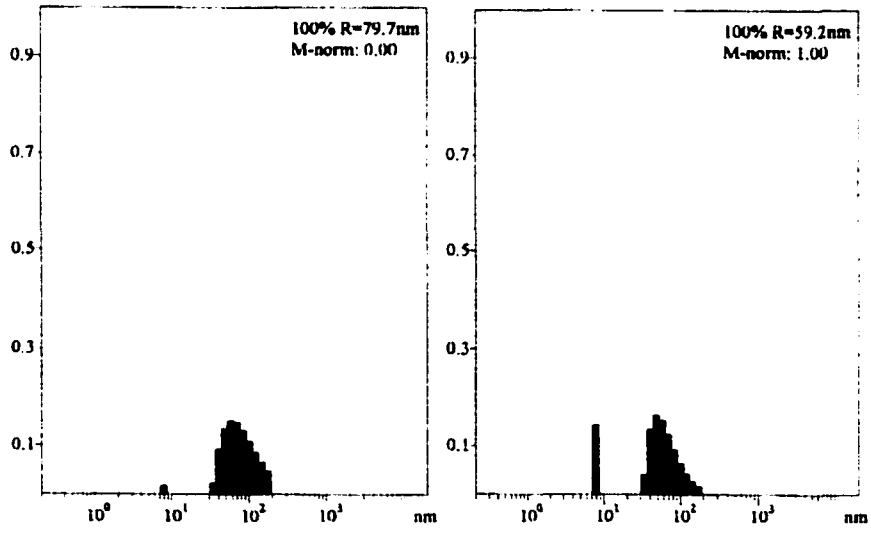

Figure 3. 20. Dynamic light scattering data of the tape product **8** in ethanol. Image on the left is intensity normalized (2% of particles with radius 8 nm and 98% of particles with average radius 81 nm). Image on the right is mass normalized to rigid rod (15% of particles with radius 8 nm and 85 % of particles with average radius 68 nm).

4.

HIERARCHICAL SELF-ASSEMBLY OF THE FREE-BASE NONAMERIC PORPHYRIN ARRAY

4. 1. Introduction

Nature repeatedly demonstrates exquisite control over the molecular forces that underpin the very existence of life. Inspired by nature, the synthetic introduction of specific molecular interactions to guide the association of matter is an overarching theme in current nanoscale materials and device design.[1] The technological and functional advantages of using nanoscaled or molecular components in a variety of devices has been recognized for decades.[1,2,3,4,5] However, the formation of functioning nanoscaled or molecular electronic devices from non-biological components began in the 1980's.

The formation of self-organized photogated transistors from porphyrins in lipid bilayers is a key example,[6,7] but the obvious limitation is the stability of the system.

---

[1] P. Ball, *Nature* **2001**, *409*, 413-416.
[2] A. P. Alivisatos, P. F. Barbara, A. W. Castleman, J. Chang, D. A. Dixon, M. L. Klein, G. L. McLendon, J. S. Miller, M. A. Ratner, P. J. Rossky, S. I. Stupp, M. E. Thompson, *Adv. Mater.* **1998**,*10* , 1297-1336.
[3] M. A. Fox, *Acc. Chem. Res.* **1999**,*32* , 201-207.
[4] A. Aviram, M. Ratner (Eds), *Annals New York Acad. Sci.* **1998**, *852*.
[5] M. A. Reed, *MRS Bull.* **2001**, *26*, 113-120.
[6] C. M. Drain, D. Mauzerall, *Biophys. J.* **1992**, *63*, 1556-1563.
[7] C. M. Drain, D. Mauzerall, *Bioelectrochem. Bioenerg.* **1990**, *24*, 263-266.

With the remarkable progress in the self-assembly of molecular components into specific arrays and polymers, there are many other recent examples of supramolecular species that are proposed as components of nanoscaled devices.[8,9,10,11] The methodologies used to create devices on the nanometer scale can be roughly categorized as those using lithography ("top down") or self-assembly ("bottom up") — approaches, with each having advantages and limitations. Certainly, self-assembly is claimed to be an important avenue toward the manufacture of the next generation of nanoscaled molecular materials, especially for use in photonic devices.[2,7-11] But, there are several critical factors to be considered. Since the vast majority of molecular self-assembly processes are carried out in solution and utilize relatively weak intermolecular forces, can the desired products be reliably deposited onto surfaces and still retain their intended structure and function? Since the components of the self-assembled structures are organic or coordination compounds, how stable are they electrochemically, thermally, and to dioxygen? If self-assembled entities are to be used in large-scale applications, an important, yet often unacknowledged requirement is that highly pure molecular components or building blocks must be readily synthesized on large scales in high yields. Herein we report the self-assembly of porphyrinic arrays and clusters that address these issues.

Specifically, we demonstrate hierarchical solution phase organization of self-assembled nonameric porphyrin arrays into columnar stacks that are about 6.2 nm in diameter and 0.4 nm to ~ 10 nm tall. These heights correspond to stacks of 1 to about 22 nonamers, and represent the self-organization of 21 to about 460 particles, respectively,

---

[8] J. -M. Lehn, *Angew. Chem. Int. Ed.***19 90**, *29*, 1304-1319.
[9] J. S. Lindsey, *New J. Chem.***19 91**, *15*, 153-180.
[10] P. J. Stang, B. Olenyuk, *Acc. Chem. Res.* **1997**,*30* , 502-518.
[11] M. Fujita (Ed.) *Structure and bonding* **2000**,*96* , 149-201.

of four different chemical types. The size of the aggregates is pre-determined by the choice of appended alkyl group, solvent, temperature, porphyrin metalation, and an understanding of the secondary organization kinetics. Moreover, these materials can be deposited onto a variety of surfaces with high structural fidelity, with the choice of surface chemistry affording an additional modality for size selection. AFM and UV-visible analysis shows that once deposited on surfaces these structures are stable in air for more than a year at room temperature, and retain their photophysical properties. Herein we present data for the hierarchical self-assembly of the free base porphyrins. This approach provides access to a wide variety of closed arrays, and defined structures. Other approaches include liquid crystalline, and polymeric porphyrin materials on surfaces,[12,13,14] and other networks.[15,16]

4. 2. Results and discussion

Earlier, Drain and coworkers reported the self-assembly and characterization of a 21 component square planar porphyrin nonamer.[17] The predefined geometry of either the metallo or free-base porphyrins as well as the coordination geometry of the metal ion linker – all in the correct stoichiometry – dictates the final structure of the self-assembled arrays. In the case of the nonamer, the 180^0 (trans) coordination geometry of the twelve $PdCl_2$ species combines with four 'L-shaped' porphyrins (3) that serve as the corners,

---

[12] D. M. Sarno, B. Jiang, D. Grosfeld, J. O. Afriyie, L. J. Matienzo, W. E. Jones, Jr., *Langmuir,* **2000**, *16*, 6191-6199

[13] X. Qiu, C. Wang, Q. Zeng, B. Xu, S. Yin, H. Wang, S. Xu, C. Bai, *J. Am. Chem. Soc.* **2000**, *122*, 5550-5556.

[14] C. -Y. Liu, H. -I. Pan, M. A. Fox, A. J. Bard, *Science* **1993**,*26 1*, 897-899.

[15] F. Wurthner, C. Thalacker, A. Sautter, *Adv. Mater.* **1999**, *11*, 754-758.

[16] D. G. Kurth, P. Lehmann, M. Schutte, *Proc. Natl. Acad. Sci. USA,* **2000**, *97*, 5704-5707.

[17] a) C. M. Drain, F. Nifiatis, A. Vasenko, J. D. Batteas, *Angew. Chem. Int. Ed.* **1998,** *37* (17), 2344-2347. b) C. M. Drain, F. Nifiatis, A. Vasenko, J. D. Batteas, *Angew. Chem.* **1998**,*11 0*, 2478-2481.

four 'T-shaped' porphyrins (2) that constitute the sides, and one 'X-shaped' porphyrin (1), which resides in the center. The self-assembly of these porphyrin nonameric array (Figure 4. 1. a), is followed by the self-organization into columnar aggregates that are about 6 nm in diameter and an average of 5 nm in height (Figure 4. 1. b).

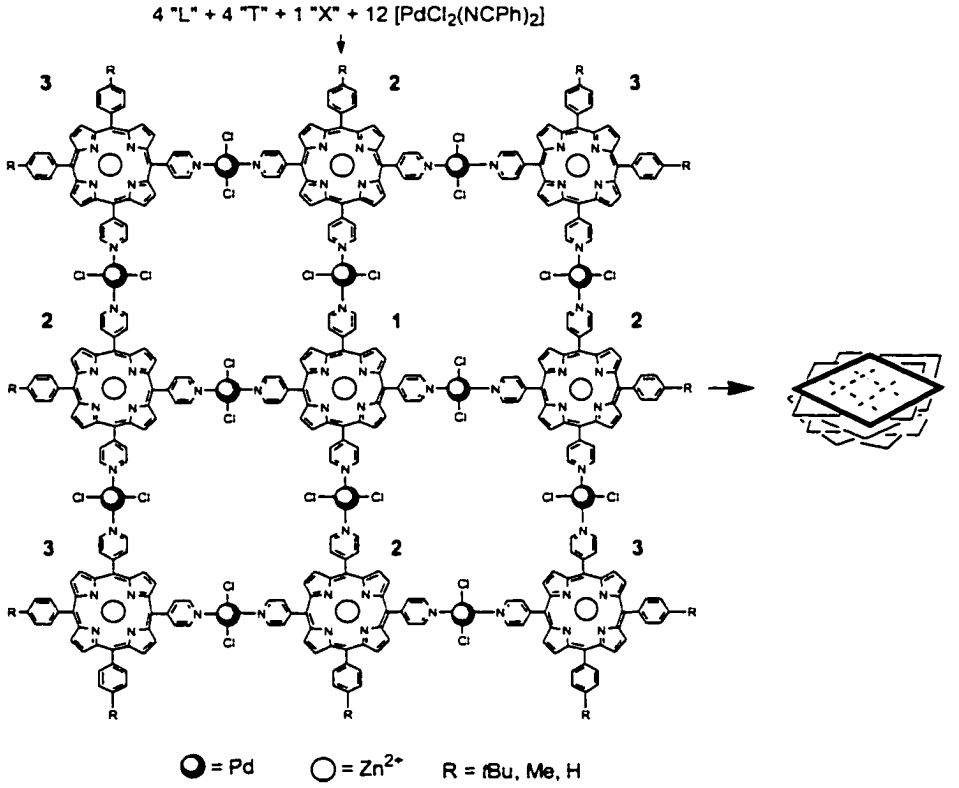

Figure 4. 1. The self-assembly of a porphyrin nonameric array **a)** is followed by the self-organization into columnar aggregates **b)**. The size of these latter entities can be directed by various means (see text).

As mentioned before, the rate of formation of the much more complex 21-particle nonameric array is only slightly slower than the formation of the simple 3-particle dimer or 8-particle tetramer- all occurring in less than 90 seconds (Table 4. 1.). The UV-visible

spectral evolution for the arrays continues, revealing a second time constant on the order of ~ 25 minutes for the nonamer. Dynamic and resonance light scattering (DLS, RLS), coupled with AFM experiments, reveal that this process is a secondary organization of these discrete self-assembled arrays into nanoscaled aggregates.

Table 4. 1. Kinetics data for the self-assembly of various porphyrin arrays

Pd linked Assembly (# particles)	t1 (min)	t2 (min)
dimer (3)	0.9 ± 0.1	14 ± 5
square tetramer (8)	1.2 ± 0.1	23 ± 3
nonamer (21)	1.4 ± 0.2	26 ± 4

A single nonamer array when R = *tert*-Bu should be approximately 6.2 x 6.2 nm from *tert*-butylphenyl to *tert*-butylphenyl and ~ 0.4 nm in thickness. DLS of aggregates in solution and AFM of aggregates on glass show that the final aggregate is ~ 6 ± 1 nm in diameter and 2-10 nm tall, respectively. However, these experiments also suggest that the aggregation process is dynamic, proceeding through several intermediate stages. The initially formed kinetic products are about 50 nm tall aggregates, and these then dissociate and re-organize until the about 6 nm tall thermodynamic products are formed. Once removed from the equilibrating solution by deposition on glass surfaces and evaporation of the solvent, the particles are trapped in the state of aggregation at the time. This affords a time-based selection of the average particle size to be deposited on surfaces (Figure 4. 2.). UV-visible and fluorescence spectra indicate the about 6 nm tall aggregates of all 4 types of nonamer (R = Me or *tert*-Bu, and M = Zn^{2+} or $2H^{+}$) are

thermally stable in toluene in air up to ~ 80 ^{0}C. After cooling to 20 ^{0}C, DLS data on these samples are identical to those before heating.

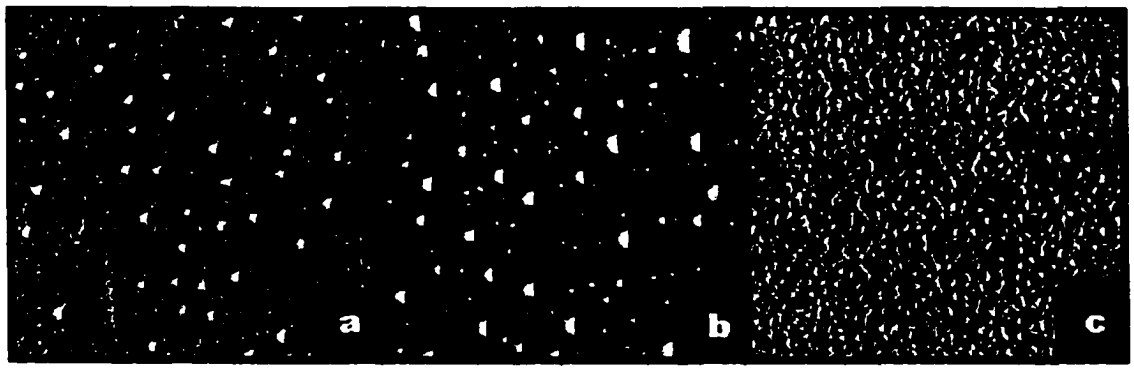

Figure 4. 2. AFM images (10 μm x 10 μm) confirm the hypothesis that the formation of the nanoscaled aggregates of free base porphyrin nonamers (R = Me) is dynamical; **a)** after 5 minutes, ~ 30 nm high aggregates are first observed, followed by the observation **b)** of a bimodal distribution of these and 100's of much smaller sub-10 nm high aggregates, and **c)** finally a uniform distribution of aggregates that are ~ 6 nm in height on average.

The energetics of the self-organization of the columnar stacks of porphyrin nonamers arises from the complex interplay between a variety of intermolecular forces. The π-stacking of porphyrins to form face-to-face (H) or edge-to-edge (J) aggregates is a well-known and understood phenomena.[18] Electronic spectra indicate both types of arrangements are present in the columnar aggregates.[17] Under the conditions described herein, however, neither solutions of individual porphyrins or a mixture of them, nor the palladium complex, results in any discernable aggregation as shown by absorption and emission spectra, DLS or AFM. Estimates of π-stacking interactions are between 3 and 5

[18] C. A. Hunter, J. K. M. Sanders, *J. Am. Chem. Soc.* **1990**,*11 2*, 5525-5534 and references therein.

kcal mol^{-1} per porphyrin face for meso-tetraphenylporphyrin.[18] Since the aryl groups are not coplanar with the porphyrin, these substituents also sterically prevent exact alignment of the two macrocycles. A second inter-nonamer interaction comes from the $PdCl_2$ groups. The electrostatic and steric interactions arising from the Pd^{2+} and the Cl^- ions would tend to place Cl^- from one nonamer over the vacant axial positions of the Pd^{2+} ions of the adjacent nonamer, over the pyrrole N-H. The nature of substituent (H, Me or *tert*-Bu), also influences the kinetics and size of the hierarchical assembly. In general, the kinetics are faster and the resultant columnar stacks are larger as one goes from R = *tert*-Bu, to Me, to H, with average columnar heights by DLS of 6 nm, 7 nm, 10 nm, respectively. Though the exact geometry of the nanoscaled aggregates is still under investigation, docking experiments suggest that one planar array may stack on top of another in either of two ways: a) one is rotated $30\text{-}60^0$ relative to the next or b) one is diagonally offset by a little more than half the diameter of a single porphyrin ~ 0.6 nm.

The size of the hierarchical stack formed on the surface may also be explained in terms of the influence of surface energetics on π-stacking (Figure 4. 3.). AFM studies reveal that glass and mica surfaces favor absorption of nonamer aggregates, while surfaces such as gold favor dislodging the nonamer in contact with the surface from its parent nanoscaled aggregate and resulting in high surface densities of individual planar nonameric arrays on the gold surface.[19,20] Interestingly, when nonamers are adsorbed on gold, multi-supramolecular stacks preferentially decorate defects and step edges, while on the atomically flat terraces we find predominantly individual nonamers.

---

[19] G. S. McCarty, P. S. Weiss, *Chem. Rev.* **1999**, *99*, 1983-1990.
[20] R. Smoluchowski, *Phys. Rev. Lett.* **1941**,*60* , 661-674.

The AFM images (Figure 4. 3.) also show the expected increase in the surface density of the nonamers as the aggregates proceed from large stacks on glass to predominantly individual nonamers on Au. This is most likely due to the local dipoles formed by the Smoluchowski effect[20] at step edges, pinning the nonamers and adding an additional degree of polarization that favors stacking.[21] STM of nonamers on Au(111) clearly show the individual arrays to be ~ 6 x 6 x 0.4 nm in size (Figure 4. 3. a inset).

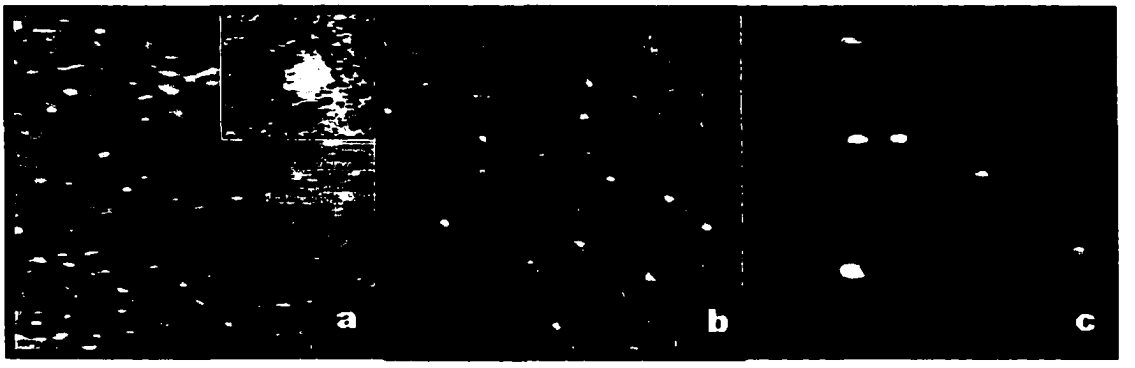

Figure 4. 3. The size of the columnar stack of free base porphyrin nonamers (R = *tert*-Bu) is also determined by the nature of the surface; **a)** single nonameric arrays are typically found on Au(111), whereas larger aggregates are observed on **b)** mica (~ 5-8 nonamer high stacks) and **c)** glass (~ 5-27 nonamer high stacks). All images are 1.15 μm x 1.15 μm, with z-scales of 14.2 nm, 3 nm and 11.9 nm respectively in panels a, b and c. The insert in panel a) is 16 nm x 14 nm with a z-scale of ~ 5 Å, and was collected in constant current mode.

Further studies are aimed at evaluating e- conductance of stacked arrays as a function of the number of nonamers in the stacks, and as a function of light intensity. The detailed photonic properties of these aggregates are also under investigation. The controlled

[21] A. P. H. J. Schenning, F. B. G. Benneker, H. P. M. Geurts, X. Y. Liu, R. J. M. Nolte, *J. Am. Chem. Soc.* **1996**, *118*, 8549-8552.

formation of nanocrystals and aggregates of inorganic,[22,23] organic,[24] and hybrid materials[17,25,26] such as those described here, is a key step in the development of nanoscaled devices. The cooperative formation of these hierarchical structures, using both specific and non-specific interactions, imparts a high degree of stability and control of size not found in most supramolecular systems (Table 4. 2).

Table 4. 2. Control of hierarchical self-assembly

	Average height (nm)
Chemistry	
R = H	10 ± 2
R = Me	7 ± 1
R = *tert*-Bu	6 ± 1
Surface type	
Glass	6 ± 2
Mica	3 ± 1
Au(111)	0.4 (single nonamer)
Au(111) edge	0.8 ± 0.3
Kinetics (R=Me)	
5 min	30 ± 5
10 min	50 ± 8
30 min	6 ± 1

4. 3. Experimental

Instruments and methods: Routine identification was performed using Cary Bio-3 UV-visible spectrometer, SPEX Tau-3 fluorometer, Agilent Technologies HP 1100 LC/MSD, Varian (500 MHz) or QE (300 MHz) NMR.

[22] V. F. Puntes, K. M. Krishnan, A. P. Alivisatos, *Science* **2001**, *291*, 2115-2117.
[23] J. F. Banfield, S. A. Welch, H. Zhang, T. T. Ebert, R. L. Penn, *Science* **2000**, *289*, 751-754.
[24] E. R. Zubarev, M. U. Pralle, E. D. Sone, S. I. Stupp, *J. Am. Chem. Soc.* **2001**, *123*, 4105-4106.
[25] J. D. Diaz, G. D. Storrier, S. Bernhard, K. Takada, H. D. Abruña, *Langmuir* **1999**, *15*, 7351-7354.
[26] T. A. Jung, R. R. Schlitter, J. K. Gimzewski, *Nature* **1997**, *386*, 696-698.

Typical Electrospray Ionization Mass Spectroscopy (ESI-MS) method: ~ 0.05mM solutions in acetonitrile:water (50 : 50) containing 1% trifluoroacetic acid, positive ion mode, and the fragmentor voltage between 100-350 V.

AFM measurements: Topometrix Explorer with ECU-plus electronics (ThermoMicroscopes) and a PicoSPM-AFM (Molecular Imaging) coupled with SPM 1000 electronics, revision 8 (RHK Technology). All measurements were made in air at room temperature using commercial Si_3N_4 AFM tips (ThermoMicroscopes) with 1:1 aspect ratios and typical radii of curvature of 30–50 nm and nominal spring constants of 0.03 N/m. All sizes referred to by AFM are the nonamer stack heights, as the horizontal dimensions are a convolution of the tip and aggregate sizes.

STM measurements: All experiments were performed in air, ambient condition using a Nanoscope III scanning tunneling microscope (Digital Instruments). The STM tip is mechanically cut from 0.25 mm diameter platinum/rhodium (87/13) wire (Omega) with an angle. The bias voltage was in the range of –1.5 V to 1.5 V, and the tunneling current was in the range of 0.25–1.0 nA.

Dynamic light scattering measurements: DLS experiments were done on Precision Detector PDDLS/Batch Instrument. The results obtained for multiporphyrin arrays indicate the presence of both small particles and large aggregates. Particles much smaller than the wavelength of incident light (800 nm), which in practice means particles with r < 20 nm, are considered small. Large particles are approximately 1/20 of the wavelength of light. The expected size of nonamer is ~ 6.3 nm in diameter, so the radius should be ~ 3.15 nm. The results have been normalized to a spherical geometry (N=3.00), and helical or cylindrical geometries cannot fit the data. Aliquots of the solutions used on the DLS

experiments were taken and deposited via a syringe fitted with a 0.2 μm filter onto glass by placing the solution onto a clean cover slip and allowing the solvent to evaporate. After rinsing (toluene, methanol or chloroform yield similar results) and drying, AFM analysis was performed. The AFM images of these aliquots taken at various times (see main text) confirm the hypothesis that the formation of the nanoscaled aggregates is dynamical. Large (> 50 nm) aggregates are first observed, followed by the observation of a bimodal distribution of these and hundreds of much smaller aggregates, and finally a uniform distribution of aggregates that are less than 10 nm.

Solvents: All solvents for synthesis and purification of the porphyrin starting materials were used as received from Aldrich or Fisher. The toluene used for self-assembly studies was distilled from CaH_2, and the chloroform from K_2CO_3. Both were filtered through a 0.2 micron filter for aggregate deposition and washing of the surfaces. Chloroform is avoided in the assembly steps because of its known reactivity with the Pd compound.

Supports: Glass cover slips, Fisher Premium 15 x 25 mm, were washed and dried in a vacuum desiccater without drying agents to avoid dust and stored for transport in PE capped vials. For optical experiments, the cover slips were affixed to glass slides, with cellophane tape on the top few mm. Mica was supplied by Polysciences and was freshly cleaved to expose a clean surface onto which nonamer was immediately deposited. Au(111) thin films on mica were supplied by Molecular Imaging and were cleaned with methanol prior to use.

Porphyrin synthesis: The synthesis of the porphyrins has been described in details in Chapter 2. The free base porphyrins used in this study were made by mixing a 2 : 2.2 : 4

mole ratio of 4-*tert*-butylbenzaldehyde (or 4-methylbenzaldehyde or benzaldehyde), 4-pyridylaldehyde, and pyrrole, respectively, in refluxing propionic acid in air for 2 hours. The solution was 0.06 M in pyrrole. Removal of the propionic acid, adsorption onto florisil, loading onto a flash silica-gel column, and elution with a pure toluene to pure chloroform solvent gradient afforded the four disubstituted porphyrins. All compounds and nonameric assemblies were characterized by ESI-MS, ^{1}H NMR, and UV-visible spectra (see Chapter 2).

Typical nonamer assembly *conditions*: Clear isosbestic points are observed in the UV-visible spectra as the trans-bis-(benzonitrile)dichloropalladium ($PdCl_2Bn_2$) is titrated into < 10 μM toluene solutions of the porphyrins in the correct 4:4:1 stoichiometry of the 5,10-bis-(4-pyridyl)-15-20-bis-(4-*tert*-butylphenyl)porphyrin, 5,10,15-tris-(4-pyridyl)-20-(4-*tert*-butylphenyl) porphyrin, and tetrakis-(4-pyridyl)porphyrin, respectively (Figure 4. 5.). The isosbestic points indicate high yield and correct formation of the self-assembled nonamer. A UV-visible titration is done for every nonamer synthesis. The UV-visible titrations reported in this work are used as an assay on every nonamer preparation to assure correct assembly. The substantial red-shift, broadening, and concomitant decreased intensity of the Soret and Q bands indicates electronic communication between the chromophores. Other characterization data are listed below.

UV-VIS Nonamer (R = *tert*-Bu): λ, nm in ethanol (ε × 10^4 $cm^{-1}M^{-1}$) 419.5 (140), 520.0 (14.5), 555.0 (7.4), 592.0 (5.6), 649 (3.0). Nonamer (R = *tert*-Bu): λ, nm in toluene (ε × 10^4 $cm^{-1}M^{-1}$) 425 (185), 520 (15.4), 557 (8.5), 593 (5.8), 649 (3.6).

^{1}H-NMR (300 MHz, $CDCl_3$) Nonamer (R = *tert*-Bu): α-pyridyl (δ = 9.051 to 9.454), β-pyridyl (δ = 8.13 to 8.32), tert-butyl (δ = 1.621 to 1.627 and 1.634), pyrrole NH (δ = -

2.816, -2.866, -2.906 to -2.786, -2.811, -2.840). The width at half-height of the methyl peaks broadens from about 2 Hz to 4.2 Hz.[17]

ESI-MS Nonamer-MeP: The ES mass spectrum (HP-1100 LC/MS, direct injection at 0.1 $mLmin^{-1}$, ionization potential 150 kV, positive-ion mode) of nonamer with methyl-phenyl substituents in chloroform with 0.3% acetic shows tri- and tetra-protonated nonamer at m/z = 2619 and 1965, respectively.[17]

DLS: Average hydrodynamic radius found for nonamer (R = *tert*-Bu) after equilibration was 3.05 ± 1 nm (N = 3.00), while for nonamer with methylphenyl groups was 3.5 ± 1 nm (N = 3.00). DLS data that followed hierarchical organization of nonamers are given in Figure 4. 4.

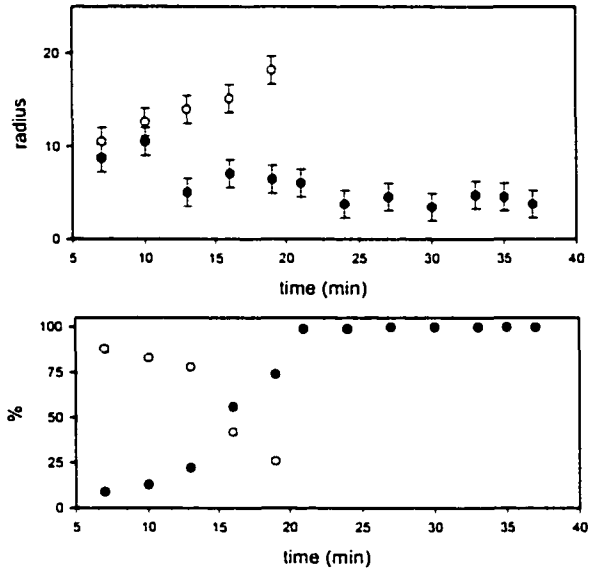

Figure 4. 4. DLS data for the hierarchical self-assembly of the nonamers (R = Me) in toluene at room temperature from a 5 μM solution of the porphyrin monomers

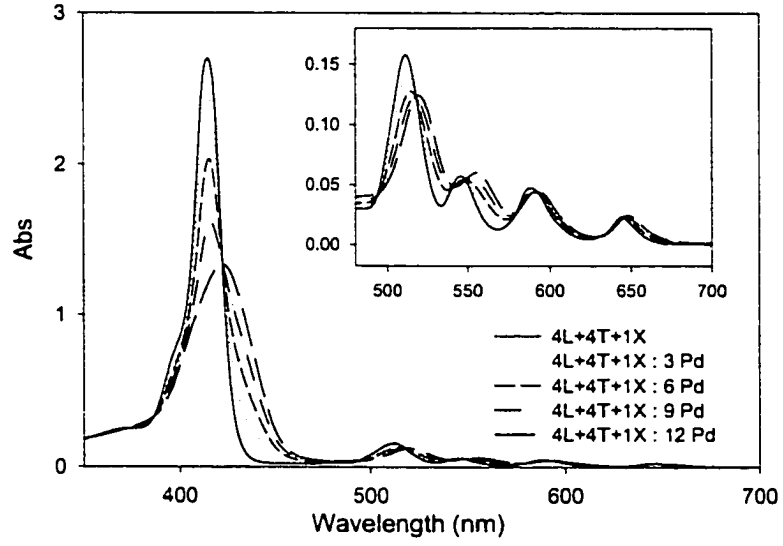

Figure 4. 5. Typical UV-Vis absorption spectrum for the titration of "4T + 4L + 1X" with bis-(benzonitrile)palladium(II) dichloride

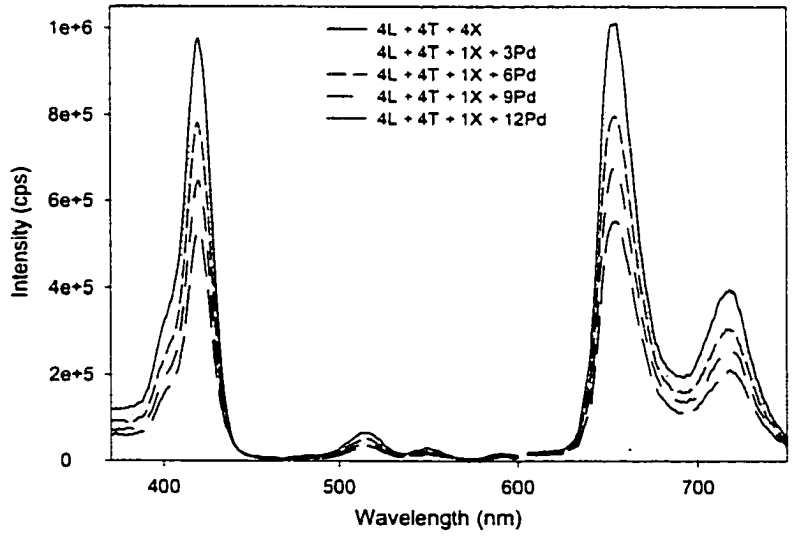

Figure 4. 6. Typical fluorescence emission and excitation spectra for the titration of "4T + 4L + 1X" with bis-(benzonitrile)Pd(II) dichloride. Intense quenching of fluorescence is due to the π-π stacking and heavy atom effects.

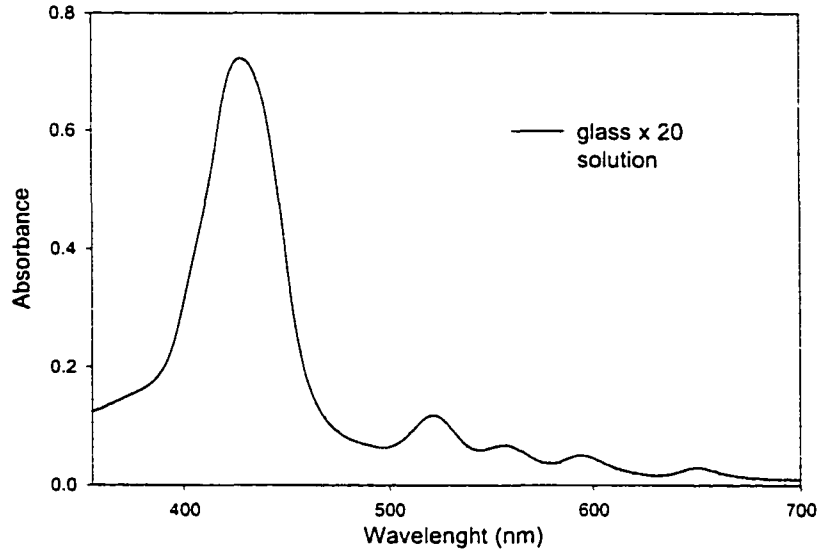

Figure 4. 7. Characteristic UV-Vis absorption spectra of the nonamer are retained if deposited onto glass substrate

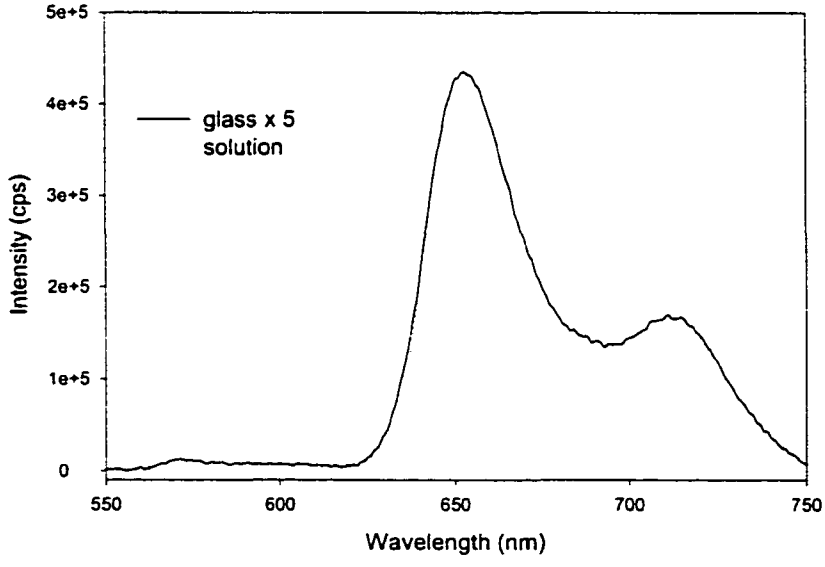

Figure 4. 8. Fluorescence emission properties of nonamer on glass are retained. The fluorescence measurement was done by front-face illumination.

The remarkable feature of these absorption and emission spectra is that they are essentially the same in solution and on glass surfaces. This is not observed when one merely absorbs porphyrins onto glass. In this latter case, the spectra are observed to be significantly broader.

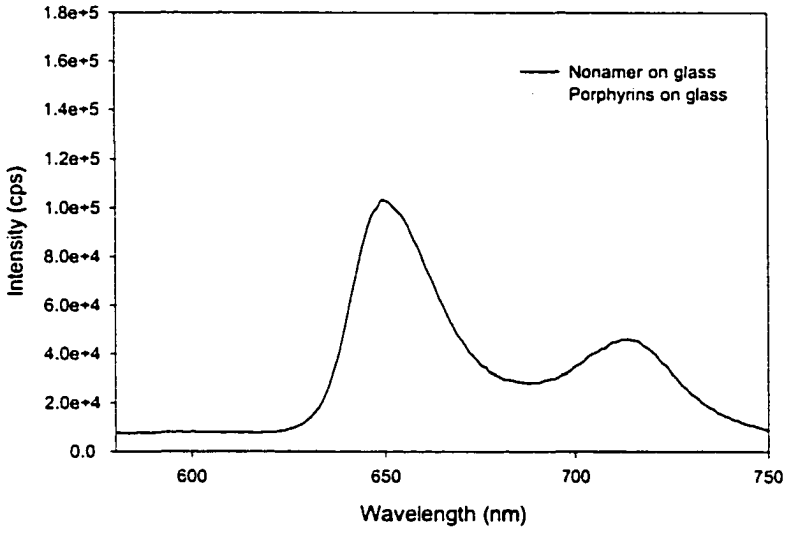

Figure 4. 9. Comparison between fluorescence emission spectra of porphyrins and nonamers on glass

5.

SELF-ASSEMBLY OF SUPRAMOLECULAR METALLOPORPHYRIN ARRAYS

5. 1. Introduction

A porphyrin core is essentially a tetradentate ligand, with an inner space with diameter ~ 3.7 Å, suitable for coordination to many metals.[1] When coordination occurs, two protons leave the pyrrole nitrogen atoms and the porphyrin ring becomes dianionic. Since metal ions behave as Lewis acids, they will accept lone pairs of electrons from a porphyrin ligand and coordinate within macrocycle.[2] Such porphyrin complexes with transition metals are very stable.

For zinc(II)tetraphenyl porphyrin, the stability constant is ~ 10^{29}.[1] Generally, for a given metalloporphyrin, the order of decreasing covalent character, and decreasing thermodynamic stability, is Pt(II) > Pd(II) > Ni(II) > Co(II) > Ag(II) > Cu(II) > Fe(II) > Zn(II) > Mg(II) > Cd(II). Subsituent effects on the porphyrin core also plays an important role for metalation kinetics.[1] Increasing the electron withdrawing character of groups

---

[1] J. E. Falk, *Porphyrins and metalloporphyrins*, Vol. 2, Elsevier **1964** and references therein.
[2] D. Marsh, L. Mink, *J. Chem. Educ.* **1996**, Vol. 73, *12*, 1188-1190.

substituted in the beta pyrroles position tends to decrease the rate of metal ion incorporation, and decrease thermodynamic stability.

There are a lot of studies on the metalation of induvidual porphyrins molecules, because metalloporphyrins are used as models for studies in biosynthesis and for the biological activity of natural compounds.[1,3] However, there is not much information available on metalation of self-assebled multi-porphyrin arrays, and how metal incorporation into the porphyrin macrocycle may affect external metal coordination. Since tessellation of nine free-base porphyrins into a supramolecular array, as described in Chapter 4, is accomplished by the self-assembly of 9 porphyrins with 12 *trans*-Pd(II) complexes, it was particularly interesting to study the effect that results from the addition of nine equivalents of a first-row transition metal to the above milieu (Scheme 5. 1.).

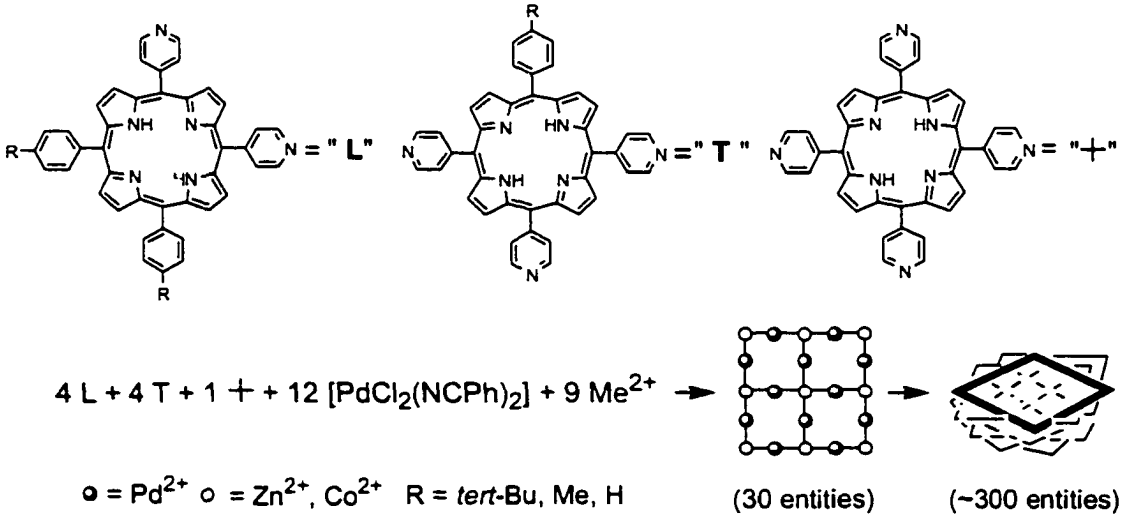

Scheme 5. 1. The self-assembly of the 30-component metalloporphyrin nonamer is followed by self-organization into columnar aggregates

[3] M. Biesaga, K. Pyrzynska, M. Trojanovicz, *Talanta* **2000**,*51* , 209-224.

In this case each porphyrin unit in the nonameric array would coordinate the same metal, such as Ni(II), Co(II) or Zn(II), but this process should not significantly interfere with the external Pd(II) coordination, *vide infra*.

Generally, the metalation of self-assembled nonameric array can be accomplished in two ways. The individual porphyrin units can be metalated prior to the self-assembly process to afford the metalloporphyrins that later can self-assemble into the nonamer. But because of the highly selective porphyrin complexation and stability for different metal-porphyrin complexes, it is possible to achieve *in situ* metalation of already self-assembled multi-porphyrin arrays. Similar to the self-assembled free-base nonamer, we can expect a secondary self-assembly process due to non-specific intermolecular interactions that will lead to the formation of nanoscaled three-dimensional aggregates. In solution, the size of the nanoscaled aggregate of the supramolecular arrays can be directed by fine-tuning the properties of the component macrocycles, by choice of metalloporphyrin, and the kinetics of the secondary self-assembly process. The choice of surface should also afford additional means to modulate the size of the particles.

5. 2. Results and discussion

5. 2. 1. Differential Metalation

When nine equivalents of a zinc(II)acetate were added simultaneously with 12 equivalents of $[Pd(PhCN)_2Cl_2]$ in toluene to a < 10 μM mixture of porphyrins in toluene at 40-50 ^{0}C, the self-assembly of the 30-component metalloporphyrin nonamer was accomplished in greater than 90% yield (Scheme 5. 1.). The formation of the metalated array was monitored by UV-Vis spectroscopy (Figure 5. 1.).

The UV-Vis spectral data indicate that after addition of palladium(II) and zinc(II) complexes, the self-assembly of nine porphyrin units via external palladium coordination happens in a first step, 5 min after metal addition, while slower zinc(II) metalation of the porphyrin macrocycles takes 3-4 hours.

The changes in UV-Vis spectrum observed are typical for porphyrin macrocycle metalation (bands I and III are collapse to an band alpha, while bands II and IV to a beta band, because the macrocycle is approaching a square-planar geometry). Formation of Zn(II) chelate is also confirmed by the characteristic ratio $\beta > \alpha$, typical for a less stable chelates.

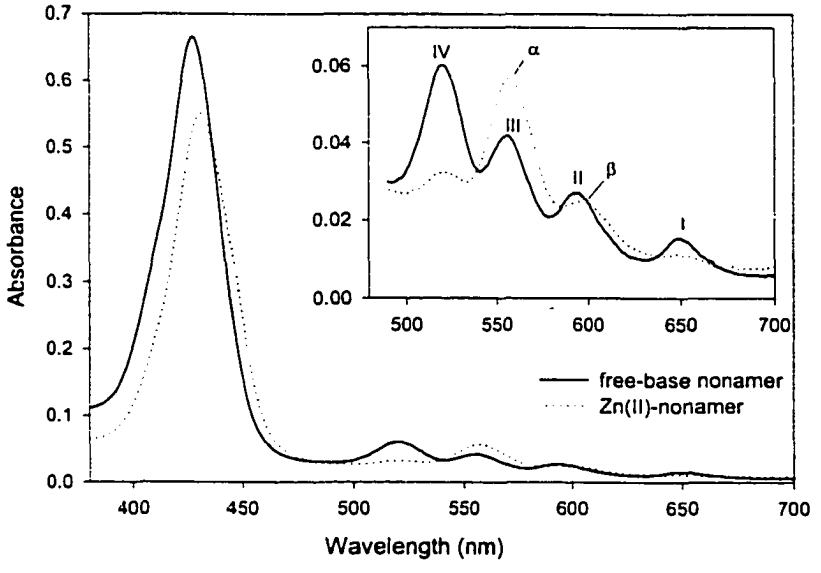

Figure 5. 1. UV-Vis spectral changes for *in situ* metalation of nonameric array (R = *tert*-Bu). Five minutes after addition of Pd and Zn(II) (solid line) and after the reaction mixture was heated at 50 °C for four hours (dashed line).

This differential metalation is possible for several reasons. First it is well known that the kinetics and thermodynamics of porphyrin metalation by the zinc is substantially different than that of palladium.[4] The size of the metal ion, the lability of the counter ions, and the energetics of the metal-porphyrin interaction all affect the yield and the rate of the reaction. Thus for most porphyrins the first row transition metals can be inserted into the core in a few hours or less at temperatures < 80 ^{0}C using an excess of the acetate salt dissolved in methanol, while palladium(II) insertion takes 8-12 hours at >120 ^{0}C. Yet, the efficiency observed for the self-assembly of the metalloporphyrin nonamer also suggests that the are additional considerations because a stoichiometric quantity of the metal to be inserted is used rather than an excess.

As we and others have observed, the insertion of Zn(II) into meso-pyridyl porphyrins increases the basicity of the pyridyl nitrogen.[4,5,7] This is indicated by a concomitant increase in the coordination bond energy between the pyridine moiety and both Pt(II) and Pd(II). The stability of dimers formed from free base mono-pyridyl porphyrins and either $PtCl_2$ or $PdCl_2$ in toluene is less than the same dimers composed of the zinc metalated porphyrins by about a factor of two. Inversely, it is reasonable to expect that the exocyclic coordination of Pd(II) or Pt(II) by the pyridyl moieties may increase the binding constant and/or lower the barrier to Zn(II) insertion into to macrocycle via similar electronic effects. Therefore, there is a synergy, or cooperativity, between the metalation of the porphyrins and the formation of the nonameric array.[6] Under these

---

[4] J. W. Buchler in *Porphyrins and Metalloporphyrins*, Kevin M. Smith (Ed.), Elsevier, **1975**, 157-224.
[5] C. M. Drain, J.-M. Lehn, *Chem. Commun.* **1994**, 2313-2315.
[6] C. V. K. Sharma, G. A. Broker, J. G. Huddleston, J. W. Baldwin, R. M. Metzger, R. D. Rogers, *J. Am. Chem. Soc.* **1999**,*12 1*, 1137-1144.

conditions the nonamer is formed prior to complete metalation of the free-base porphyrins.

This is supported by the observation of the same kinetics for porphyrin metalation of the pre-assembled nonamer under the same conditions. The electronic perturbation of the macrocycle by exocyclic ligand coordination to these square planar metals is also demonstrated by 2-5 nm red shifts observed in the visible spectra.[4,6,7]

5. 2. 2. Formation of Surface Bound Structures as Device Precursors

In order to convert these materials into useful nanoscale devices, their organization and stability following surface deposition must be evaluated. A myriad of devices can be envisioned utilizing these materials. These include a) chemical sensor arrays utilizing changes in the optoelectronic properties of the materials for signaling, b) complex 3-D storage devices based on the ability of Co(II)porphyrin nonamers to form organized nanoscale stacks of magnetic materials with varying magnetic properties depending on number of nonamers in a stack, c) photo-gated magnetic material wherein the magnetism is gated on or off depending the metalloporphyrin used.

As a precursor to the formation of such devices, we have investigated and compared the adsorption of free-base and metallo-nonamers on a variety of surfaces including glass, mica, graphite and Au(111) thin films.

The adsorption properties of the nonamers have been detailed using a combination of atomic force and scanning tunneling microscopies. As reported before in Chapter 4, the free-base materials have shown remarkable stability on glass surfaces and have found to remain intact for more than one year from deposition.

In Chapter 4 we reported that the free-base nonamer forms aggregates of ~ 5-6 nm^3 in size in solution (as observed by DLS) that remain intact when deposited on a glass surface. Nonamer aggregates on glass are deposited fairly uniformly in density over the surface with heights of 2-6 nm, which corresponds to ~ 4-12 stacked nonamer arrays. When the free-base is deposited on graphite, the stacks are found to cluster together and are generally shorter. On surfaces such as mica, or the electron rich Au surface, the nonamer aggregates break apart and form smaller structures of ~ 3 nm in height on mica, down to single nonameric array when the aggregates are deposited on Au. Interestingly, single nonameric arrays (~ 0.3 nm) appear almost exclusively on Au(111) terraces, while two nonamer high stacks are found to bind to defects such as step edges on the Au surface. This suggests that the aggregate height, thus its optoelectronic properties, may be tuned at the level of single arrays by controlling the strength of the surface dipole of the metal formed from the Smoluchowski effect.[7,8,9] Thus one can envision that the organization of these materials on metal nanoparticles of varying dimensions will exhibit tuned photonic properties due to the number of supramolecules stacked together as controlled by the varying surface dipoles of the metal nanoparticles.

Upon metalation, zinc(II)-nonamers and cobalt(II)nonamers exhibit different properties in terms of solution aggregation and surface absorption than the free-base nonamers. In general, zinc metalation of nonamer (R = *tert*-Bu) should increase the degree of intermolecular nonamer interactions, due to the additional axial interactions between the zinc(II) ion and pyridyl groups on the porphyrin macrocycle.

---

[7] G. S. McCarty, P. S. Weiss, *Chem. Rev.***19 99**, *99*, 1983-1990.
[8] R. Smoluchowski, *Phys. Rev. Lett.***19 41**, *60*, 661-674.
[9] A. P. H. J. Schenning, F. B. G. Benneker, H. P. M. Geurts, X. Y. Liu, R. J. M. Nolte, *J. Am. Chem. Soc.* **1996**,*11 8*, 8549-8552.

In fact, a significant broadening of Soret band was observed by UV-Vis that is indicative of aggregation. Also DLS measurements confirmed that in case of zinc(II)-nonamers there is a higher degree of aggregation as compared to the free-base nonamer. More specifically, DLS data of the zinc(II)-nonamer solution indicate presence of the particles with average hydrodynamic radius of ~ 9 ± 1.5 nm, while the data of the same free-base nonamer type indicate presence of particles with average hydrodynamic radius of 3.5 ± 1.5 nm. However, similar to the previous results for the free-base nonamers, the final size of aggregates on surfaces is influenced by the nature of a substrate.

When zinc(II)-nonamer solution is deposited on Au(111) surface, mostly an individual zinc(II)-nonamers or side-by-side aggregates of several nonamers are found. In the case of free-base nonamer we found that typically columnar aggregates are found on step-edges, while individual nonamers were typically located on terraces. Because of the zinc metalation, it could be expected that the binding energy between the zinc-nonamers and gold atoms increases and this reduces the intermolecular π-π stacking interaction in the z-direction. So even if we had columnar aggregates formed in solution, upon deposition they will break apart due to the stronger interaction with the surface.

This hypothesis is confirmed by changing the substrate from electron-rich Au(111) to atomically flat and electron-poor mica. When zinc(II)-nonamers are deposited on mica, the size of the metalated aggregates is greater compared to the free-base nonamers. Typically for the free-base nonamers, the height of the aggregates indicates 4 to 5 π-stacking nonamers.

In a case of zinc metalated porphyrin nonamer (Figure 5. 2.), height of the aggregates indicates 6 to 13 π-stacks of individual nonamers.

The particle density also decreases compared to the free base nonamer. Because, the binding energy between the zinc metalated nonamer and mica is similar to the binding energy of the free-base nonamer and mica, the height of the stacks is more influenced by intermolecular interactions between zinc(II)-nonameric arrays.

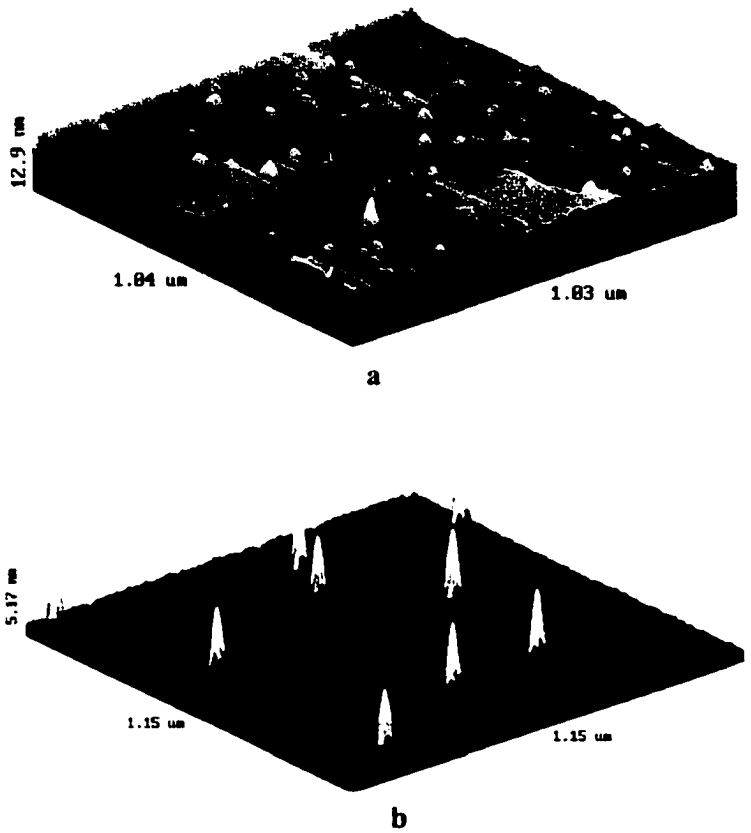

Figure 5. 2. 3D-AFM images of the zinc(II)-nonamers on Au(1 1 1) **a)**, and mica **b)**

These differences can be explained by electronic and steric effects that arise upon surface adsorption. Because the zinc(II) ion has a filled d_z^2 orbital, generally we can expect more electron density in the zinc(II)-nonamers then in the free-base nonamers. The increased proclivity for zinc porphyrins to π-stack results from both electronic and symmetry considerations.

Students in Professor Batteas's lab in the College of Staten Island conducted preliminary AFM studies on Co(II) nonamer. In an experiment that utilized 20% less Co(II) than needed to fully metalate the porphyrin nonamer, one observes two populations of columnar stacks on glass surfaces as expected. One height is nearly equivalent to the free base and one is about twice this height, which suggests that the Co(II)nonamers aggregate into larger columnar stacks due to an additional magnetic or electrostatic attraction between the layers. It is expected that the tunability of the stack height (dictated by the surface chemistry and electronic properties) will afford the controlled formation of nanoscale aggregates with designed magnetic properties, a feature we are currently exploring. This work dovetails well with other recent work on nanoscaled materials based in inorganic, organic, and organometallic systems.[10,11,12,13,14,15]

5. 3. Experimental

All compounds used for synthesis of 'L-shaped' 5,10-bis-(4-pyridyl)-15,20-bis-(4-alkylphenyl)porphyrins, 'T-shaped' 5,10,15-tris(4-pyridyl)-20-(4-alkylphenyl)porphyrins one 'X-shaped' tetrakis-(4-pyridyl)porphyrins are commercially available. The porphyrins are synthesized as described in Chapter 2. Bis-(benzonitrile)palladium(II) dichloride used for the synthesis of nonamer is purchased from Aldrich.

---

[10] V. F. Puntes, K. M. Krishnan, A. P. Alivisatos, *Science* **2001**, *291*, 2115-2117.
[11] J. F. Banfield, S. A. Welch, H. Z. Zhang, T. T. Ebert, R. L. Penn, *Science* **2002**,*28 9*, 751-754.
[12] E. R. Zubarev, M. U. Pralle, E. D. Sone, S. I. Stupp, *J. Am. Chem. Soc.* **2001**, *123*, 4105-4106.
[13] J. D. Diaz, G. D. Storrier, S. Bernhard, K. Takada, H. D. Abruna, *Langmuir* **1999**, *15*, 7351-7354.
[14] J. K. Gimzewski, T. A. Jung, M. T. Cuberes, R. R. Schlitter, *Surface Science* **1997**, *386*, 101-114.
[15] F. Wurthner, C. Thalacker, A. Sautter, *Adv. Mater.* **1999**, *11*, 754-758.

Solvents for synthesis and purification of the porphyrin starting materials were used as received from Aldrich or Fisher.

The toluene used for self-assembly studies was distilled from CaH_2. For UV-Vis measurements Varian Cary Bio-3 UV-visible spectrophotometer was used, typically in double beam mode in the range 350 – 700 nm in 1cm cuvette. All NMR measurements were done on a QE 300 MHz instrument in the solution of $CDCl_3$. Electron spray ionization (ESI) mass spectroscopy was done on Agilent Technologies HP 1100 LC/MSD, using a common electrospray ionization method: Typically the sample is dissolved in a mixture of toluene/acetonitrile 1:1 and 1% of trifluoroacetic acid. 5 microliters of this mixture is injected. Solvent acetonitrile/water 1:1 + 0.1% HOAC, positive ion mode, and the fragmentor voltage 100-350 mV.

AFM measurements were made with a PicoSPM-AFM (Molecular Imaging) coupled with SPM 1000 electronics, revision 8 (RHK Technology) All AFM measurements were made in air at room temperature using commercial Si_3N_4 AFM tips (ThermoMicroscopes) with 1:1 aspect ratios and typical radii of curvature of 30 – 50 nm and nominal spring constants of 0.032 N/m.

All the STM measurements were performed in air, ambient condition (16 °C) using a Nanoscope III scanning tunneling microscope (Digital Instruments) with 0.5μm x 0.5 μm head. The STM tip is mechanically cut from 0.25 mm diameter platinum/rhodium (87/13) wire (Omega) with an angle. The bias voltage was in the range of –1.5 V to 1.5 V, and the tunneling current was in the range of 250 pA to 1.0 nA.

Glass cover slips used were purchased from Fisher (*Fisher Premium*). The glass slides were washed in *aqua regia*, rinsed with water and dried in oven until use. Au(111)

thin films on mica were supplied by Molecular Imaging and were cleaned with methanol prior to use.

5. 3. 1. Metalation of nonameric array with zinc(II)

In 3mL solution of toluene, tetrakis-(4-pyridyl)porphyrin (1.7×10^{-6} mmol, 0. 6 μM) was mixed with 5,10-bis-(4-pyridyl)-15,20-bis-(4-*tert*-butylphenyl)porphyrin (6.7×10^{-6} mmol, 2.2 μM) and 5,10,15-tris-(4-pyridyl)-20-(4-*tert*-butylphenyl)porphyrin ($6. 7 \times 10^{-6}$ mmol, 2.2 μM) in 1:4:4 ratios. A solution of bis-(benzonitrile)palladium(II) dichloride (20.0×10^{-6} mmol, 6.67 μM) was added to the reaction mixture, followed by addition of zinc(II)acetate dihydrate (15×10^{-6} mmol, 5.0 μM). The reaction mixture was stirred at 50°C for four hours and monitored by UV-Vis. After 210 minutes the metalation was completed. The control experiment performed under the same experimental conditions with only Pd(II) present in a solution confirmed that Pd(II) does not bind internally to the porphyrin macrocycle, but coordinates exocyclic pyridyl meso-substituents. If only a zinc metal is present in a similar solution of porphyrins, it will bind porphyrin macrocycle completely after 4 hours at 50 °C.

Table 5. 1. UV spectral data for the metalation of nonamer (R = *tert*-Bu) with Zn(II) in toluene

	λ_{max} (nm)	Q_1, (nm)	Q_2, (nm)	Q_3, (nm)	Q_4, (nm)
4L + 4T + 1X	419	514	548	590	648
4L + 4T + 1X + $9Zn^{2+}$	423	514	551		
4L + 4T + 1X + $12Pd^{2+}$	428	520	556	593	654
4L + 4T + 1X + $12Pd^{2+}$ + $9Zn^{2+}$	431	520	560		

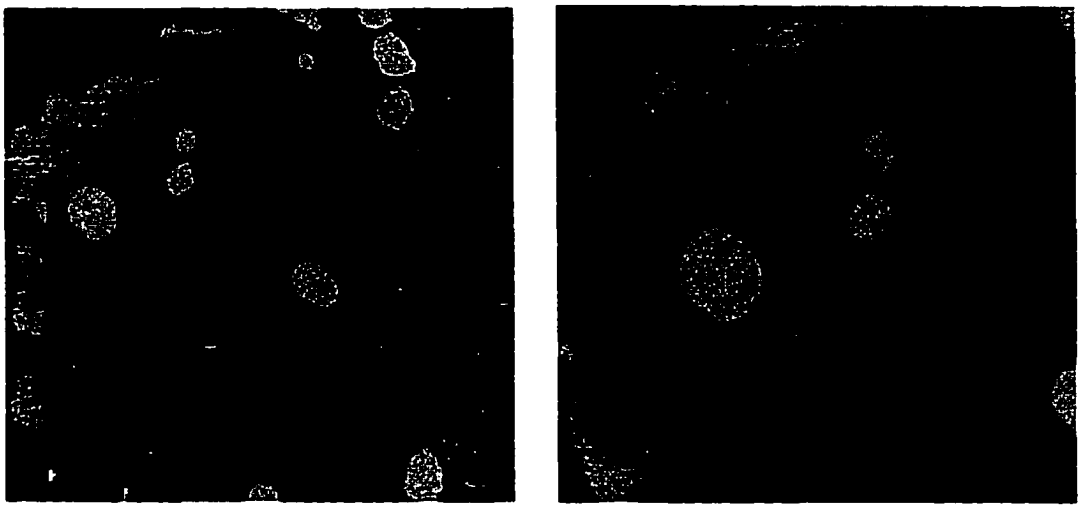

a) b)

Figure 5. 3. a) 150 x 150 nm constant current STM image of Zn(II)-nonamers deposited on Au(III). Image was collected at – 800 mV and 600 pA; **b)** 90 x 90 nm constant current STM image, which is an enlarged portion of a).

The images (Figure 5. 3.) were collected at -800 mV and 250 pA. The zinc(II)-nonamers are formed with the stoichiometric amount of zinc(II). The larger particle (Figure 5. 3. b) measures ~ 12 nm x 13 nm x 0.3 nm while the smaller particles are ~ 6.6 nm x 6.7 nm x 0.3 nm. These dimensions are consistent with approximately two zinc(II)-nonameric particles aggregated side-by-side and those of a single zinc(II)-nonamer, respectively. The Au(111) plates were rinsed with methanol to remove traces of unreacted material. The zeroth order flattening procedure has been utilized to normalize the vertical offset produced in the constant current operating mode.

5. 3. 2. Metalation of nonameric array with Co(II)

A divalent Co(II) metal ion chelates the porphyrin core, forming the square planar tetracoordinated chelate with zero residual charge. However, Co(II) is very sensitive to

oxidation. If exposed to the air, Co(II)porphyrin will oxidize to Co(III) complex that has a unit positive charge. It was experimentally observed and later confirmed by literature,[1] that the rate of Co(II) incorporation is particularly sensitive to the nature of the solvent, and that small percentages of water inhibit the reaction. This is probably due to the hydration of the metal ion, which prevents facile metal incorporation.[1] Therefore reaction should be done either in dry toluene or in absolute ethyl alcohol.

Cobalt(II) acetate was dissolved in methanol (5.46 x 10^{-4}M). Tetrakis-(4-pyridyl) porphyrin (28.00 μL of 1.07x10^{-4} M in chloroform) was mixed with 5,10-bis-(4-pyridyl)-15,20-bis-(4-tert-butylphenyl) (39.8 μL of 3.02 x 10^{-4} M in toluene) and 5,10,15-tris-(4-pyridyl)-20 (4-tert-butylphenyl) porphyrin (47.5 μL of 2.52 x 10^{-4} M in toluene) and then the cobalt(II) acetate solution was added to x mL ethanol. The reaction was done under nitrogen gas (to prevent cobalt(II) oxidation) at the temperature 70-80 °C overnight.

Table 5. 2. UV spectral data for the metalation of nonamer (R = *tert*-Bu) with cobalt(II) in ethanol

	λ_{max} (nm)	Q_1, (nm)	Q_2, (nm)	Q_3, (nm)	Q_4, (nm)
4L + 4T + 1X	415	512	546	591	645.5
4L + 4T + 1X + $12Pd^{2+}$	419.5	519.5	554.5	593	647
4L + 4T + 1X + $12Pd^{2+}$ + $9Co^{2+}$	413.5	523	580		

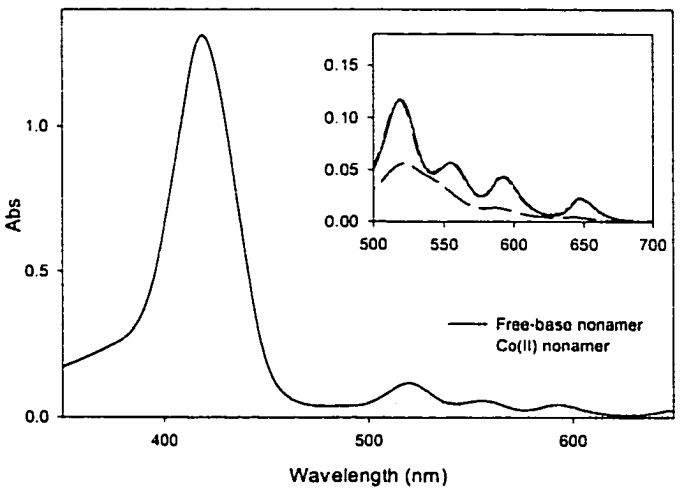

Figure 5. 4. UV spectra of the free-base and cobalt(II)-nonamer in an ethanol solution. The observed blue-shift of Soret band and collapse of Q-band are indicative for Co(II) metalation.

6.

SELF-ASSEMBLED PORPHYRIN ARRAYS WITH PERIPHERAL LONG-ALKYL CHAINS

6. 1. Introduction

Molecules in liquid phases are characterized by their random movement and loss of positional and orientational order.[1] Therefore, deposition of molecules from solution phase onto surfaces can rarely yield highly organized structures. Deposition methods, such as evaporation, sputtering or spin coating can produce monolayer molecular assemblies but these methods lack control over final molecular organization. However, it is well known that in order to make many functional organic material, such as for use in photonics, both molecular structure and alignment are important.

There are several methods for more controlled formation of monolayers. The Langmuir-Blodgett technique is based on the application of increased surface pressure on molecules, oriented between organic and water phases, until a nearly incompressible "solid" monolayer phase is formed. This method is mostly applied to molecules that posses distinct hydrophilic and hydrophobic parts, so that they can spontaneously form a

[1] Peter J. Collings, *Liquid Crystals*, Princeton University Press, Princeton, New Jersey **1990**.

films between two liquid phases of different polarity. Further transfer of ordered monolayers onto substrates can be achieved only if the surface pressure is very carefully controlled. Another method to obtain uniform monolayers is by attaching molecules to the substrate chemically, by means of covalent bonding. These are refered to as self-assembled monolayers (SAMs). However, attachment of molecules to the substrate may induce distortion of molecular physico-chemical properties, which may not be desirable for some applications.

In the liquid crystalline phase molecules are moving freely, but they retain certain spontaneous orientational order. Furthermore, liquid crystals respond much more to weak electric and magnetic fields than solids, liquids or gases and this change induce significant structural reorganization. Because of these latter properties and their potential to form ordered structures on surfaces, preparation of liquid crystalline films has received a lot of attention in recent years, and are used in liquid crystalline displays, for example.

Phthalocyanines with long, flexible hydrocarbon chains have been extensively investigated as thermotropic mesogenic materials.[2,3] They usually form discotic mesophases at elevated temperature, with molecules stacked in columnar phases with planes perpendicular to the columnar axis. Such arrangement is very suitable for applications, such as in ion or electron channels. It was also demonstrated that some phthalocyanines derivatives can be self-assembled into columnar phases in Langmuir-Blodgett films and in solution.[4]

---

[2] M. S. Suslick, *Comprehensive Supramolecular Chemistry; Bioinorganic Systems*; Elsevier Oxford **1996**, Vol. 5.
[3] J. Simon, P. Bassoul, *Phtalocyanines: Properties and Applications*; C. C. Leznoff, A. B. P. Lever, (Eds.), VCH New York **1989**, Vol. 2.
[4] C. F. van Nostrum, R. J. M. Nolte, *Chem. Commun.* **19 96**, 2385-2392.

Liquid crystal-forming derivatives of porphyrins and metalloporphyrins have not been explored as extensively as the phthalocyanines, but they are interesting due to the their rich photophysical properties, ease of functionalization and lower melting points comparing with phthalocyanines.[5] Shimizu and co-workers showed that meso-tetrasubstituted porphyrins have properties of liquid crystalline columnar phases.[6] It is usually expected that porphyrins will form discotic mesophases due to the stacking of the large, flat core. However, Bruce *et. al.* demonstrated that long alkyl chain substitution at the 5 and 15- meso position elongates the molecule so that aggregates of porphyrins with rod-like properties can be made.[7] Therefore, appropriate substitution can change porphyrin materials from discotic to rod-like calamitic mesophases.[8]

It was reported that tetrakis(4-n-alkyloxyphenyl) porphyrins form monolayer assemblies using the Langmuir-Blodgett technique.[9] Metal-free 5,10,15,20-tetrakis-(4-dodecyloxyphenyl)porphyrins have been investigated previously, and they showed three mesomorphic phase transitions (at 77 °C, 90.2 °C and 136.8 °C), and between the isotropic liquid and crystalline phases (below 5.9 °C).[6]

---

[5] J. -H. Chou, M. E. Kosal, H. S. Nalwa, N. A. Rakow and K. S. Suslick, *The Porphyrin Handbook*, Kadish, Smith, Guilard (Eds.), Adademic Press New York **2000**, Vol 6, 43-131 and references therein.
[6] Y. Shimizu, M. Miya, A. Nagata, K. Ohta, A. Matsumura, I. Yamamoto, S. Kusabayashi, *Chem. Lett.* **1991**, 25-28.
[7] D. W. Bruce, M. A. Wali, Q. M. Wang, *Chem. Commun.***19 94**, 2089-2090.
[8] Q. M. Wang, D. W. Bruce, *Angew. Chem. Int. Ed.* **1997**, *36*, 150-152.
[9] G. A. Schick, I. C. Schreiman, R. W. Wagner, J. S. Lindsey, D. F. Bocian, *J. Am. Chem. Soc.* **1989**, *111*, 1344.

Thus, four long alkyl chains per porphyrin ring are sufficient to impart liquid crystalline properties with structural transitions over wide range of temperature. Also para substitution of tetraphenyl porphyrin seems essential for liquid crystalline properties, perhaps because 2, 3, 5, 6 substitution results in four rotomeric isomers that may (3 or 5) or may not (2 or 6) interconnect ar room temperature.

Other advantages that peripheral long-alkyl chain functionalization of the porphyrin can bring are improved solubility in nonpolar solvents and better immobilization of porphyrin molecules on inert surfaces under ambient conditions.[10]

Herein we report the self-assembly of porphyrinic tetramer arrays made of four 5,15-bis-(4-pyridyl)-10,20-bis-(4-*tert*-butylphenyl)porphyrins or 5,15-bis-(4-pyridyl)-10,20-bis-(4-dodecyloxyphenyl)porphyrins linked together by coordination to *cis*-platinum(II) dichloride. We made comparison of surface organization of these tetrameric arrays with or without peripheral long-alkyl chain in order to obtain more information about role that long-alkyl chain may play in improving porphyrin surface organization. Atomic force and scanning tunneling microscopy have been utilized for imaging of the final surface structures on glass, gold and graphite.

We have also examined the self-assembly of squares formed from palladium(II) and 5,10-bis-(4-pyridyl)-15,20-bis-(4-dodecyloxyphenyl)porphyrin. This version of the square forms well in solution and has the advantage that the dodecyloxyphenyl groups face away from the center of the structure. UV-Vis titration, ^{1}H-NMR and ESI-MS indicate that the palladium(II) square indeed forms (see Chapter 3), but we find that they

---

[10] X. Qui, C. Wang, Q. Zeng, B. Xu, S. Yin, H. Wang, S. Xu, C. Bai, *J. Am. Chem. Soc.***20 00**, *122*, 5550-5556.

disassemble in the deposition process (on glass, gold and graphite). Therefore we turned to the more robust assemblies that result from using platinum(II) as the linker.

6. 2. Results and discussion

Porphyrins **1** and **2** (Scheme 6. 1.) have been synthesized using Adler procedure from 4-pyridylcarboxaldehyde, appropriate benzaldehyde (4-*tert*-butylbenzaldehyde for **1** or 4-dodecyloxybenzaldehyde for **2**) and pyrrole in propionic acid.[11] They were purified by flash column chromatography using toluene/ethyl acetate (5%) for **1**, and toluene/ethyl acetate (5:1) for **2**. Both **1** and **2** had satisfactory UV-Vis, ^{1}H-NMR and MS data.

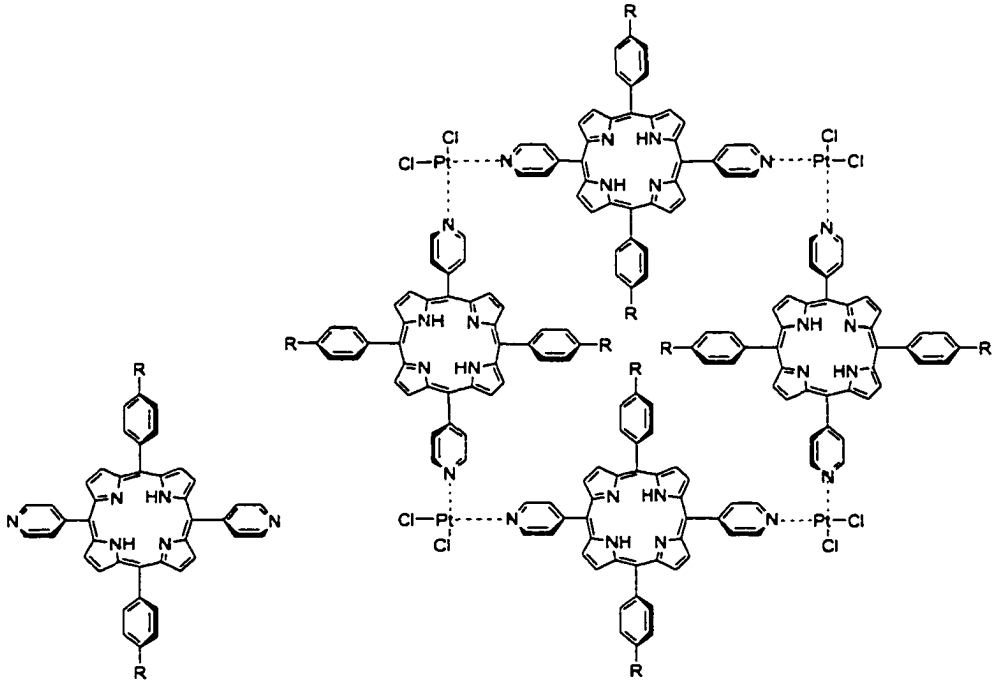

1 - R = *tert*-butyl
2 - R=dodecyloxyphenyl

3 - R = *tert*-butyl
4 - R=dodecyloxyphenyl

Scheme 6. 1. Porphyrin buiding blocks **1** and **2** and self-assembled arrays **3** and **4**

[11] A. D. Adler, F. R. Longo, J. D. Finarelli, J. Goldmacher, J. Assour, L. Korsakoff, *J. Org. Chem.*, **1967**,*32* , 476-480.

Compounds **3** and **4** (Scheme 6. 1.) are prepared at concentrations 1×10^{-6} M by mixing solution of **1** or **2** (1.21 μmol) with bis-(benzonitrile)platinum(II) dichloride (1.21 μmol) in 3 mL of refluxing toluene for 17 hours. A high reaction temperature is necessary in order to ensure complete binding of platinum(II) to pyridyl groups of porphyrin. Resulting platinum(II)-porphyrin complexes are usually very stable.[12] The higher solubility of array **4** in toluene, allows preparation at higher concentrations (1×10^{-4} M). The isolation of the products may be achieved by column chromatography on flash silica-gel using toluene/ethyl acetate gradient (5:1) as eluent. The reaction product **4** is a mixture of two compounds with very close R_f values, both less than the starting compound **2**. There was virtually no unreacted starting material. Similar results are found for the formation of **3**.

The UV-Vis absorption spectra of **3** and **4**show little change between the free porphyrin and the platinum(II) porphyrin assemblies. A red-shift of 2 nm was observed for both **3** and **4**, but with no significant broadening of Soret band. The similar results are previously reported and there are probably due to the small perturbation caused by platinum(II) to the electronic properties of the porphyrin ring.[13] The presence of four Q-bands indicate the macrocycles remain as free bases.

The ^{1}H-NMR of **4** is more complex than the spectrum of **2** (Figure 6. 1.) and shows a downfield shift for pyridyl protons, consistent with platinum(II)-pyridine complexation.

---

[12] H. Yuan, L. Thomas and L. K. Woo, *Inorg. Chem.***19 96**, *35*, 2808-2817.
[13] C. M. Drain, J.-M. Lehn, *Chem. Commun.* **1994**, 2313-2315.

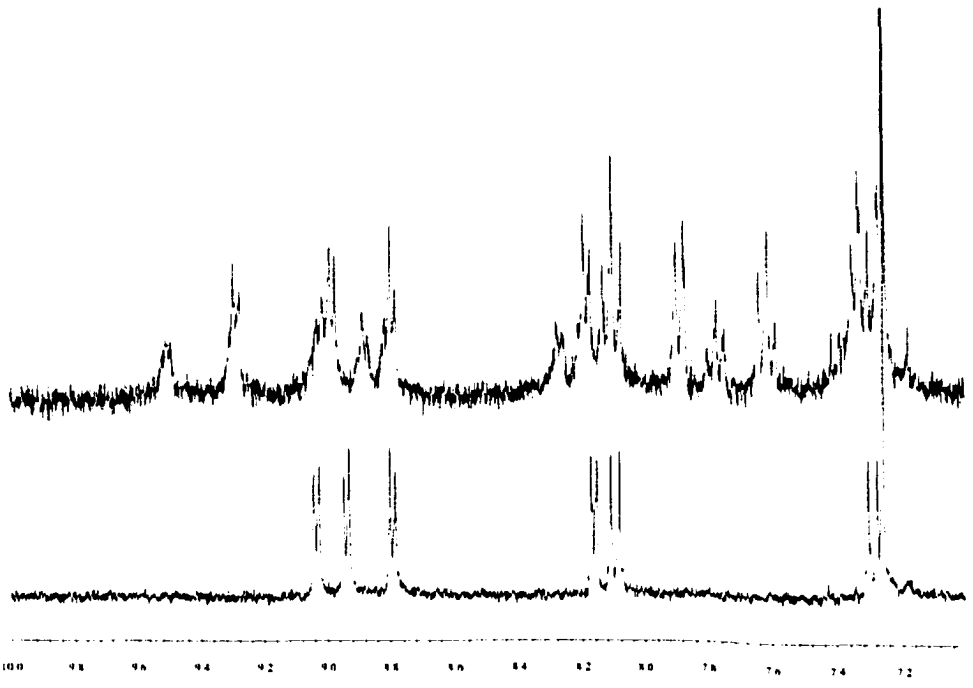

Figure 6. 1. NMR spectra of **2** and **4**. Image on the bottom is aromatic region of compound **2**, image above is the same region for the tetramer **4**.

The NMR spectrum of **2** (Figure 6. 1.) exhibits a doublet for both the alpha pyridyl protons centered at 9.04 ppm (J = 5.5 Hz) and and a second doublet fot the beta pyridyl protons at 8.17 ppm (J = 5.5 Hz). After platinum(II) binds the pyridyl groups the alpha protons in **4** significantly shift downfield, split, and broaden at 9.51 and 9.29 ppm (d, J = 6.6 Hz), while the splitting of the beta protons is less prounounced since they are located at 8.28 and 8.20 ppm (d, J = 6.6 Hz). Splitting of peaks indicate loss of symmetry in the system. An increased number of peaks may also be explained by the presence of a products, which can consist of dimers or trimers in addition to the tetramer.

The loss of chemical equivalence of the pyridyl protons and the integration of the pyridyl peaks ~ 1:1:1:1 suggests that there are now two different environments, inside the supramolecular square and outside (Figure 6. 2.). Similar findings for **3** were reported

earlier.[13] The peak due to the internal pyrrole protons at – 2.8 ppm confirms that platinum(II) is not inserted into porphyrin cavity but coordinated to the porphyrin periphery.

ESI-mass spectral analysis of **4** didn't indicate presence of mass corresponding to the tetrameric compound, however it is known that these compounds are not stable under the conditions employed in mass spectroscopic measurements.[14]

Elucidating the molecular structure of assemblies **3** and **4** is of considerable interest. We applied molecular modeling based on MM-2 steric energy minimization, to obtain insight into the structural organization (Figure 6. 2.).

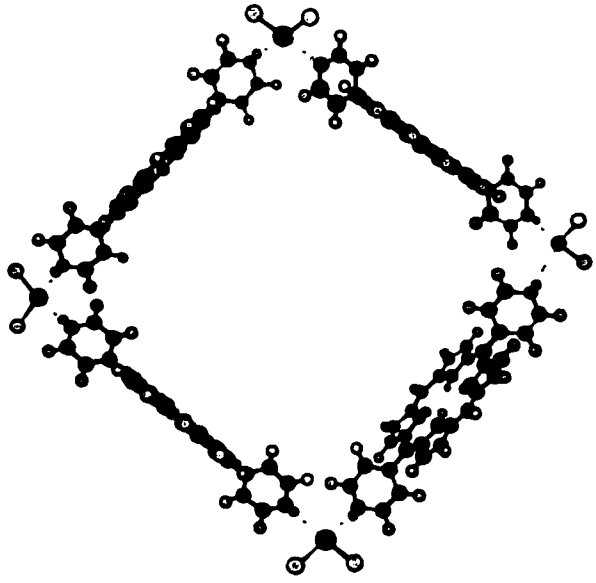

Figure 6. 2. Molecular model of *cis*-platinum(II)porphyrin assembly based on MM-2 energy minimization.[15] The figure corresponds to the tetramer array coordinated to four platinum(II) chlorides. Substituents are omitted for simplification. This arrangement

[14] J. Foekema, A. P. H. J. Schenning, D. M. Vriezema, F. B. G. Benneker, K. Norgaard, J. K. M. Kroon, T. Bjornholm, M. C. Feiters, A. E. Rowan, R. J. M. Nolte, *J. Phys. Org. Chem.* **2001**, *14*, 501-512.

[15] MM2 calculations and geometry optimization was performed with CS Chem3D Pro, Pro version 5.0, CambridgeSoft Corporation.

would leave the eight dodecyloxyphenyl groups pointing away from opposite sides of the trapezoid structure (Scheme 6. 2.)

Because of the steric constraints it is not likely that all four porphyrin units and metal complexes lie in the same plane. It is more reasonable that the porphyrin rings are orientated in such a way, so that they face each other and are perpendicular to the plane of metal complex. As a result a trapezoidal structure is more likely to be formed, with an approximate distance of ~ 20 Å from side to side and diagonal distance of ~ 31 Å between two platinum atoms opposite to each (Scheme 6. 2.).

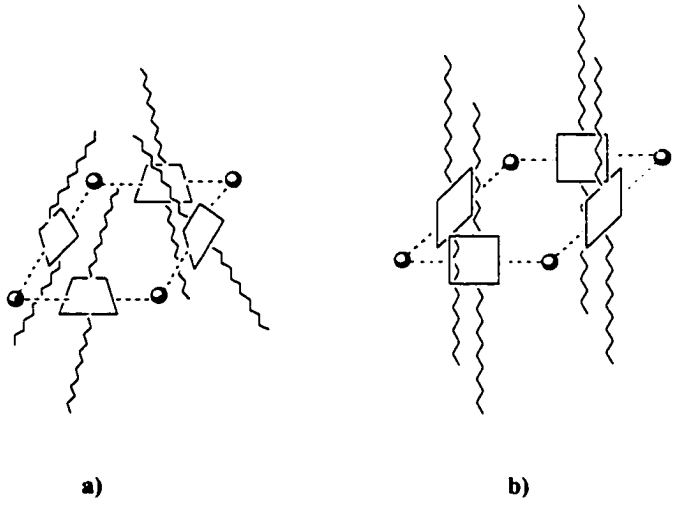

Scheme 6. 2. Simplified models of possible structures of tetrameric array **4**; **a)** a square-pyramidal shaped structure where the four porphyrins are canted inward on one face, maximizing the interactions of the four dodecyl groups on one side but cradling the corners; **b)** a cubic shaped structure minimizing inter-porphyrin contacts. For ease of illustration the dodecyl groups are shown in an extended conformation.

As found for other porphyrinic self-assembled tetramers, the plains of the macrocycle are likely larger then 60° from the plains of the square planar metal center.[16] Preliminary sterically minimized structure indicates that the supramolecule is in a square-pyramidal type structure (Scheme 6. 2. a), that allows the dodecyloxyphenyl groups on one side to interact. This leaves each side of the porphyrin in a different chemical environment. This also means there is an inside and outside of the structure (see Scheme 6. 1. for a flattened out version).

It can be supposed that the number of proton resonances should double as there are now inner-facing and outer-facing protons. If **4** is a flat as in Scheme 6. 1. then only pyrrole protons would split into inner and outer. If **4** is a cube (Scheme 6. 2. b), then only the protons on the pyridyl and phenyl groups face in and out. If **4** is trapezoidal, the pyridyl and phenyl protons face in or out. In this case we could expect porphyrins on opposite sides of the tetramer to be the same but different from the dodecyl ones, i. e. two pairs. Therefore, in principle there should be four times the number of pyrrole peaks compared to the starting porphyrin (3 to 12). If **4** is square-pyramidal-like then the phenyl and pyridyl protons face in or out, and so does the pyrrole protons; thus there should be a splitting of each set. Additionally, if there are supramolecular conformational changes that are near the NMR time scale, then there may be further broadening in addition to the increased molecular size.

---

[16] a) M. S. Ram, C. S. Johnson, R. L. Blackbourn, J. T. Hupp, *Inorg. Chem.* **1990**, *29*, 238-244
b) K. E. Splan, M. H. Keefe, A. M. Massari, K. A. Walters, J. T. Hupp, *Inorg. Chem.***20 02**, *41*, 619-621.

Deposition on glass

In order to obtain more information about molecular organization on surfaces for compound **3** and **4**, a series of atomic force microscopy measurements have been done using glass as a substrate. The solutions of **3** and **4** have been prepared in toluene at the same concentrations and deposited at room temperature on a clean glass substrate by solvent evaporation. Representative surface structures are given in Figures 6. 3. and 6. 4.

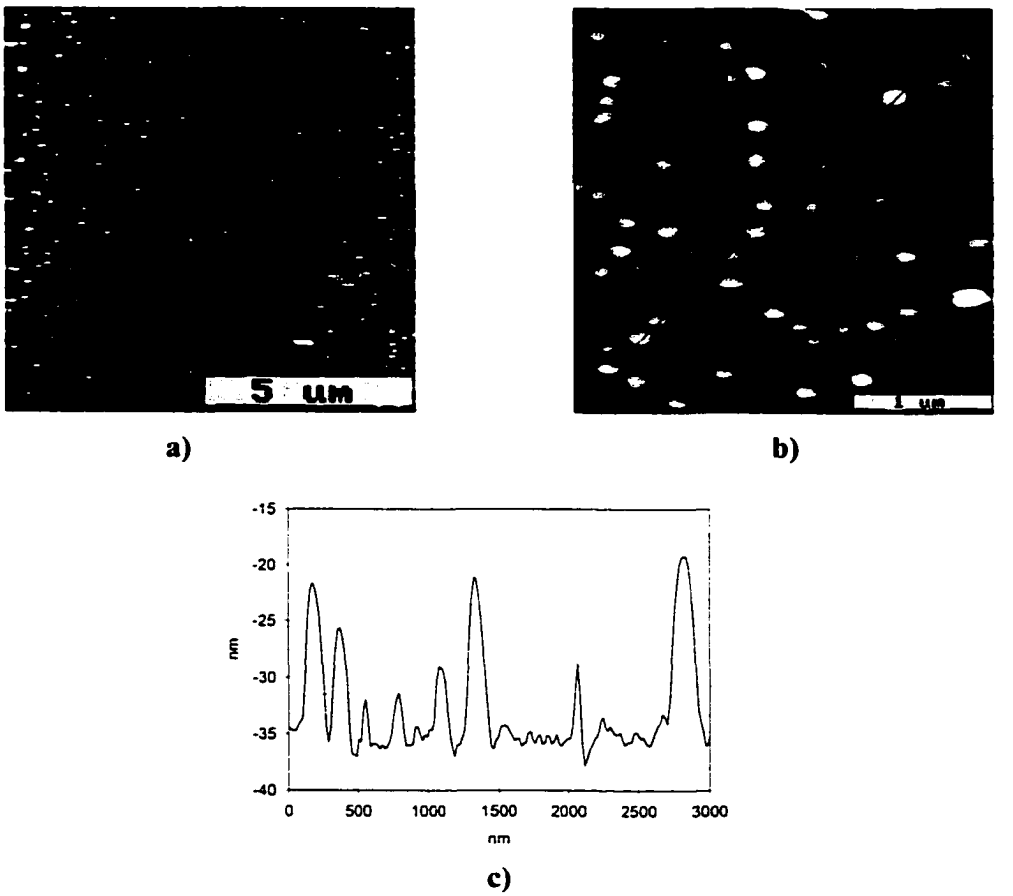

Figure 6. 3. AFM topographical images of porphyrin arrays **3** on glass. **a)** 10 × 10 μm (z-scale = 30 nm), **b)** 3 × 3 μm (z-scale = 25 nm), **c)** line scan of b). The deposition on glass from toluene (1×10^{-6} M) results in nanoclusters of 3-5 nm and 11-15 nm in height.

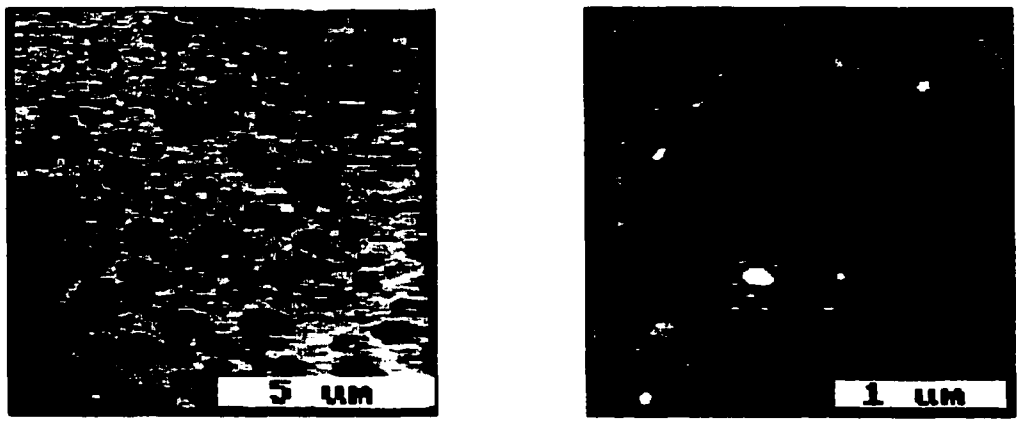

a) b)

Figure 6. 4. AFM topographical images of porphyrin arrays **4** on glass; **a)** 10 x 10 μm (z-scale = 15 nm), **b)** 2.5 x 2.5 μm (z-scale = 10 nm). Deposition was done by solvent evaporation from toluene solution (1×10^{-6} M). A film of ~ 2 nm is formed. Rinsing the plate with toluene did not produce any significant change in surface morphology, indicating a stable film.

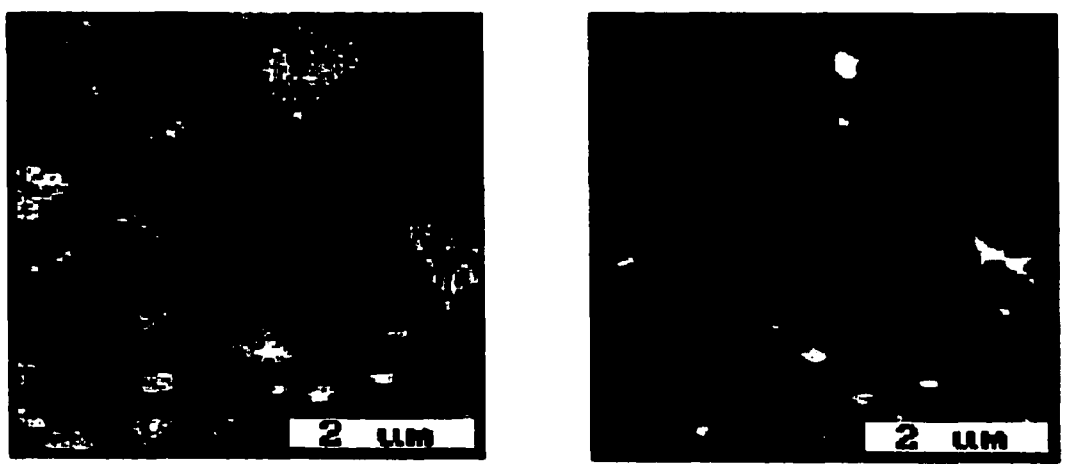

a) b)

Figure 6. 5. Frictional and topographical AFM data for porphyrin arrays **4** on glass are collected simultaneously. **a)** 5 x 5 μm frictional and **b)** corresponding topographical image.

We can see from Figures 6. 3 and 6. 4. that under ambient conditions and deposition by the solvent evaporation method, the tetrameric array with *tert*-butylphenyl peripheral groups, **3**, yields isolated nano-aggregates dispersed randomly over large areas, while the tetrameric array with peripheral long-alkyl chain, **4**, yields a more consistent coverage on the surface with a few isolated nanocrystals found. This is most likely due to the additional horizontal hydrophobic interactions of the peripheral long alkyl chains as represented in Scheme 6. 3.

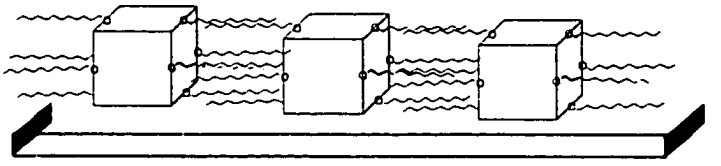

Scheme 6. 3. Lateral hydrophobic interactions between nano-aggregates with terminal long-alkyl chains

As reported previously for the cases of self-assembled nonameric arrays with *tert*-butylphenyl or methylphenyl substituents, individual self-assembled porphyrin arrays π-π stack in an offset fashion on glass substrates to form 2-10 nonamer high aggregates.[17,18] For supramolecule **3**, similar surface organization is found, with distinct nano-aggregates 3-5 and 11-15 nm in height which corresponds to 1-2 aggregates or 4-6 aggregates stacked one upon the other. However, film organization as found for square array **4** was not previously observed. The film organization at room temperature of square tetrameric array, **4**, is observed in repetitive experiments.

---

[17] a) C. M. Drain, F. Nifiatis, A. Vasenko, J. D. Batteas, *Angew. Chem. Int. Ed.* **19 98**, *37*, 2344-2347.
b) C. M. Drain, F. Nifiatis, A. Vasenko, J. D. Batteas, *Angew. Chem.* **1998**, *110*, 2478-2481.

[18] T. Milic, N. Chi, D. Yablon, G. Flynn, J. D. Batteas, C. M. Drain, *Angew. Chem.* **2002**,*41* (12), 2117-2119.

Typically, film coverage extends over large surface areas with some empty domains found. Therefore, we tried the deposition at ten times higher concentration of **4** in order to see if the monolayer film will extend more uniformly over larger areas on the glass substrate. However, more island-like domains on surfaces with height ~ 10 nm are observed with lot of individual aggregates in the same height range lying on the top of the surface film (Figure 6. 6.). The hard, straight edges and the corners are highly indicative of nanocrystalline particle that is about four layers of **4**.

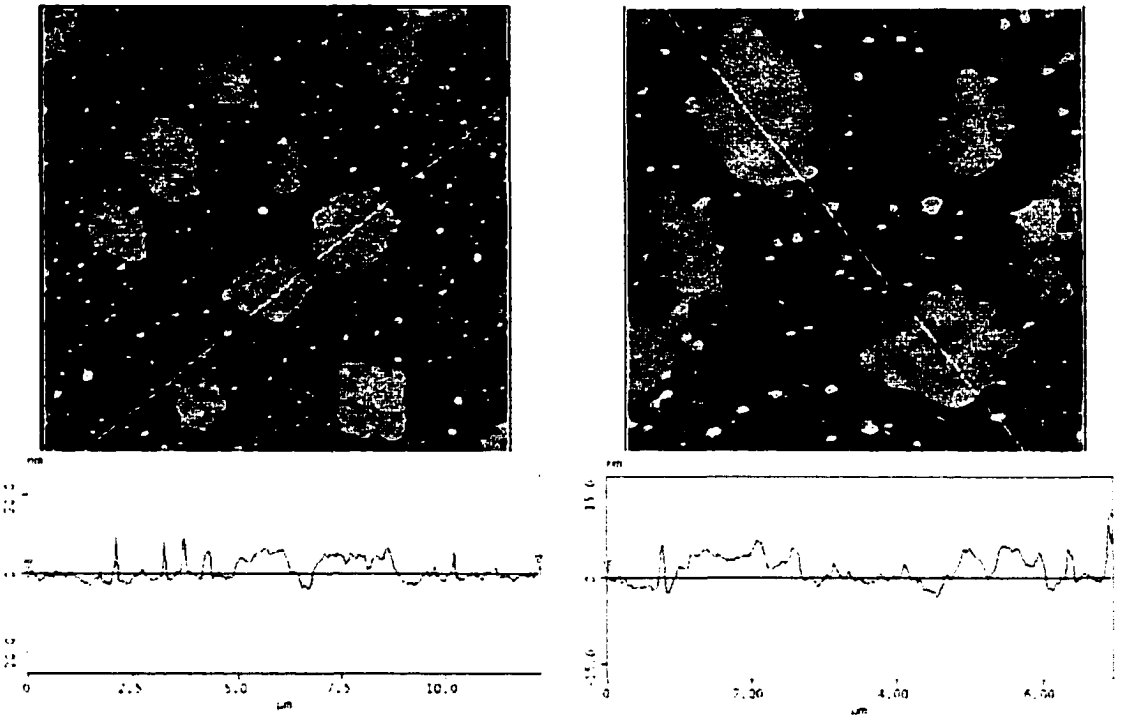

a) **b)**

Figure 6. 6. a) 12.2 × 12.2 μm (z-scale = 50 nm) topographical AFM image and line scan of porphyrin array **4** on glass, **b)** 7.0 x 7.0 μm (z-scale = 20 nm) topographical AFM image and line scan of porphyrin array **4** on glass.

In both Figures 6. 6. a) and 6. 6. b) deposition was done by solvent casting from toluene solution at 10 times higher concentration (4×10^{-5} M). The glass plate was rinsed with toluene and dried at room temperature. The height of the island like domains is between 9-11 nm. The height of smaller isolated nanocrystals is 9-12 nm. The control experiments with bis-(benzonitrile)platinum(II) dichloride solution (4×10^{-6} M) did not produce any similar surface morphology and most of the substrate seems without particles.

Another way of modifying existing film structures was to anneal the glass substrate with the film of **4** in an oven. Because of the liquid crystalline properties that the long alkyl chain we might see some change in surface morphology. The results have shown that after heating the glass substrate with **4** in oven at 80 °C overnight and cooling to room temperature, there is a decrease in overall film coverage with an increase in the number of isolated nano-aggregates (Figure 6. 7.).

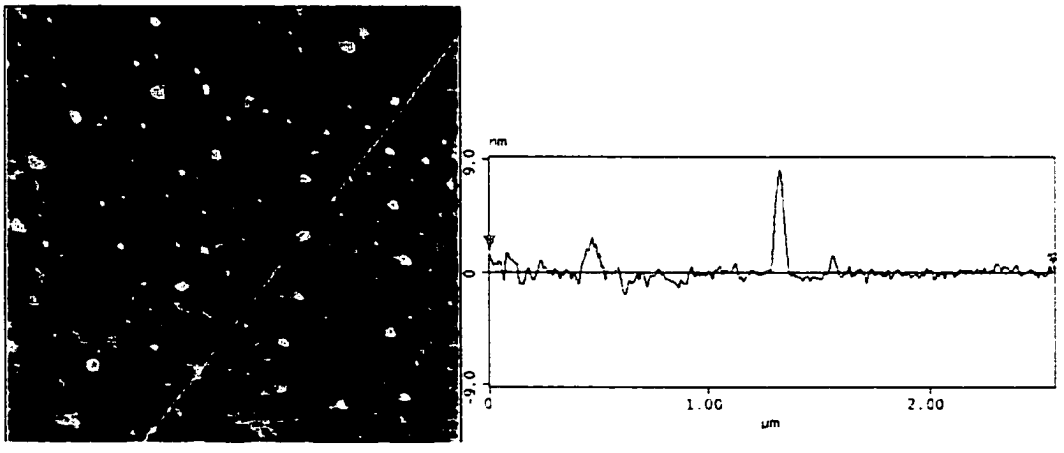

Figure 6. 7. 2.2 × 2.2 µm (z-scale = 9 nm) AFM topographical images of **4** (1×10^{-5} M) on glass after annealing in oven overnight; the average aggregate height is 8-10 nm. The smaller particles are embedded in the monolayer film, which is ~ 1.5 nm high.

Deposition from ten times more concentrated solution and annealing in oven under same conditions produced very similar results. Rinsing the glass plate with toluene didn't induce any significant change in surface structure.

The behavior of the tetrameric array, **4**, film on glass at low temperatures was also investigated. If there are some liquid crystalline properties due to the peripheral dodecyloxyphenyl groups on the self-assembled porphyrin, upon cooling to 5 °C we could expect transition from the mesogenic liquid crystalline to solid phase, as previously reported.[19] The atomic force measurements were done in a dry box with humidity 2 - 5% and sample was placed on a temperature stage. The tip was brought into contact and same area was imaged under room temperature 25 °C (298 K), 10 °C (283 K) and 5 °C (278 K). Though the quality of images is poor (probably due to the insufficient system equilibration) we can see that the film structure of **4**, present at room temperature slowly degrades (Figure 6. 8.).

Figure 6. 8. a) 10 × 10 μm AFM topographical image collected at 25 °C (298 K) and **b)** 3.0 × 3.0 μm AFM topographical image collected at 5 °C (278 K). The film of **4** in image

[19] S-i. Kugimiya, M. Takemura, *Tetrahedron Letters* **1990**,*31* (22), 3157-3160.

a) is between 4 to 7 nm high, while height of nano-aggregates of **4** in image **b)** varies more, from 1.5 to 8 nm.

Deposition on graphite

The deposition of arrays **4** on HOPG graphite did not yield more extensively organized structures as might be expected based on previous reports in the literature.[20] Large aggregates of various size were seen, particularly at the step edges on the graphite. However, the graphite surface appeared to have extended film coverage (Figure 6. 9.).

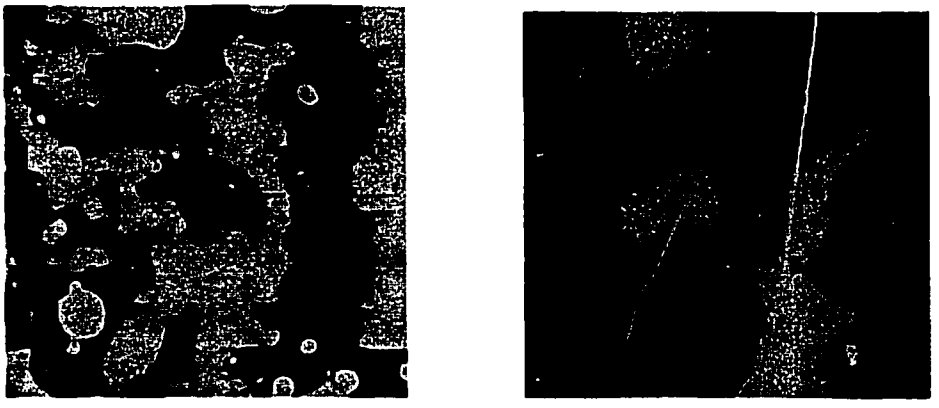

a) **b)**

Figure 6. 9. AFM images of tetrameric arrays **4** on graphite; **a)** 100 × 100 μm topographical image (z-scale = 250 nm), deposition from 4×10^{-6} M solution in toluene. Nano-aggregates range in height from 69.3-110.8 nm's, film height varies from 16-36.6 nm's; **b)** 20 × 20 μm topographical image of array **4** on graphite (z-scale = 90 nm), deposition from 4×10^{-5} M solution in toluene. Sample was annealed in oven for 90 min and cooled again to the room temperature before imaging. The film on graphite is smoother and around 25 nm high.

[20] X. Qui, C. Wang, Q. Zeng, B. Xu, S. Yin, H. Wang, S. Xu, Chunli Bai, *J. Am. Chem. Soc.***20 00**, *122*, 5550-5556.

6. 3. Experimental

All compounds used for synthesis of **1** and **2** are commercially available. Bis-(benzonitrile)palladium(II) dichloride used for synthesis of **3** and **4** was purchased from Aldrich. Solvents for synthesis and purification of the porphyrin starting materials were used as received from Aldrich or Fisher. The toluene used for self-assembly studies was distilled from CaH_2. For UV-Vis measurements Varian Cary Bio-3 UV-visible spectrophotometer was used, typically in double beam mode in the range 350 – 700 nm in 1cm cuvette. All NMR measurements were done on a QE 300 MHz instrument in the solution of $CDCl_3$. Electron spray ionization (ESI) mass spectroscopy was done on Agilent Technologies HP 1100 LC/MSD. Typical ESI method: Sample is dissolved in a mixture of toluene/acetonitrile 1:1 and 1% of trifluoroacetic acid. 5 microliters of this mixture is injected. Solvent acetonitrile/water 1:1 + 0.1% HOAC, positive ion mode, and the fragmentor voltage 100-350 mV.

AFM measurements were made with a PicoSPM-AFM (Molecular Imaging) coupled with SPM 1000 electronics, revision 8 (RHK Technology) and a Nanoscope III Multi-mode (Digital Instruments). All AFM measurements were made in air at room temperature using commercial Si_3N_4 AFM tips (ThermoMicroscopes) with 1:1 aspect ratios and typical radii of curvature of 30 – 50 nm and nominal spring constants of 0.032 N/m. All the STM measurements were performed in air, ambient condition using a Nanoscope III scanning tunneling microscope (Digital Instruments). The STM tip is mechanically cut from 0.25 mm diameter platinum/rhodium (87/13) wire (Omega) with an angle. The bias voltage was in the range of –1.5 V to 1.5 V, and the tunneling current was in the range of 250 pA to 1.0 nA.

Glass cover slips, Fisher Premium were used for deposition of **3** and **4**. Glass slides were washed in aqua regia, rinsed with water and dried in oven until use. Au(111) thin films on mica were supplied by Molecular Imaging and were cleaned with methanol prior to use.

*5, 15-bis(4-*pyridyl*)-10,20-bis(4-tert-butylphenyl) porphyrin,* **1**: To a solution of 448 mL of propionic acid (preheated to 80°C), 4-*tert*-butylbenzaldehyde (1.87 mL, 11 mmol) and 4-pyridenecarboxaldehyde (1.34 mL, 14 mmol) were added and mixed, followed by addition of pyrrole (1.55 mL, 22.4 mmol). The reaction mixture was refluxed for 90 minutes in the dark, cooled and the propionic acid removed at reduced pressure. The oily black-purple products were dissolved in 15 mL of toluene and allowed to crystallize in 400 mL of methanol overnight. Filtration and washing with methanol afforded 0.8g (~17 % yield) of a purple crystalline product that contained the expected six statistical porphyrin compounds. The desired porphyrin **1**, was isolated and purified by flash silica gel column chromatography using toluene/ethyl acetate (5%) as an eluent. **^{1}H-NMR** (300 MHz, $CDCl_3$): δ 9.04 (4H, d, o-pyridyl, J = 5.9 Hz), 8.95 (4H, d, β-pyrrole, J = 4.4 Hz), 8.79 (4H, d, β-pyrrole, J = 4.8 Hz), 8.17 (4H, d, m-pyridyl, J = 5.9 Hz), 8.13 (4H, d, o-phenyl, J = 8.4 Hz), 7.78 (4H, d, m-phenyl, J = 8.4 Hz), 1.70 (18H, s, *tert*-butyl), -2.86 (2H, s, internal pyrrole). **ESI-MS** calculated for $C_{50}H_{44}N_6$ (relative intensities theoretical): 728 (100), 729 (57), 730 (15), 731 (3), 732 (0.4). m/z ($M + H^+$ relative intensities found): 729.5 (100), 730.3 (60), 731.3 (18). **UV-Vis** λ, nm in toluene ($\varepsilon \times 10^4$ $cm^{-1}M^{-1}$) 419.5 (26), 515 (1.2), 548 (0.5), 589 (0.36), 648 (0.23).

5, 15-bis(4-pyridyl)-10,20-bis(4-dodecyloxyphenyl) porphyrin, **2**: A statistical mixture of 4-pyridylcarboxaldehyde (0.3286 ml, 3.443 mmol), 4-dodecyloxybenzaldehyde (1g,

3.443 mmol) and pyrrole (0.4777 mL, 6.886 mmol) was refluxed for 90 min in 138 ml of propionic acid (0.05 M) in the dark. A black-purple liquid remained after the propionic acid has been removed. Separation and purification of desired product **2** from the six statistical compounds was achieved by flash chromatography column with toluene/ethyl acetate (5:1) eluent. **^{1}H-NMR** (300 MHz, $CDCl_3$): δ 9.04 (4H, d, J = 5.5 Hz, o-pyridyl), 8.94 (4H, d, J = 4.8 Hz, β-pyrrole), 8.79 (4H, d, J = 4.8 Hz, β-pyrrole), 8.17 (4H, d, J = 5.5 Hz, m-pyridyl), 8.10 (4H, d, 8.4 Hz, o-phenyl), 7.30 (4H, d, J = 8.4 Hz, m-phenyl), 4.26 (4H, t, J = 6.4 Hz, $-CH_2$), 2.07-1.97, 1.69-1.27 and 0.92-0.88 (50H, m, $-(CH_2)_{10}CH_3$), - 2.82 (2H, s, internal pyrrole). **ESI-MS** calculated for $C_{66}H_{76}N_6O_2$ (rel. intensities); 985 (100), 986 (28), 988 (7), 989 (1). m/z ($M + H^+$)(relative intensities) found: 985.5 (100), 986.5 (80), 987.5 (18), 988.5 (7). **UV-Vis** λ, nm in toluene ($\varepsilon \times 10^{-4}$ $cm^{-1}M^{-1}$) 421.5 (41), 516 (1.8), 551.5 (0.91), 593 (0.54), 649 (0.40).

Tetrameric array, **3**: Solution of **1** (3.1×10^{-6} mol, 2.3 mg) was mixed with cis-bis-(benzonitrile)platinum(II) dichloride (3.1×10^{-6} mol, 1.5 mg) in 6mL of toluene. The reaction was refluxed overnight at 110 °C. Because of the poor product solubility further purification and characterization of the product was difficult. Therefore further sythesis and deposition on surfaces was done using a solution of **3** prepared at much lower concentrations. Typically, 5,15-bis-(4-pyridyl)-15,20-bis-(4-*tert*-butylphenyl)porphyrin (4.06 μM) was mixed in 1:1 ratio with bis-(benzonitrile)platinum(II) dichloride (4.06 μM) in 3 mL of toluene, and heated overnight at temperature ~ 100 °C. **UV-Vis** λ, nm in toluene 421, 515, 550, 590, 648.

Tetrameric array, **4**:*Cis* -bis-(benzonitrile)platinum(II) dichloride (2.4×10^{-6} mol, 1.1 mg) was added with stirring to the solution of **2** (2.4×10^{-6} mol, 2.4 mg) in 6 mL of

toluene. Solution was refluxed overnight for 17 hours. Purification of the product was done by column chromatography on flash silica gel using toluene/ethyl acetate 15% as eluent. **UV-Vis** λ, nm in toluene 423, 516, 553, 593, 650. **^{1}H-NMR** (300 MHz, $CDCl_3$): δ 9.51 (b, pyridyl), 9.29 (d, J = 6.6 Hz, pyridyl), 9.02 (d, J = 6.23 Hz), 8.99 (d, J = 4.76 Hz, pyrrole), 8.88 (d, J = 4.76 Hz, pyrrole), 8.80 (d, J = 4.76 Hz, pyrrole), 8.28 (d, J = 6.6 Hz, pyridyl), 8.2 (d, J = 6.6 Hz, pyridyl), 8.17 (t, J = 8.8 Hz), 7.89 (d, J = 6.96 Hz), 7.62 (t, J = 7.69 Hz), 7.43 – 7.287 (m), 7.27 (s, chloroform), 4.45-4.36 (m), 2.10 – 0.8 (m), - 2.8 (d, internal pyrrole). **ESI-MS** calculated: 5005. Found 2231.3 $(dimer)^{4+}$, 2114.0 $(dimer)^{+}$ – 1Cl, 2077.7 $(dimer)^{+}$ – 2Cl, 1409.5 $(monomer)^{+}$ + 2Pt + 1Cl), 1375.0 $(monomer)^{+}$ + 2Pt, 494.2 $(monomer)^{2+}$, 401 $(PtPhCN)_2$.

AFM control experiments: Deposition of bis-(benzonitrile)platinum(II) dichloride (4 μM in toluene) solution on glass didn't yield any similar result as shown for tetrameric arrays **3** and **4** in figures. Most of the surface didn't have much material present and only few particles and circular structures have been observed due to the film rupture during solvent evaporation. The particles found are around 10 nm tall.

7.

CONCLUSIONS

Among many types of noncovalent interactions, metal-ion coordination has proved to be a successful approach for design of multi-porphyrin arrays because of its directionality, stability and tunability of the photophysical and electronic properties of the final assemblies. Therefore, in this work we utilized external ligand-metal interactions to bring together various meso-(4-pyridyl)porphyrin derivatives using platinum(II) or palladium(II) dichloride complexes. By choosing the appropriate porphyrin substitution and metal ion binding geometry, various structures can be formed. In case of the formation of the most complex array made of nine porphyrin, the 12 *trans*-palladium(II) dichloride units combines with 4 "L"-shaped 5,10-bis(4-pyridyl)-15,20-bis(4-alkylphenyl)porphyrins that serve as corners, 4 "T"-shaped 5,10,15-tris-(4-pyridyl)-20-(4-alkylphenyl)porphyrins that as sides, and 1 "+"-shaped tetrakis-(4-pyridyl)porphyrin that is the center. Self-assembly reaction was followed by UV-Vis spectroscopy. The UV-visible spectral evolution for the arrays reveals two reaction stages. The initial self-assembly process, that brings 21 particles together, is directed by metal-ion coordination and is finished in less than 2 minutes. The second time constant on the order of ~ 25

minutes is due to the secondary self-organization of the discrete self-assembled arrays into nanoscaled aggregates, that arises from the complex interplay between a variety of non-specific intermolecular forces, such as π-π bonding.

Because, the aggregation process is dynamic, proceeding through several intermediate stages, it also affords a time-based selection of the average particle size to be deposited on surfaces. It is observed that the final thermodynamic products are columnar stacks that are ~ 6 nm in diameter and 0.4 nm to ~ 10 nm tall.

The nature of the R groups, and their position on the aryl ring, also influences the kinetics and size of the secondary assembly. In general, the kinetics are faster and the resultant hierarchical assemblies are larger as one goes from R = *tert*-Bu, to Me, to H (upon reaching equilibrium the respective average columnar heights by DLS are 6.2 nm, 7.1 nm, 10 nm). The small differences between the various pendant -R groups, -H, $-CH_3$, -*tert*-Bu, can be attributed to packing and somewhat to electronic effects on the π-system. Since the aryl groups are not coplanar with the porphyrin, these substituents also sterically prevent exact alignment of the two macrocycles. Though the exact geometry of the nanoscaled aggregates is still under investigation, it is most likely that one planar array may stack on top of another by rotation by $30\text{-}60^0$ or they are off-set randomly by little more than half the diameter of a single porphyrin ~ 0.6 nm.

Nonamer aggregates are remarkably robust and may be deposited on a variety of surfaces. The adsorption properties of the nonamers have been investigated using a combination of atomic force and scanning tunneling microscopies. The free-base nonamer forms aggregates of ~ 5-6 nm^3 in size in solution (as observed by DLS) that

remain intact when deposited on the glass surface. While the nonamer aggregates on glass are deposited fairly uniformly in density, when deposited on graphite, the nonamer aggregates are found to cluster together. As the free-base is deposited on more electron rich surfaces such as mica and Au(111), the nonamer aggregates break apart and form smaller structures, down to single nonameric array when deposited on Au(111). However, the internal structure of nonamers could not be elucidated, possibly due to their extended pi-conjugated system and scanning conditions whereby multiple tunneling pathways may impact the image.

Since tessellation of 9 equivalents of free-base porphyrins into a supramolecular array is accomplished with 12 equivalents of trans-Pd(II) dichloride linkers, it was particularly interesting to study the effect that results from the addition of 9 equivalents of a first-row transition metal to the same milieu. It is observed that if nine equivalents of Co(II) or Zn(II) are added to the solution that forms the self-assembled multi-porphyrin array, each porphyrin in the array coordinates the same metal internally, without any significant interaction with the external Pd(II) coordination. Upon metalation, the Zn(II) and Co(II)-porphyrin nonamers deposited on glass exhibit divergent properties. In general the Zn(II) nonamers show smaller stack heights on glass than the free base, most likely due to the enhanced d_{z^2}- orbital electron density on the Zn(II) ions, leading to a reduction in pi-stacking capabilities by the nonamers.

Addition of long-alkyl chain on the periphery of self-assembled tetrameric array yielded a more consistent surface coverage, due to the additional horizontal hydrophobic interactions of the peripheral long-alkyl chains. The more detailed studies of the structure and adsorption of tetrameric arrays are under investigation.

BIBLIOGRAPHY AND NOTES

Chapter 1. Introduction

1. *Supra* – prefix meaning "above" or "beyond limits" of molecule.
2. J. M. Lehn, *Angew. Chem. Int. Ed.* **1990**, *29*, 1304-1319.
3. D. Philp, J. F. Stoddart, *Angew. Chem. Int. Ed.* **1996**, *35*, 1154-1196.
4. L. F. Lindoy, I. M. Atkinson, *Self-assembly in supramolecular systems*, RSC, October **2000**.
5. J. S. Lindsey, *New. J. Chem.* **1991**, *15*, 153-180.
6. P. J. Stang, B. Olenyak, *Acc. Chem. Res.* **1997**, *30*, 502-518.
7. M. Fujita (Ed.), *Structure and Bonding* **2000**, *96*, 149-201.

Chapter 2. Preparation and characterization of porphyrin building blocks

1. J. Wojaczynski, L. Latos-Grazynski, *Coord. Chem. Rev.* **2000**, *204*, 113-171 and references therein.
2. Z. Qin, H. Jenkins, S. Coles, K. Muir, R. Puddephatt, *Can. J. Chem.* **1999**, *77*, 155-157.
3. L. F. Lindoy and I. M. Atkinson, *Self-assembly in Supramolecular Systems*, RSC, October **2000** and references therein.
4. C. M. Drain, J.-M. Lehn, *J. Chem. Soc. Chem. Commun.* **1994**, 2313-2315.
5. C. M. Drain, F. Nifiatis, A. Vasenko, J. D. Batteas, *Angew. Chem. Int. Ed.* **1998**, *37* (17), 2344-2347.
6. Peter M. Maitlis, *The Organic Chemistry of Palladium*, Academic Press **1971**.
7. M. S. Kharasch and T. A. Ashford, *J. Am. Chem. Soc.* **1936**, *58*, 1733.
8. M. M. Olmstead, P. Wei, A. S. Ginwalla and A. L. Balch, *Inorg. Chem.* **2000**, *39* (20), 4555-4559.

9. A. D. Adler, F. R. Longo, J. D. Finarelli, J. Goldmacher, J. Assour, L. Korsakoff, *J. Org. Chem.* **1967**, *32*, 476.

10. A. D. Adler, F. R. Longo, W. Shergalis, *J. Am. Chem. Soc.* **1964**, *86*, 3145-3149.

11. R. G. Little, J. A. Anton, P. A. Loach, J. A. Ibers, *J. Heterocycl. Chem.* **1975**, *12*, 343-349.

12. Lionel R. Milgrom, *The colors of life*, Oxford University Press **1997**.

13. J. S. Lindsey, I. C. Schreiman, H. C. Hsu, P. C. Kearney, A. M. Marguerettaz, *J. Org. Chem.* **1987**, *52*, 827-836.

14. J. S. Lindsey, K. A. MacCrum, J. S. Tyhonas, Y.-Y. Chuang, *J. Org. Chem.* **1994**, *59*, 579.

15. D. Gryko, J. S. Lindsey, *J. Org. Chem.* **2000**, *65* (7), 2249-2252.

16. P. D. Rao, B. J. Littler, G. R. Geier III, J. S. Lindsey, *J. Org. Chem.* **2000**, *65*, 1084-1092.

17. R. A. W. Johnstone, M. L. P. G. Nunes, M. M. Pereira, A. M. d'A. Rocha Gonsalves, A. C. Serra, *Heterocycles* **1996**, *43* (7), 1423-1437.

18. J. E. Falk, *Porphyrins and Metalloporphyrins*, Vol. 2, Elsevier New York, **1964**.

19. E. Dufour, *American Laboratory*, May **2002**, *34* (10), 50-56.

Chapter 3. Multi-porphyrin arrays: synthesis and characterization

1. J. Seth, V. Palaniappan, R. W. Wagner, T. E. Johnson, J. S. Lindsey, D. F. Bocian, *J. Am. Chem. Soc.* **1994**, *116*, 10578.

2. R. W. Wagner, J. S. Lindsey, *J. Am. Chem. Soc.* **1994**, *116*, 9759.

3. V. Marvaud, J. P. Launay, *Inorg. Chem.* **1993**, *32*, 1376.

4. J. J. Hopfield, J. N. Onuchic, D. N. Beratan, *J. Phys. Chem.* **1989**, *93*, 6350.

5. E. J. Brandon, R. D. Rogers, B. M. Burkhart, J. S. Miller, *Chem. Eur. J.* **1998**, *4*, 1938.

6. D. Gust, T. A. Moore, *Top. Curr. Chem.* **1991**, *159*, 103.

7. S. Prathapan, T. E. Johnson, J. S. Lindsey, *J. Am. Chem. Soc.* **1993**, *115*, 7519.

8. H. J. Anderson, S. J. Martin, D. D. C. Bradley, *Angew. Chem. Int. Ed. Engl.* **1994**, *33*, 655.

9. J. Sojaczynski, L. Latos-Grazynski, *Coor. Chem. Rev.* **2000**, *204*, 113-171.

10. Lionel R. Milgrom, *Colours of Life*, Oxford University Press **1997**.

11. a) C. M. Drain, X. Shi, T. Milic, F. Nifiatis, *Chem. Commun.* **2001**, 287-288.

    b) X. Shi, K. M. Barkigia, J. Fajer, C. M. Drain, *J. Org. Chem.* **2001**, *66* (20), 6513-6522.

12. A. P. Alivisatos, P. F. Barbara, A. W. Castleman, J. Chang, D. A. Dixon, M. L. Klein, G. L. McLendon, J. S. Miller, M. A. Ratner, P. J. Rossky, S. I. Stupp, M. E. Thompson, *Adv. Mater.* **1998**, *10* (16), 1297-1336.

13. H-J. Schneider, A. Yatsimirsky, *Principles and methods in supramolecular chemistry*, Wiley **2000**.

14. R. F. Pasternack, P. J. Collings, *Science* **1995**, *269*, 935-939.

15. M. Przybylski, M. O. Glocker, *Angew. Chem. Int. Ed.* **1996**, *35*, 806-826.

16. A. Ikai, *Surface Science Reports* **1996**, *26*, 261-332.

17. R. Margalit, N. Shaklai, S. Cohen, *Biochem. J.* **1983**, *209*, 547.

18. T. N. Milic, N. Chi, D. G. Yablon, G. W. Flynn, J. D. Batteas, C. M. Drain, *Angew. Chem. Int. Ed. Eng.* **2002**, *41* (12), 2117-2119.

19. C. M. Drain, F. Nifiatis, A. Vasenko, J. D. Batteas, *Angew. Chem. Int. Ed.* **1998**, *37* (17), 2344-2347.

20. H. Yan, L. Thomas, L. K. Woo, *Inorg. Chem.* **1996**, *35*, 2808-2817.

21. D. L. Akins, H.-R. Zhu, C. Guo, *J. Phys. Chem.* **1996**, *100*, 5420-5425.

22. A. P. H. J. Schenning, D. Hubert, M. Feiters, R. J. M. Nolte, *Langmuir* **1996**, *12*, 1572-1577.

23. K. Kano, H. Minamizono, T. Kitae, S. Negi, *J. Phys. Chem. A*, **1997**, *101*, 6118-6124.

24. R. F. Khairutdinov, N. Serpone, *J. Phys. Chem. B*, **1999**, *103*, 761-769.

25. C. M. Drain, J. –M. Lehn, *Chem. Commun.* **1994**, 2313-2315.

26. P. J. Stang, J. Fan, B. Olenyuk, *Chem. Commun.* **1997**, 1453.

27. A. P. H. J. Schenning, F. B. G. Benneker, H. P. M. Geurts, X. Y. Liu, R. J. M. Nolte, *J. Am. Chem. Soc.* **1996**, *118*, 8549-8552.

28. J. Hofkens, L. Latterini, P. Vanoppen, H. Faes, K. Jeuris, S. De Feyter, J. Kerimo, P. F. Barbara, F. C. De Schryver, *J. Phys. Chem. B.* **1997**, *101*, 10588-10598.

29. H. A. M. Biemans, A. E. Rowan, A. Verhoeven, P. Vanoppen, L. Latterini, J. Fockema, A. P. H. J. Schenning, E. W. Meijer, F. C. De Schryver, R. J. M. Nolte, *J. Am. Chem. Soc.* **1998**, *120*, 11054-11060.

30. L. Latterini, R. Blossey, J. Hofkens, P. Vanoppen, F. C. De Schryver, A. E. Rowan, R. J. M. Nolte, *Langmuir* **1999**, *15*, 3582-3588.

31. R. M. Weis, H. M. McConnell, *J. Phys. Chem.* **1985**, *89*, 4453.

32. J. H. Wang, C. Bohm, T. S. Ramalingam, E. Betzig, M. Edidin, *Science* **1995**, *270*, 610.

33. M. Maillard, L. Motte, A. T. Ngo, M. P. Pileni, *J. Phys. Chem B.* **2000**, *104*, 11871-11877.

Chapter 4. Hierarchical self-assembly of the free-base nonameric array

1. P. Ball, *Nature* **2001**, *409*, 413-416.

2. A. P. Alivisatos, P. F. Barbara, A. W. Castleman, J. Chang, D. A. Dixon, M. L. Klein, G. L. McLendon, J. S. Miller, M. A. Ratner, P. J. Rossky, S. I. Stupp, M. E. Thompson, *Adv. Mater.* **1998**, *10*, 1297-1336.

3. M. A. Fox, *Acc. Chem. Res.* **1999**, *32*, 201-207.

4. A. Aviram, M. Ratner (Eds), *Annals New York Acad. Sci.* **1998**, *852*.

5. M. A. Reed, *MRS Bull.* **2001**, *26*, 113-120.

6. C. M. Drain, D. Mauzerall, *Biophys. J.* **1992**, *63*, 1556-1563.

7. C. M. Drain, D. Mauzerall, *Bioelectrochem. Bioenerg.* **1990**, *24*, 263-266.

8. J.-M. Lehn, *Angew. Chem. Int. Ed.* **1990**, *29*, 1304-1319.

9. J. S. Lindsey, *New J. Chem.* **1991**, *15*, 153-180.

10. P. J. Stang, B. Olenyuk, *Acc. Chem. Res.* **1997**, *30*, 502-518.

11. M. Fujita (Ed.) *Structure and bonding* **2000**, *96*, 149-201.

12. D. M. Sarno, B. Jiang, D. Grosfeld, J. O. Afriyie, L. J. Matienzo, W. E. Jones, Jr., *Langmuir* **2000**, *16*, 6191-6199.

13. X. Qiu, C. Wang, Q. Zeng, B. Xu, S. Yin, H. Wang, S. Xu, C. Bai, *J. Am. Chem. Soc.* **2000**, *122*, 5550-5556.

14. C.-Y. Liu, H.-I. Pan, M. A. Fox, A. J. Bard, *Science* **1993**, *261*, 897-899.

15. F. Wurthner, C. Thalacker, A. Sautter, *Adv. Mater.* **1999**, *11*, 754-758.

16. D. G. Kurth, P. Lehmann, M. Schutte, *Proc. Natl. Acad. Sci. USA* **2000**, *97*, 5704-5707.

17. a) C. M. Drain, F. Nifiatis, A. Vasenko, J. D. Batteas, *Angew. Chem. Int. Ed.* **1998**, *37* (17), 2344-2347.

b) C. M. Drain, F. Nifiatis, A. Vasenko, J. D. Batteas, *Angew. Chem.* **1998**, *110*, 2478-2481.

18. C. A. Hunter, J. K. M. Sanders, *J. Am. Chem. Soc:* **1990**, *112*, 5525-5534 and references therein.

19. G. S. McCarty, P. S. Weiss, *Chem. Rev.* **1999**, *99*, 1983-1990.

20. R. Smoluchowski, *Phys. Rev. Lett.* **1941**, *60*, 661-674.

21. A. P. H. J. Schenning, F. B. G. Benneker, H. P. M. Geurts, X. Y. Liu, R. J. M. Nolte, *J. Am. Chem. Soc.* **1996**, *118*, 8549-8552.

22. V. F. Puntes, K. M. Krishnan, A. P. Alivisatos, *Science* **2001**, *291*, 2115-2117.

23. J. F. Banfield, S. A. Welch, H. Zhang, T. T. Ebert, R. L. Penn, *Science* **2000**, *289*, 751-754.

24. E. R. Zubarev, M. U. Pralle, E. D. Sone, S. I. Stupp, *J. Am. Chem. Soc.* **2001**, *123*, 4105-4106.

25. J. D. Diaz, G. D. Storrier, S. Bernhard, K. Takada, H. D. Abruña, *Langmuir* **1999**, *15*, 7351-7354.

26. T. A. Jung, R. R. Schlitter, J. K. Gimzewski, *Nature* **1997**, *386*, 696-698.

Chapter 5. Self-assembly of supramolecular metalloporphyrin arrays

1. J. E. Falk, *Porphyrins and metalloporphyrins*, Vol. 2, Elsevier **1964** and references therein.

2. D. Marsh, L. Mink, *J. Chem. Educ.* **1996**, Vol. 73, *12*, 1188-1190.

3. M. Biesaga, K. Pyrzynska, M. Trojanovicz, *Talanta* **2000**, *51*, 209-224.

4. J. W. Buchler in *Porphyrins and Metalloporphyrins*, Kevin M. Smith (Ed.), Elsevier, **1975**, 157-224.

5. C. M. Drain, J.-M. Lehn, *Chem. Commun.* **1994**, 2313-2315.

6. C. V. K. Sharma, G. A. Broker, J. G. Huddleston, J. W. Baldwin, R. M. Metzger, R. D. Rogers, *J. Am. Chem. Soc.* **1999**, *121*, 1137-1144.

7. G. S. McCarty, P. S. Weiss, *Chem. Rev.* **1999**, *99*, 1983-1990.

8. R. Smoluchowski, *Phys. Rev. Lett.* **1941**, *60*, 661-674.

9. A. P. H. J. Schenning, F. B. G. Benneker, H. P. M. Geurts, X. Y. Liu, R. J. M. Nolte, *J. Am. Chem. Soc.* **1996**, *118*, 8549-8552.

10. V. F. Puntes, K. M. Krishnan, A. P. Alivisatos, *Science* **2001**, *291*, 2115-2117.

11. J. F. Banfield, S. A. Welch, H. Z. Zhang, T. T. Ebert, R. L. Penn, *Science* **2002**, *289*, 751-754.

12. E. R. Zubarev, M. U. Pralle, E. D. Sone, S. I. Stupp, *J. Am. Chem. Soc.* **2001**, *123*, 4105-4106.

13. J. D. Diaz, G. D. Storrier, S. Bernhard, K. Takada, H. D. Abruna, *Langmuir* **1999**, *15*, 7351-7354.

14. J. K. Gimzewski, T. A. Jung, M. T. Cuberes, R. R. Schlitter, *Surface Science* **1997**, *386*, 101-114.

15. F. Wurthner, C. Thalacker, A. Sautter, *Adv. Mater.* **1999**, *11*, 754-758.

Chapter 6. Self-assembled porphyrin arrays with peripheral long-alkyl chains

1. Peter J. Collings, *Liquid Crystals*, Princeton University Press, Princeton, New Jersey **1990**.

2. M. S. Suslick, *Comprehensive Supramolecular Chemistry; Bioinorganic Systems*, Elsevier Oxford **1996**, Vol. 5.

3. J. Simon, P. Bassoul, *Phtalocyanines: Properties and Applications*; C. C. Leznoff, A. B. P. Lever, (Eds.) VCH New York, **1989**, Vol. 2.

4. C. F. van Nostrum, R. J. M. Nolte, *Chem. Commun.* **1996**, 2385-2392.

5. J. -H. Chou, M. E. Kosal, H. S. Nalwa, N. A. Rakow and K. S. Suslick, *The Porphyrin Handbook*, Kadish, Smith, Guilard, (Eds), Adademic Press, New York **2000**, Vol. 6, 43-131 and references therein.

6. Y. Shimizu, M. Miya, A. Nagata, K. Ohta, A. Matsumura, I. Yamamoto, S. Kusabayashi, *Chem. Lett.* **1991**, 25-28.

7. D. W. Bruce, M. A. Wali, Q. M. Wang, *Chem. Commun.* **1994**, 2089-2090.

8. Q. M. Wang, D. W. Bruce, *Angew. Chem. Int. Ed. Engl.* **1997**, *36*, 150-152.

9. G. A. Schick, I. C. Schreiman, R. W. Wagner, J. S. Lindsey, D. F. Bocian, *J. Am. Chem. Soc.* **1989**, *111*, 1344.

10. X. Qui, C. Wang, Q. Zeng, B. Xu, S. Yin, H. Wang, S. Xu, C. Bai, *J. Am. Chem. Soc.* **2000**, *122*, 5550-5556.

11. A. D. Adler, F. R. Longo, J. D. Finarelli, J. Goldmacher, J. Assour, L. Korsakoff, *J. Org. Chem.* **1967**, *32*, 476-480.

12. H. Yuan, L. Thomas and L. K. Woo, *Inorg. Chem.* **1996**, *35*, 2808-2817.

13. C. M. Drain, J.-M. Lehn, *Chem. Commun.* **1994**, 2313-2315.

14. J. Foekema, A. P. H. J. Schenning, D. M. Vriezema, F. B. G. Benneker, K. Norgaard, J. K. M. Kroon, T. Bjornholm, M. C. Feiters, A. E. Rowan, R. J. M. Nolte, *J. Phys. Org. Chem.* **2001**, *14*, 501-512.

15. MM2 calculations and geometry optimization was performed with CS Chem3D Pro, Pro version 5.0, CambridgeSoft Corporation.

16. a) M. S. Ram, C. S. Johnson, R. L. Blackbourn, J. T. Hupp, *Inorg. Chem.* **1990**, *29*, 238-244.

b) K. E. Splan, M. H. Keefe, A. M. Massari, K. A. Walters, J. T. Hupp, *Inorg. Chem.* **2002**, *41*, 619-621.

17. C. M. Drain, F. Nifiatis, A. Vasenko, J. D. Batteas, *Angew. Chem. Int. Ed.* **1998**, *37* (17), 2344-2347.

18. T. Milic, N. Chi, D. Yablon, G. Flynn, J. D. Batteas, C. M. Drain, *Angew. Chem. Int. Ed.* **2002**, *41* (12), 2117-2119.

19. S-i. Kugimiya, M. Takemura, *Tetrahedron Letters* **1990**, *31* (22), 3157-3160.

20. X. Qui, C. Wang, Q. Zeng, B. Xu, S. Yin, H. Wang, S. Xu, Chunli Bai, *J. Am. Chem. Soc.* **2000**, *122*, 5550-5556.